Subsurface Structural Variability of the Himalayan Foreland Basin, Nepal

by

Michael John Duvall

A thesis submitted in partial fulfillment of the requirements for the degree of

Master of Science

Department of Earth and Atmospheric Sciences

University of Alberta

Abstract

The Himalayan orogen is segmented along its strike at the scale of hundreds of kilometres. This segmentation is apparent from along-strike changes in earthquake rupture patterns, thickness changes, deformation styles, topographic gradients, thermal evolution, and faults at oblique angles to the orogen. Understanding the driving mechanisms of this longitudinal variability could further our understanding of the orogen, and potentially improve earthquake hazard assessment. This thesis attempts to explain longitudinal variability of the Himalaya by observing how the Himalayan foreland basin varies along-strike, and determining what mechanisms drive the observed changes.

The geometry of the Nepali part of the Ganga Basin is assessed through interpretation of two-dimensional seismic reflection data. The study area covers ~26 000 km^2 of the foreland basin, and incorporates 5134 km of seismic reflection data imaged by 181 profiles. The data have been depth-converted using time-depth relationships derived from wells, so as to highlight structures. Regionally interpreted surfaces include: two horizons internal to the Cenozoic succession; an angular unconformity at the base of the Cenozoic succession where older stratified units, ranging in age from Proterozoic to possibly Mesozoic, are truncated; and the nonconformity that separates sedimentary strata from acoustic basement representing Archean granitoids and Proterozoic gneisses. In addition, faults and damage zones are identified in both the foreland basin strata and the underlying basement. Because much of the foreland basin fill was deposited in continental environments close to sea level, thickness can be used as a proxy for subsidence rate. The interpreted horizons have been used to produce isopach maps for each of the main stratigraphic intervals.

The seismic interpretations show that basement depth fluctuates dramatically, ranging from > 12 km to < 3 km. These variations define two sets of depressions and ridges, and several large graben oriented at high angles to the orogen. The Cenozoic succession thins and thickens in step with the basement below. Thickness maps of units within the Cenozoic succession reveal maxima above basement depressions, and minima above basement ridges, indicating that the basement features were inherited by the foreland basin, and controlled accommodation in the foreland basin. A system of six tear faults oriented NNE-SSW and NNW-SSE is spatially localized in the sedimentary succession above a basement ridge in eastern Nepal. An E-W striking blind thrust fault is interpreted in the subsurface, ~2.8 km below sea level, bounded by two tear faults, soling on a detachment surface below the top of the Lower Siwalik subgroup. The geometry of the fault system is interpreted as a series of blocks soling on a basal décollement, with strike-slip movement on tear faults accommodating differential slip between the blocks. The faults represent the subsurface propagation of shortening associated with the Main Himalayan Thrust into the Ganga Basin that is recognized for the first time as a 'New Frontal Thrust'. The faults are interpreted to be localized by basement ridges that influence lithofacies, basin thickness, overpressure and/or the topography of the basin floor. Cumulative slip between 42 and 124 m is calculated to have accumulated on these faults over the last ~0.5 Ma. Present-day fault development in the Himalayan foreland basin may have implications for seismicity patterns varying along the strike of the orogen.

Basement-controlled differential subsidence has played (and likely continues to play) a significant role in the development of the Ganga foreland basin. Accommodation generation varied along strike during foreland basin fill, and was controlled by NE-SW oriented basement ridges and their bounding faults. Spatial localization of tear faults above basement ridges suggests that the ridges may influence lateral ramp and transfer zone distribution in the developing Himalayan foreland thrust belt.

Preface

This thesis is the original work of M. Duvall. The thesis is in paper format.

In the development of this project, Y. Najman obtained access to seismic data from the Ganga Basin in Nepal. We thank John Clayburn and Cairn Energy for their contribution to the project. L. Godin introduced the author and J.W.F. Waldron to the data in the summer of 2017. The present project, designed by L. Godin and J.W.F.Waldron, started in the fall of 2017. L. Godin organized and supported logistics for field work in Nepal in April to May 2018 with additional contributions from Y. Najman and J.W.F. Waldron. Subsequent work on the seismic data was carried out at the University of Alberta under the supervision of J.W.F. Waldron, with additional guidance from E. Konstantinovskaya.

In this thesis, Chapter One outlines the content and methodologies, and places this work in a regional context.

Chapter Two is formatted as a paper intended for submission for publication under the authorship M.J. Duvall, J.W.F Waldron, L.Godin, and Y. Najman in a structural geology or tectonics journal. The chapter focuses on the regional geometry of the Ganga basin of Nepal, and how the basin changes along-strike. I was responsible for data interpretation and manuscript preparation. Waldon provided edits and supervision. L. Godin designed the research project and the guiding hypotheses, helped organize the field research, provided access to data, and provided editorial input during preparation of the chapter. Y. Najman helped organize the field research, provided access to data, and provided editorial input during preparation.

Chapter Three is formatted as a short form paper intended to be submitted for publication under the authorship M.J. Duvall, J.W.F Waldron, L.Godin, and Y. Najman in a geology journal. The chapter is a detailed summary of fault and fold systems identified within the study area, interpreted as the subsurface propagation of the Main Himalayan Thrust into the foreland basin. I was responsible for data interpretation and manuscript preparation. J.W.F. Waldron provided edits, supervision, and assistance in data interpretation. L. Godin and Y. Najman provided access to the data, and editorial input during the preparation of this chapter.

Chapter Four summarizes the main conclusions, and explores avenues for future work.

Acknowledgements

Thank you to all the people that made this thesis happen.

First and foremost, thank you to my supervisor Dr. John Waldron, whose feedback, patience, and sheer force of will helped craft this thesis from chaos, to something slightly less chaotic. This project never would have materialized without Dr. Laurent Godin, whose passion for Himalayan geology and support was invaluable at every step of the thesis. Dr. Yani Najman's sharp wit and careful guidance made the sweaty lowlands an extremely enjoyable place, despite the heat.

Thank you to my examination committee composed of Drs. Catuneanu, Godin, Konstantinovskaya, Unsworth, and Waldron for their time and effort.

Thank you to John Clayburn and Cairn Energy for their contribution to the project. Workstation interpretation was aided by Schlumberger's Petrel program. This work was supported by NSERC Discovery Grants to Godin and Waldron, and a teaching assistantship from the University of Alberta. Presentation of this work was supported by a University of Alberta Graduate Students' Association travel grant, and the Himalaya Karakorum Tibet Workshop student stipend.

Thank you to Alison Martin for being an excellent and cheerful field assistant. Dawa and Pradip Tamang ensured I not only survived in Nepal, but I actually got some research done – thank you for keeping me out of trouble.

The camaraderie of Jared, Alison, Wenbo, Morgan, Augusto and Martin made this two-year experience feel like two months. Thank you for your friendship, and for the games of cribbage played on slow afternoons.

Dr. Elena Konstantinovskaya's expertise in Petrel was extremely helpful on numerous occasions. Thank you for your willingness to sit down with a struggling student.

Thank you to my sugar momma Angie Wu for supporting my disgusting academia habit, and for being by my side on this long winding path full of diversions. Thanks to my parents Mary and Mel Duvall for their support at every step of my academic journey.

Table of Contents

List of Figures

List of symbols and abbreviations in the text

2D	Two-dimensional
3D	Three-dimensional
ASL	Above sea level
BDF	Below drilling floor
BSL	Below sea level
DEM	Digital elevation model
ITSZ	Indus-Tsangpo Suture Zone
KB	Elevation of Kelly Bushing
MBT	Main Boundary Thrust
MCT	Main Central Thrust
MD	Measured depth
MFT	Main Frontal Thrust
MHT	Main Himalayan Thrust
M_w	Moment Magnitude
NFT	New Frontal Thrust
STD	South Tibet Detachment
TWT	Two-way travel time
USGS	United States Geological Survey
V_s	Volume of shortening (or extension)
V_{sr}	Volume of structural relief
Z_i	Distance of subsidence at the intersection of a N-S and an E-W line
Z_x	Distance of subsidence at position x on an E-W line
Z_y	Distance of subsidence at position y on a N-S line

Chapter 1: Introduction

1.1 The Himalayan system

The continent-continent collision between India and Eurasia has given rise to the Himalaya, and dramatically reshaped climate, topography, geology, and life in Asia (Yin, 2006). The Himalaya, the world's highest orogen, began rising between 60 and 40 Ma (Bouilhol et al., 2013; Hu et al., 2016; Najman et al., 2017) and spans over 2500 km from syntaxis to syntaxis (Fig. 1-1a). Lithospheric flexure caused by the mass of the Himalaya resulted in a significant depression to the south, the Himalayan collisional foreland basin (Lyon-Caen and Molnar, 1985). The foreland basin (also known as the Indo-Gangetic trough) has been filled by kilometres of sedimentary strata, and these strata preserve detritus from the early Himalaya (Burbank et al., 1996). The foreland basin documents the progressive southward march of the Himalaya, with an overall coarsening depositional pattern indicating progradation through time (DeCelles et al., 1998a). This study focuses on the geometry of the Himalayan foreland basin in Nepal, dissecting the geometry, and determining how pre-Himalayan inherited structures are propagated into the basin.

The Himalayan foreland basin is longitudinally extensive, and has a surface area over 50 000 km^2 (Raiverman, 2002). The Siwalik Group that fills most of the foreland basin has been described along the entire length of the orogen (Burbank et al., 1996; Garzanti, 2019). Despite the laterally continuous basin fill, aeromagnetic and gravity anomalies indicate a series of basement ridges and depressions (Fig. 1-1b) that segment the foreland basin (Sengupta, 1962; Sastri et al., 1971; Rao, 1973; Valdiya, 1976; Karunakaran and Rao, 1979). Crustal-scale faults at a high angle to the orogen (Fig. 1-3) have also been identified under the foreland basin (Godin and Harris, 2014), segmenting the Indian crust into a series of horsts and graben (Godin et al., 2019). Along-strike changes of topography (Duncan et al., 2003), incision patterns (van der Beek et al., 2016), crustal density (Basuyau et al., 2013), structure (Yin, 2006), rates of convergence and exhumation (Burgess et al., 2012; McQuarrie et al., 2014), seismicity (Monsalve et al., 2006; de la Torre et al., 2007; Gahalaut and Kundu, 2012), and climate (Anders et al., 2006; Vögeli et al., 2017) in the Himalaya also suggest that segmentation is occurring along the orogen. An objective of this thesis is to explain these patterns of lateral segmentation in both the Himalaya and the foreland basin by studying how the foreland basin of Nepal changes along-strike.

1.2 Study objectives

The main objective of this study is to understand how and why the geometry of the Himalayan foreland basin varies along strike. To do this, we focus on the Nepali portion of the Ganga Basin, and use 2D seismic data to map several regional marker horizons and interpret faults across the basin. In studying the basin geometry, we hope to determine what mechanisms drive lateral variability, and where their effects are most pronounced. Finally, we want to assess how structures are propagating and forming in the foreland basin fill. In addressing these objectives, we aim to make insights as to where and why there is longitudinal structural variability in the Himalaya, and how this variability influences seismicity in the region.

1.3 The Himalayan Orogen

The Himalayan orogen comprises four laterally extensive lithotectonic units, bounded by faults. These lithotectonic units from north to south are: the Tethyan Himalaya, composed of sedimentary strata deposited on the passive margin of India; the Greater Himalayan high grade metamorphic rocks and granites; the Lesser Himalaya, predominantly composed of low grade metasedimentary and metavolcanic rocks sourced from continental India; and the Sub-Himalaya, uplifted deposits of the foreland basin (Yin, 2006 and references therein). The Tethyan Himalaya is bracketed to the north by the Indus-Tsangpo Suture Zone (ITSZ), the suture between the Indian plate and the Eurasian Plate (Fig. 1-1), and to the south by the South Tibet Detachment system (STD; Burchfiel et al., 1992; Ratschbacher et al., 1994). The Greater Himalaya (Fig. 1-2) is bounded to the north by the STD, and to the south by the Main Central Thrust (MCT; Heim and Gansser, 1939; Searle et al., 2008). The Lesser Himalaya (Fig. 1-2) lies between the MCT to the north and the Main Boundary Thrust to the south (MBT; Heim and Gansser, 1939; Gansser, 1964). The Sub-Himalaya (Fig. 1-2) is bounded by the MBT to the north, and the Main Frontal Thrust to the south. The southward propagating MCT, MBT, and MFT all root into a regional subsurface décollement (Fig. 1-2) – the Main Himalayan Thrust (MHT; Zhao *et al.* 1993; Brown *et al.* 1996; Nelson *et al.* 1996; Hauck *et al.* 1998).

1.4 The Ganga Basin

The Himalayan foreland basin is divided into a series of sub-basins and depressions. Overall, the foreland basin is approximately cylindrical in the region between two sharp bends, or syntaxes, in the Himalayan Orogen (Fig. 1-1a). In this central segment, convergence across the Himalaya is approximately orthogonal to the belt, and stratigraphic units can be correlated hundreds to thousands of kilometres along strike. A subtle topographic high separates the west- and south-draining Indus river system from the east-draining Ganges River. A prominent topographic high in the eastern extremity of this basin, the Shillong Plateau, reflects a thick-skinned basement uplift within the foreland basin. Within and beyond the syntaxes, convergence is oblique and foreland basin structure is more complex. Subsurface topography of the basement rock has been used to define four sub-basins (Fig. 1-1a): the Indus basin, the Punjab Basin, the Ganga Basin, and the Brahmaputra Basin (Sastri et al., 1971; Rao, 1973). Modern drainage divides have also been used to segment the foreland; the Ganga Basin is defined as the drainage area of the Ganges River, and the Indus Basin is the drainage area of the Indus river (Burbank et al., 1996). The basement topography definition is preferred in this study, as modern drainage areas have little influence on the sedimentary fill patterns of the foreland basin (and as Chapter 2 discusses, basement structures do). We focus on the Ganga Basin, defined here as the portion of the Himalayan foreland basin that stretches from the Delhi-Haridwar ridge in the west, to the eastern edge of the Munger Saharsa ridge (Fig. 1-3). The northern boundary of the Ganga Basin is the Main Frontal Thrust, and the southern boundary is the outcrop location of Precambrian continental Indian rocks (Fig. 1-4).

The Ganga Basin is the largest of the Himalayan foreland basins (Rao, 1973), underlying a large portion of Northern India and Southern Nepal (Fig. 1-1). The basin varies dramatically in thickness, from < 3 km to > 7 km total thickness (Raiverman, 1983). It has been a target of hydrocarbon exploration for over 50 years on both its Indian (Sastri et al., 1971; Rao, 1973; Valdiya, 1976; Karunakaran and Rao, 1979; Raiverman, 1983; Fuloria, 1996) and Nepali (Bashyal, 1998) sides; however no commercially viable plays have been found by the 12+ wells drilled.

The fill of the foreland basin (Fig. 1-5) is mostly Cenozoic, although Cretaceous strata have been mapped in the Sub-Himalaya of India and Nepal conformable with the foreland basin fill (Valdiya, 1980; Sakai, 1983; DeCelles et al., 1998a). The Ganga basin trends roughly E-W, following the strike of the Himalaya, and has been further subdivided into two ‘depressions,’ the Gandak depression in the east and the Sarda depression in the west (Rao, 1973) (Fig. 1-1c). These depressions are bordered by three major basement rock ridges, the Delhi-Haridwar, Faizabad, and Munger-Saharsa ridges oriented NNE-SSW (Fig. 1-1b). The ridges have been interpreted to be subsurface extensions of Indian plate mobile belts and cratons, seen along

Fig. 1-1. Regional geology maps

a) Regional political map of Asia and the Himalayan Orogen. Subdivisions of the Himalayan foreland basin after Rao (1973) are labelled. Blue triangle marks the eastern Himalayan syntaxis; red triangle marks the western Himalayan syntaxis (Yin, 2006). (b) Satellite map superimposed on a generalized geology map of Northern India, Nepal, and adjacent areas after Yin (2006), Goscombe *et al.,* (2018), Kellett & Grujic (2012), Soucy la Roche *et al.*, (2018), Mohanty (2012), Casshyap & Khan (2000), Godin *et al.,* (2019) and USGS public data. Approximate traces of basement ridges after Godin & Harris (2014). ITSZ: Indus-Tsangpo Suture Zone; STD: South Tibet Detachment; MCT: Main Central Thrust; MBT: Main Boundary Thrust; MFT: Main Frontal Thrust; KF: Kishangang Fault; MSF Munger-Saharsa Ridge fault, WPF West Patna Fault; EPF: East Patna Fault; LF: Lucknow fault; GBF: Great Boundary Fault; NSNF: North Son-Narmada Fault. (c) Detailed map of available seismic lines and wells within the study area (location shown in b). Seismic surveys used in this study are shown, and were shot in four blocks: the Western Block, the Eastern Block, the Central Block, and 'Block 10.' Gaps between the blocks range from 60 km to 9 km. Of the seven wells drilled close to the seismic, Biratnagar-1 acted as the sole well tie, while the Madhubani-1 and Raxaul-1, and Matera -1 wells were used as supplementary controls on stratigraphy in the Eastern and Western Blocks. Highlighted lines (i) and (ii) are shown in Fig. 1-8.

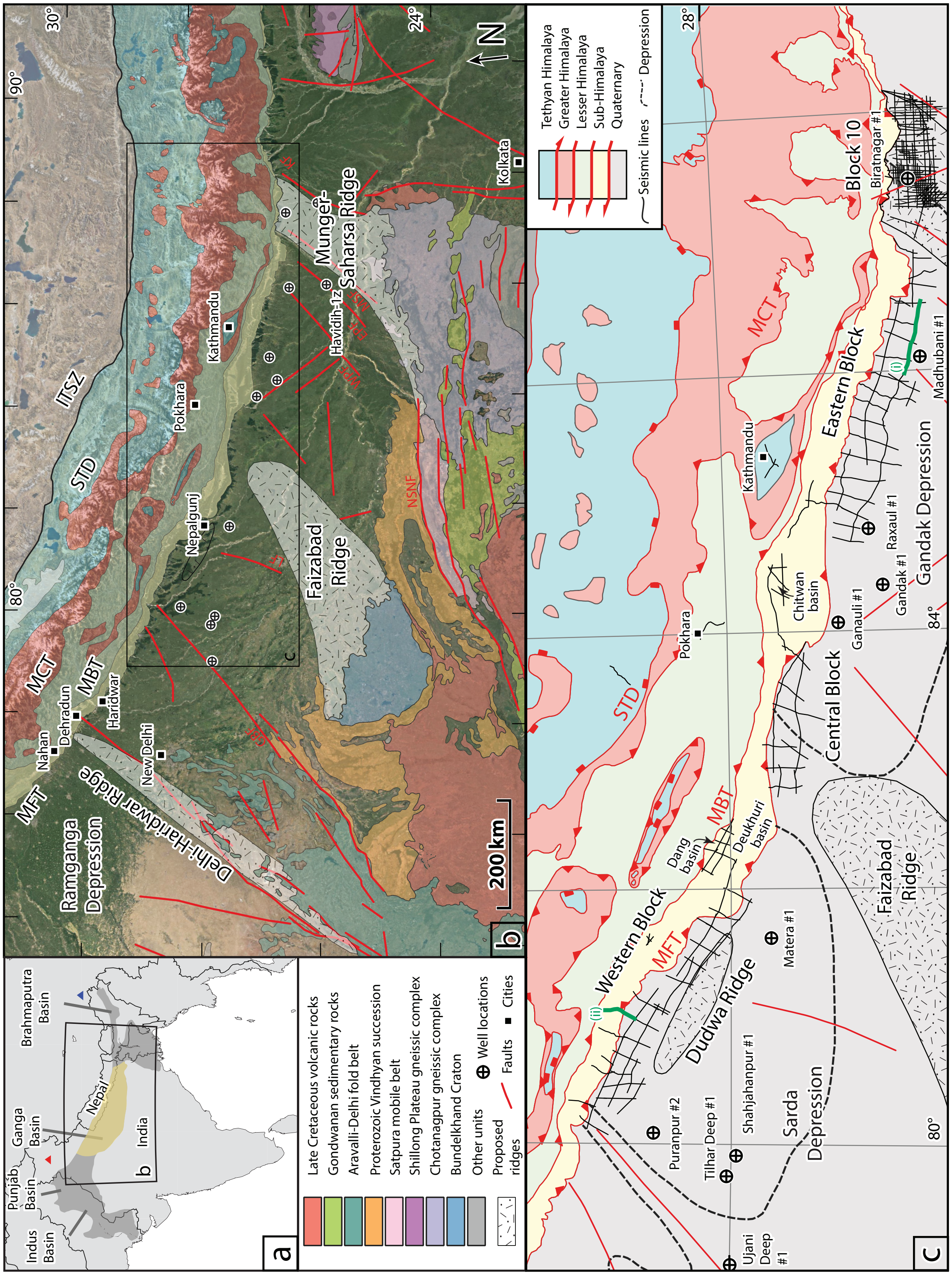

a
Indus Basin
Punjab Basin
Ganga Basin
Brahmaputra Basin
Nepal
India
b
Late Cretaceous volcanic rocks
Gondwanan sedimentary rocks
Aravalli-Delhi fold belt
Proterozoic Vindhyan succession
Satpura mobile belt
Shillong Plateau gneissic complex
Chotanagpur gneissic complex
Bundelkhand Craton
Other units
Proposed ridges
Faults
Well locations
Cities
MFT
MBT
MCT
STD
ITSZ
Ramganga Depression
Delhi-Haridwar Ridge
Nahan
Dehradun
Haridwar
New Delhi
Nepalgunj
Pokhara
Kathmandu
Faizabad Ridge
Havidih-1z
Munger-Saharsa Ridge
Kolkata
NSNF
200 km
N
80°
90°
30°
24°
c
Tethyan Himalaya
Greater Himalaya
Lesser Himalaya
Sub-Himalaya
Quaternary
Seismic lines
Depression
28°
80°
84°
MFT
MBT
MCT
STD
Western Block
Central Block
Eastern Block
Block 10
Dudwa Ridge
Faizabad Ridge
Sarda Depression
Gandak Depression
Dang basin
Deukhuri basin
Chitwan basin
Pokhara
Kathmandu
Ujani Deep #1
Tilhar Deep #1
Shahjahanpur #1
Puranpur #2
Matera #1
Ganauli #1
Gandak #1
Raxaul #1
Madhubani #1
Biratnagar #1
(i)
(ii)

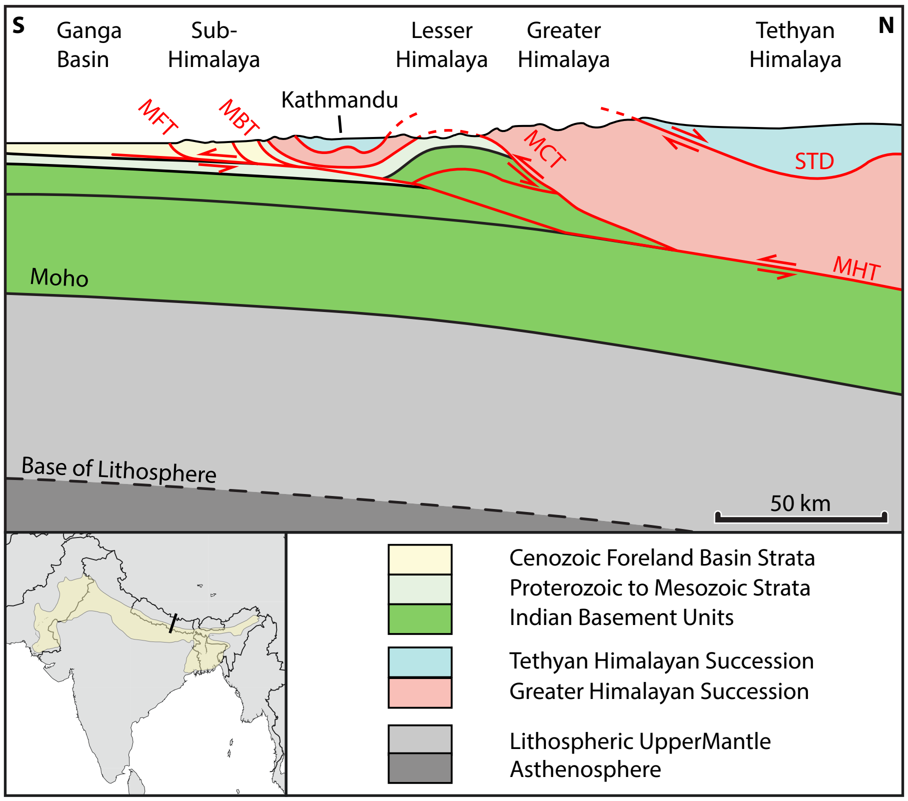

Fig. 1-2. Schematic cross-section through the Himalaya and the Himalayan foreland basin showing major structural units and boundaries.

MBT: Main Boundary Thrust. MCT: Main Central Thrust. MFT: Main Frontal Thrust. MHT: Main Himalayan Thrust. STD: South Tibet Detachment. Modified from Avouac (2003). Inset shows location.

the Ganga Basin's southern perimeter (Fig. 1-1). The foreland basin fill oversteps Precambrian metamorphic/igneous basement rocks, Proterozoic sedimentary strata, and Cretaceous sedimentary strata along its strike (Srinivasan and Khar, 1996; McQuarrie et al., 2014), depending on whether the basin is above a ridge or a depression (Rao, 1973; Karunakaran and Rao, 1979).

Heterogeneities in the Indian plate have been remotely sensed beneath the Ganga Basin using Bouguer gravity and aeromagnetic anomalies (Sengupta, 1962; Sastri et al., 1971; Rao, 1973; Valdiya, 1976; Karunakaran and Rao, 1979; Godin and Harris, 2014). A system of crustal-scale faults at oblique angles to the Himalaya has been mapped beneath the Ganga Basin (Sastri et al., 1971; Rao, 1973; Aditya et al., 1979; Karunakaran and Rao, 1979; Dasgupta, 1993; Raiverman et al., 1994; Dasgupta et al., 2013; Godin and Harris, 2014)(Fig. 1-1b). These deep-seated faults predominantly strike NE-SW, and seismic reflection data indicate that they show normal offsets in pre-foreland basin strata (Raiverman et al., 1994). A number of these crustal-scale faults spatially align with the edges of basement ridges, and are interpreted as the bounding surfaces of basement horsts and graben (Godin and Harris, 2014; Godin et al., 2019). In our study, we seek to address whether reactivation of these basement features influenced the sedimentary fill and geometry of the Ganga Basin along-strike.

1.4.1 Ganga Basin tectonostratigraphic framework

Five megasequences (or first-order sequences) can be found within the Ganga Basin, spanning a depositional history of over 1.6 Ga (Srinivasan and Khar, 1996). These sequences indicate a long and varied tectonic history, preserving strata of continental India well before it began its journey towards Eurasia. This section gives a brief summary of the main stratigraphic units found within the Ganga Basin (Figs. 1-4, 1-5), and the tectonic setting in which they were deposited. A more detailed summary of each stratigraphic interval is presented in Chapter 2.

The basement rock underlying the Ganga Basin is poorly characterized. It has been intersected by the wells Madhubani-1 and possibly Ujhani-1 (Rao, 1973; Fuloria, 1996)(Fig. 1-1c). Bouguer gravity anomalies (Sastri et al., 1971; Godin and Harris, 2014), aeromagnetic surveys (Sengupta, 1962), and seismic reflection data (Rao, 1973)(Fig. 1-1b) suggest the igneous and metamorphic rock domains of the Indian shield to the south of the Ganga Basin extend below the foreland basin fill. Thus the Ganga Basin likely oversteps the Proterozoic Satpura mobile belt, the Archean Bundelkhand Craton, and the Proterozoic Aravalli-Delhi fold belt from east to west (Rao, 1973). These same rock domains are thought to form the subsurface basement ridges (Rao, 1973; Karunakaran and Rao, 1979). The basement rock units underneath the intervening depressions are not characterized.

Above the igneous/metamorphic basement rock, appreciable thicknesses of Proterozoic strata accumulated between basement ridges (Rao, 1973). Figure 1-4 shows a regional correlation between Proterozoic strata deposited in the Vindhyan Basin, the Ganga Basin, and the Lesser Himalaya of Nepal. Two unconformity-bounded sequences of strata were deposited: the Paleoproterozoic to Mesoproterozoic Bahraich Group, and the Mesoproterozoic to Neoproterozoic Madhubani Group (McQuarrie et al., 2014; Xiao et al., 2016) (Fig. 1-4). Acritarch biostratigraphy has placed the Madhubani Group as young as Silurian (Prasad and Asher, 2001). However, according to Xiao *et al.,* (2016) detrital zircon maximum depositional ages and modern acritarch studies place the same units as Meso-Neoproterozoic. Seismic data, well data, and chronological data all suggest the Bahraich and Madhubani Groups correlate to strata deposited in the Vindhyan Basin to the south of the Ganga Basin (Fig. 1-1)(Xiao et al., 2016). They were likely deposited in a similar tectonic setting to the Vindhyan basin – an intracratonic basin – and possibly represent a northward extension of the Vindhyan Basin (Ojha, 2012; Bose et al., 2015).

Sedimentary strata that formed during the Early Carboniferous to Cretaceous on continental India are collectively known as the Gondwanan Succession (Wadia, 1919; Sitaula, 2009). Gondwanan deposits of continental India are found in long, thin basins (~300 km x ~75 km), that formed due to extension and rifting during the breakup of Gondwana (Veevers and Tewari, 1995). Gondwanan rift basins have been interpreted under the Himalayan foreland basin east of the Munger-Saharsa Ridge (Fig. 1-1b) based on palynofossils and stratigraphic correlation of contacts in wells (Prasad and Pundir, 2017). The Gondwanan succession in the Lesser Himalaya of Central Nepal comprises the Sisne Formation, the Taltung Formation, and the Amile Formation (Sakai, 1991). The Lesser Himalayan Gondwanan succession has been interpreted as rift basin deposits (Sakai, 1989). However their extreme lateral extent and sedimentology are also interpreted to record deposition on the northern continental margin of India (Valdiya, 1997; Sitaula, 2009). A sequence of Gondwanan strata has been interpreted within Ganga Basin (Bashyal, 1998), and could be either rift basin or passive continental margin deposits (Fig. 1-5).

Gondwanan strata in the Lesser Himalaya of Nepal are overlain by the Paleogene Bhainskati Formation, a fossiliferous marine mudstone interval (Sakai, 1983). The basal

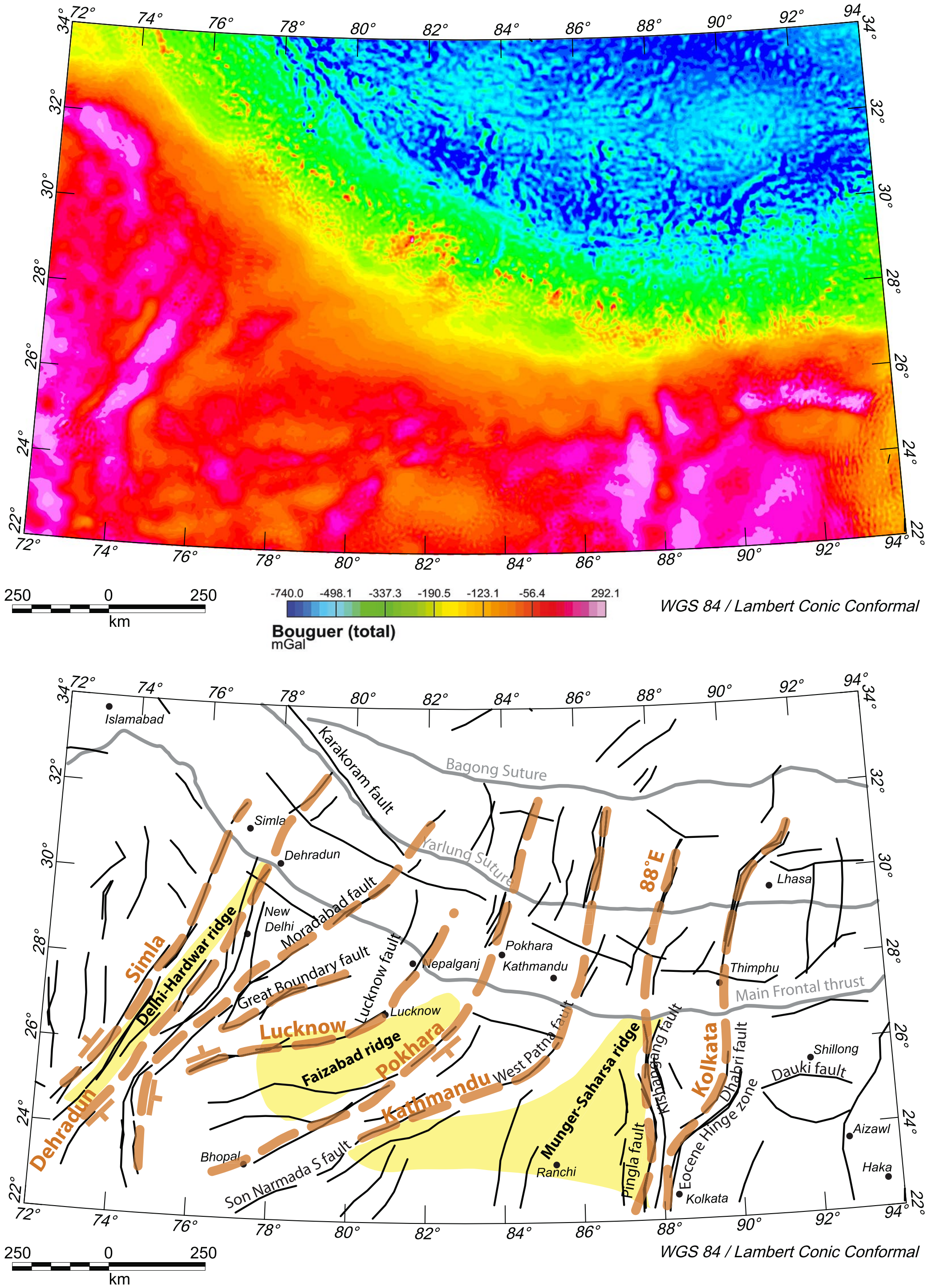

Fig. 1-3. Maps showing major subsurface features of the Ganga Basin, and the Himalaya Bouguer anomaly map (top) and major tectonic features of the Himalaya and Ganga Basin (bottom). Approximate trace of Indian plate basement ridges shown in yellow. Crustal-scale basement lineaments (brown dashed lines) and major faults (black lines) mapped using different wavelength components of Bouguer gravity data. Dip direction of basement lineaments is indicated for non-vertical lineaments (from Godin & Harris, 2014).

Fig. 1-4. Correlation of Paleozoic strata in the Vindhyan Basin, Ganga Basin, and Lesser Himalaya of Nepal

Chronostratigraphic correlation of Proterozoic strata, from the Indian shield to the Lesser Himalaya of Nepal. Possible age ranges are indicated by black bars. Vindhyan Basin stratigraphy after Rasmussen *et al.,* (2002)*,* McKenzie *et al.* (2011)*,* Gopalan *et al.,* (2013), and Tripathy & Singh (2015). Ganga basin stratigraphy based on McKenzie *et al.* (2011)*,* and Xiao *et al.,* (2016). Western Nepal stratigraphy after DeCelles *et al.,* (2000, 2001), and Martin *et al.,* (2011).

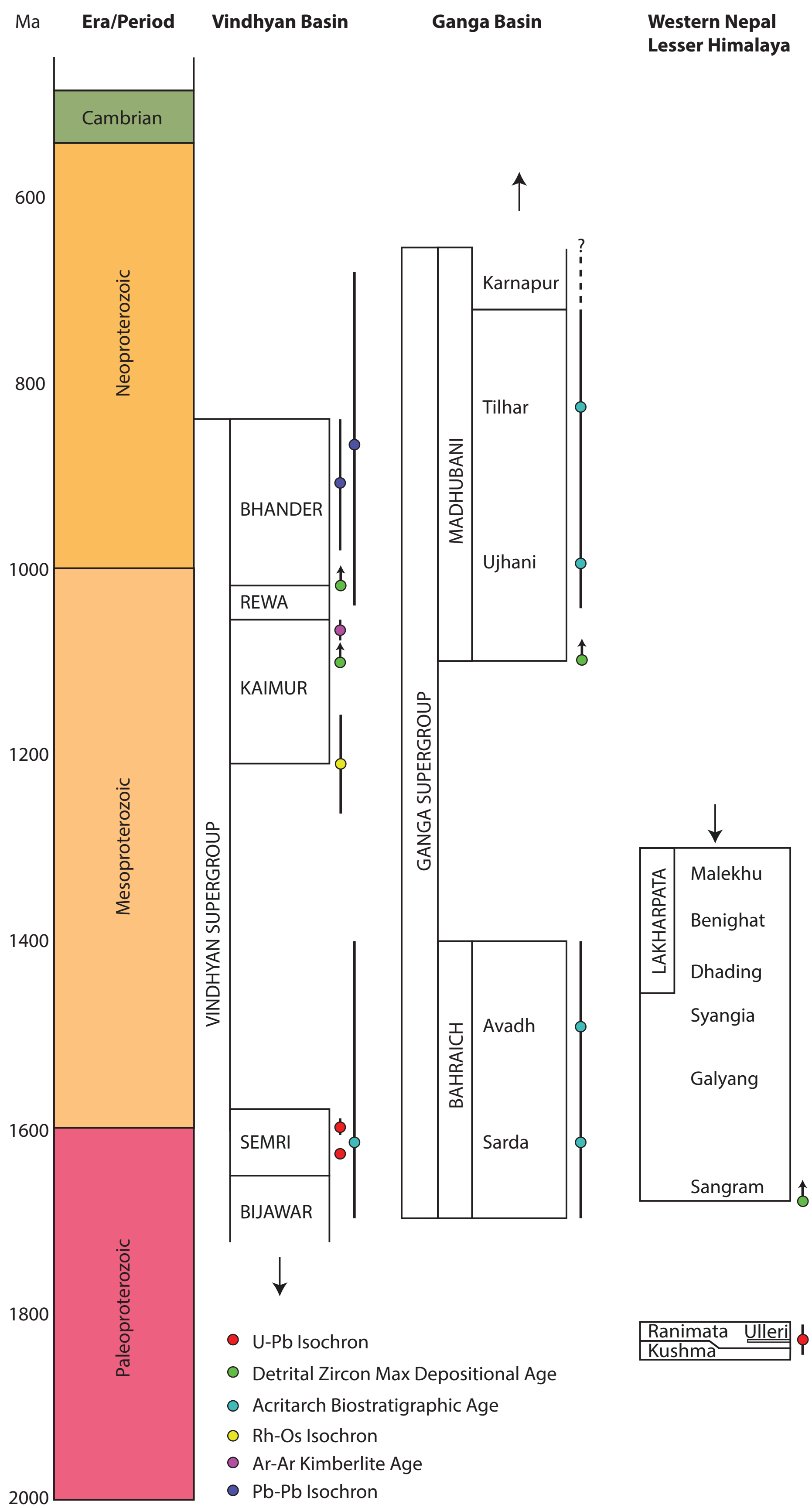
Ma
Era/Period
Vindhyan Basin
Ganga Basin
Western Nepal Lesser Himalaya
600
800
1000
1200
1400
1600
1800
2000
Cambrian
Neoproterozoic
Mesoproterozoic
Paleoproterozoic
VINDHYAN SUPERGROUP
BHANDER
REWA
KAIMUR
SEMRI
BIJAWAR
GANGA SUPERGROUP
MADHUBANI
Karnapur
Tilhar
Ujhani
BAHRAICH
Avadh
Sarda
?
LAKHARPATA
Malekhu
Benighat
Dhading
Syangia
Galyang
Sangram
Ranimata
Ulleri
Kushma
U-Pb Isochron
Detrital Zircon Max Depositional Age
Acritarch Biostratigraphic Age
Rh-Os Isochron
Ar-Ar Kimberlite Age
Pb-Pb Isochron

Fig. 1-5. Generalized lithostratigraphic chart of the Ganga Basin and Sub-Himalaya Tectonic framework column (a) after Sakai (1983), Bose *et al.,* (2015), and Burbank *et al.,* (1996). Ages of major stratigraphic surfaces and tectonic phases (b) after Sakai (1983), Upreti (1999), Najman *et al.,* (2005), and Ojha *et al.,* (2009). Idealized stratigraphic column (c) representing units potentially present in the Ganga basin. Alluvium & Siwalik Group thicknesses represent those in the Biratnagar-1 well; outcrop thicknesses from Sakai (1983) were used for older strata.

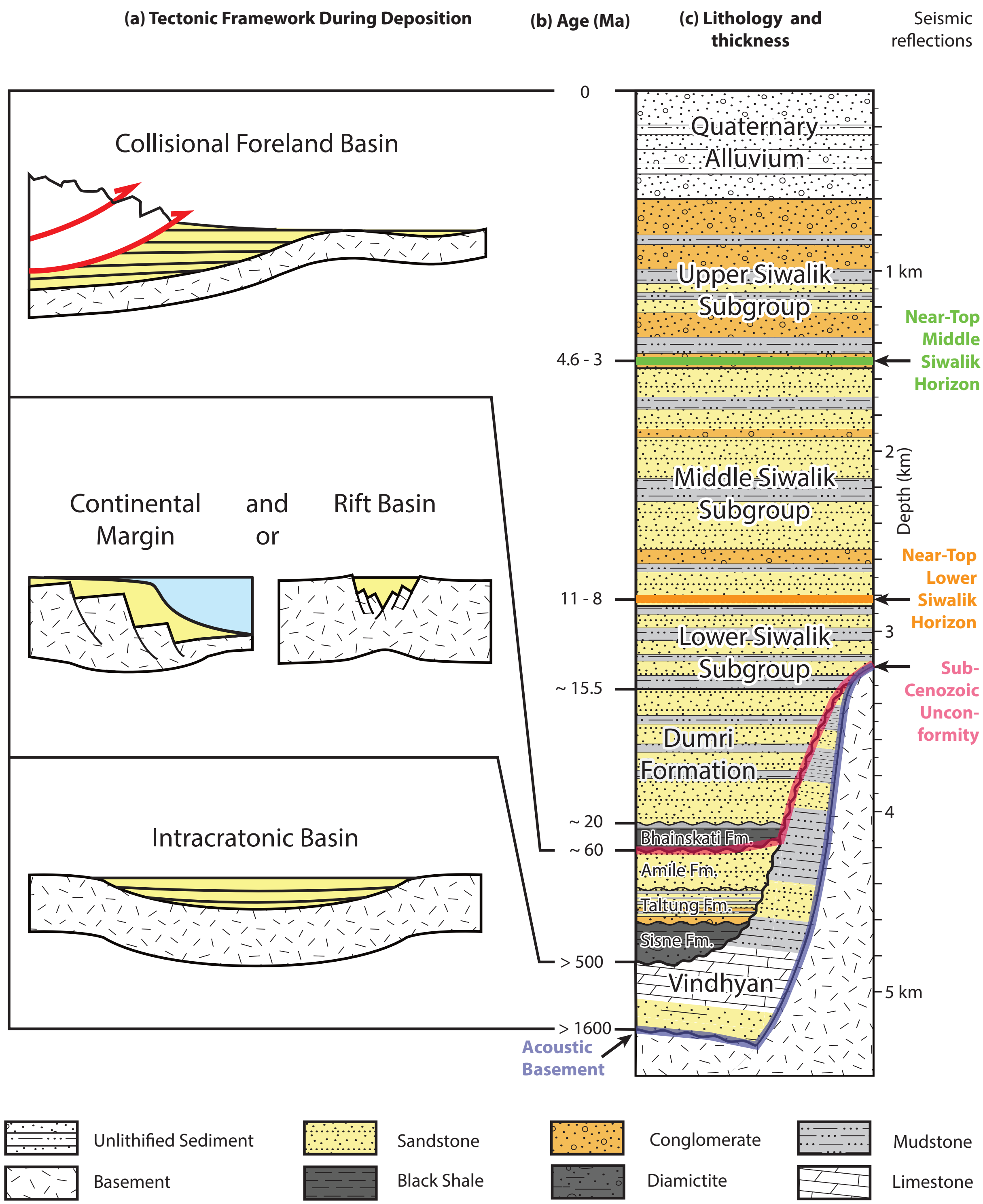

(a) Tectonic Framework During Deposition
(b) Age (Ma)
(c) Lithology and thickness
Seismic reflections
Collisional Foreland Basin
Continental Margin
and or
Rift Basin
Intracratonic Basin
0
4.6 - 3
11 - 8
~ 15.5
~ 20
~ 60
> 500
> 1600
Quaternary Alluvium
Upper Siwalik Subgroup
Middle Siwalik Subgroup
Lower Siwalik Subgroup
Dumri Formation
Bhainskati Fm.
Amile Fm.
Taltung Fm.
Sisne Fm.
Vindhyan
1 km
2
3
4
5 km
Depth (km)
Near-Top Middle Siwalik Horizon
Near-Top Lower Siwalik Horizon
Sub-Cenozoic Uncon-formity
Acoustic Basement
Unlithified Sediment
Sandstone
Conglomerate
Mudstone
Basement
Black Shale
Diamictite
Limestone

contact of the Bhainskati Formation has been described as both conformable (Sakai, 1983) and disconformable (Sitaula, 2009). The Bhainskati Formation correlates with the Subathu Formation and represents the earliest foreland basin deposits (DeCelles et al., 2004)(Fig. 1-5). The Bhainskati/Subathu Formations have not been intersected by a well within the Ganga Basin. However, they are present in appreciable thicknesses within the Himalaya, and have been hypothesized to extend into the northern fringes of the modern Ganga Basin (Raiverman et al., 1994; Srinivasan and Khar, 1996; Raiverman, 2002). The top surface of the Bhainskati Formation is an unconformity (DeCelles et al., 2004). The unconformity spans part of the Eocene and most of the Oligocene (Najman et al., 2018); it is attributed to migration of a peripheral bulge (DeCelles et al., 1998a), a redistribution of the load of the Himalaya (Najman et al., 2004), or mantle processes like slab break-off (Najman et al., 2018; Garzanti, 2019).

Above the Bhainskati/Subathu Formations is the thickest foreland basin sequence, comprising the continental Dumri Formation and Siwalik Group in Nepal (DeCelles et al., 1998b)(Fig. 1-5). This sequence is bounded by the Eocene-Oligocene unconformity at its base, and Quaternary alluvial deposits near the surface (Srinivasan and Khar, 1996); however, the nature of the contact between the Dumri Formation and the Siwalik Group is unknown. These rock units have been dated as Neogene and younger, via magnetostratigraphy (Ojha et al., 2009), and are the main rock units exposed in the Sub-Himalaya. This sedimentary sequence coarsens upwards, becoming dominated by fluvial deposits of increasing energy levels, reflecting the southward migration of the MFT (Burbank et al., 1996; DeCelles et al., 1998a).

In summary, a well drilled through the Ganga Basin would likely intersect some combination of the following rock units from bottom to top (Fig. 1-5): igneous/metamorphic basement rock, either from Archean craton or Precambrian mobile belts; Vindhyan strata, in the form of the Proterozoic (to possibly Paleozoic) Bahraich and Madhubani Groups, comprising sedimentary strata likely deposited in a intracratonic rift basin; Carboniferous to Jurassic Gondwanan strata, deposited in a rift basin or on a passive continental margin; Paleogene Subathu/Bhainskati Formations, marine mudstone beds deposited in the juvenile Himalayan foreland basin; and Neogene Siwalik Group (and underlying Dumri Formation and equivalents), representing continental deposition within the southward migrating Himalayan Foreland Basin.

1.5 Data used

1.5.1 Study area

This thesis focuses on the Ganga Basin of Nepal at a regional scale. The study area is a thin strip of land that runs from the political border of Eastern Nepal to the political border of Western Nepal. All the seismic data are north of the political boundary between Nepal and India. The northern boundary of the dataset straddles the Ganga Basin and the Sub-Himalaya (Fig. 1-6). The study area has a length of 840 km running parallel to the strike of the Himalaya, and a width ranging from 30 to 40 km.

1.5.2 Seismic data

The main dataset of this thesis is a pre-processed 2D seismic reflection dataset (Appendix 1) spanning the Ganga Basin and Sub-Himalaya of Nepal. The dataset consists of 181 seismic reflection profiles (Fig. 1-6) that were acquired in four surveys, between 1982 and 1984. The 2D lines cover a combined total of 5134 km. These surveys are known as 'blocks:' the Western Block, Central Block, Eastern Block, and Block 10 (Fig. 1-1c). These blocks are separated by data gaps. The vast majority of the lines are within the Ganga Basin, but there are ~10 lines that cross into the Sub-Himalaya, in the area of the Dang, Deukhuri, and Chitwan intermontane basins (Fig. 1-1c). Beyond the 2D seismic profiles, a set of regional interpretations were also provided by the original industry interpreters of the data. Six regional marker horizons were given, as well as fifteen local scale horizons. Because of inconsistencies, these horizons were not used in our interpretation; all regional horizons were re-picked.

The seismic data are Society of Exploration Geophysicists positive polarity: an increase in acoustic impedance produces a peak. The regional datum for the seismic dataset is 50 m above sea level. The vast majority of lines image to depths of 6 seconds two-way travel time (TWT), with some lines imaging up to 8 seconds of TWT. The vertical resolution of the data is relatively low, resolving ~20 m units at shallower depths, and ~50 m units in the deepest parts of the survey. Each trace is spaced at a 25 m interval. The spacing between the 2D seismic profiles varies in the study area, dependent on the survey. The Western, Central and Eastern blocks all had a coarse line spacing about 15 km between N-S lines, and 20 km between E-W lines. Block 10 had a much closer profile spacing of ~8 km between N-S lines, and 5 km between E-W lines.

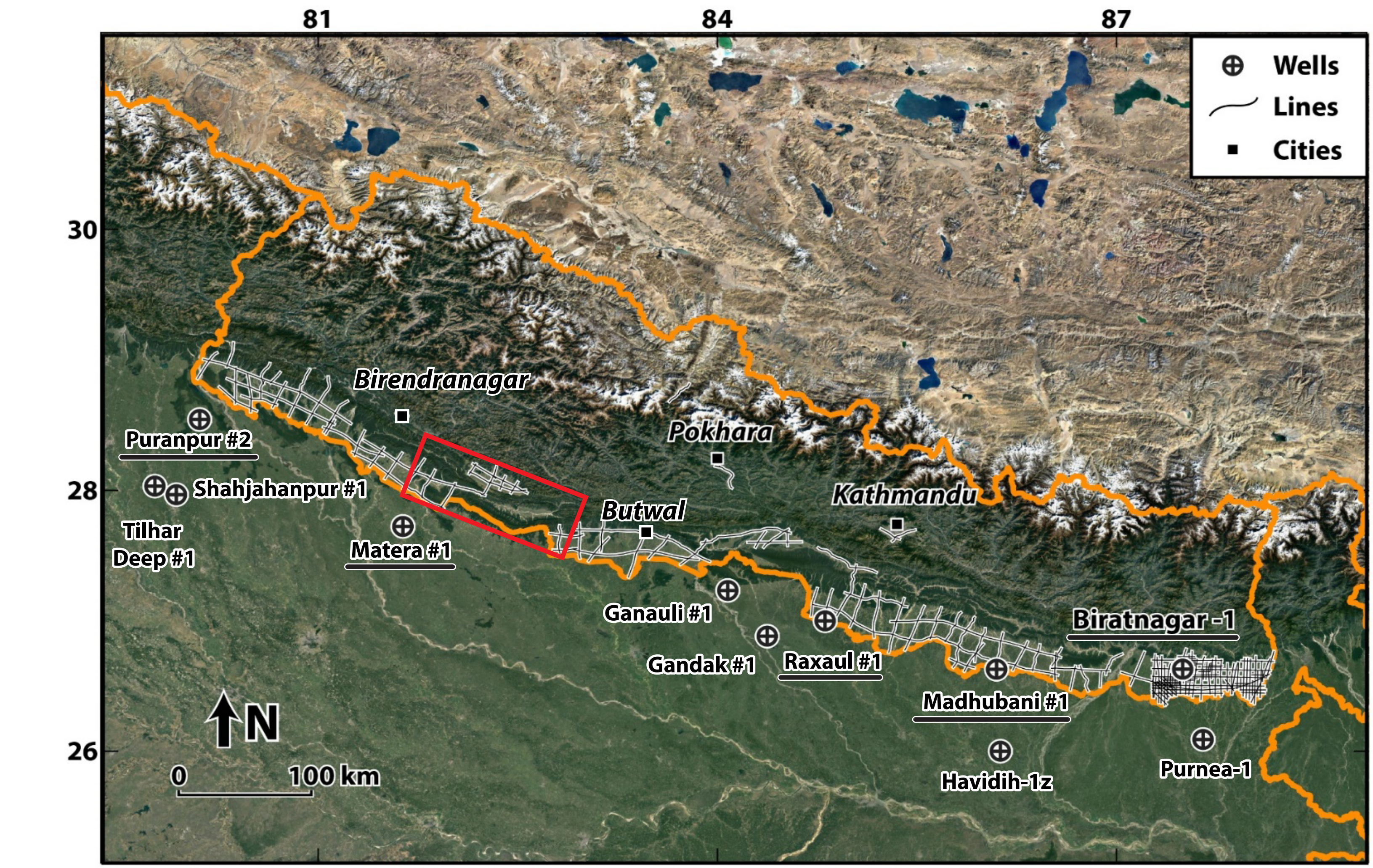

Fig. 1-6. Map of data used

Satellite map of Nepal and surrounding areas, with surficial trace of 2D seismic profiles superimposed. Field study area is highlighted in red. Wells shown in Fig. 1-7 are underlined.

The seismic data were originally sourced from sepia films, but were scanned, vectorized and migrated by Fugro-Robertson for workstation interpretation (Cairn Energy, 2006).

This seismic dataset is accompanied by well reports for 9 wells (Appendix 2) drilled in the Ganga Basin that summarize well tops for stratigraphic boundaries, well head locations, total depths, drilling procedures, sampling procedures, palynology where studied, geophysical well logs in raster format, and mud logs. Selected wells are shown in Fig. 1-7. Regional gravity anomaly and magnetic surveys were also used in interpretation. Checkshot data were given for three wells (Shahjahanpur-1, Havidih-1z, and Biratnagar-1; Fig. 1-1c). Of these three wells, only Biratnagar-1 fell within the seismic grid. Biratnagar-1 was used to create a seismic well tie for the Cenozoic succession intersected by the well. The well reached total depth of 3530 m before penetrating the basement and pre-Cenozoic succession. Three other wells fell within 30 km of the seismic grid (Raxaul-1, Majhubani-1, and Matera-1; Fig. 1-6, 1-7). These were used as quality controls to ensure consistency in our horizon picking, and accuracy of our depth conversion.

1.5.3 Outcrop data

The subsurface dataset is accompanied by surficial data in the Sub-Himalaya, mostly restricted to the area between Birendranagar and Butwal (shown in Fig. 1-6). We acquired the surficial dataset in April and May 2018, through field mapping of lithological units. The Siwalik Group was described and mapped in detail, by taking structural measurements on seven traverses. In addition, structural orientations were interpreted from a digital elevation model (DEM) provided as part of the Cairn data package. A complete listing of field sites and structural measurements is provided in Appendix 3. We used the field dataset to ensure that the boundaries we have interpreted in the subsurface are laterally extensive and consistent with field observations.

1.6 Methods

1.6.1 Data preparation

Before seismic interpretation, quality control steps were taken to ensure the seismic profiles were correctly levelled and tied to each other. Petrel's mis-tie manager was used to identify 2D lines that had a statistically poor correlation with intersecting lines. Lines that had

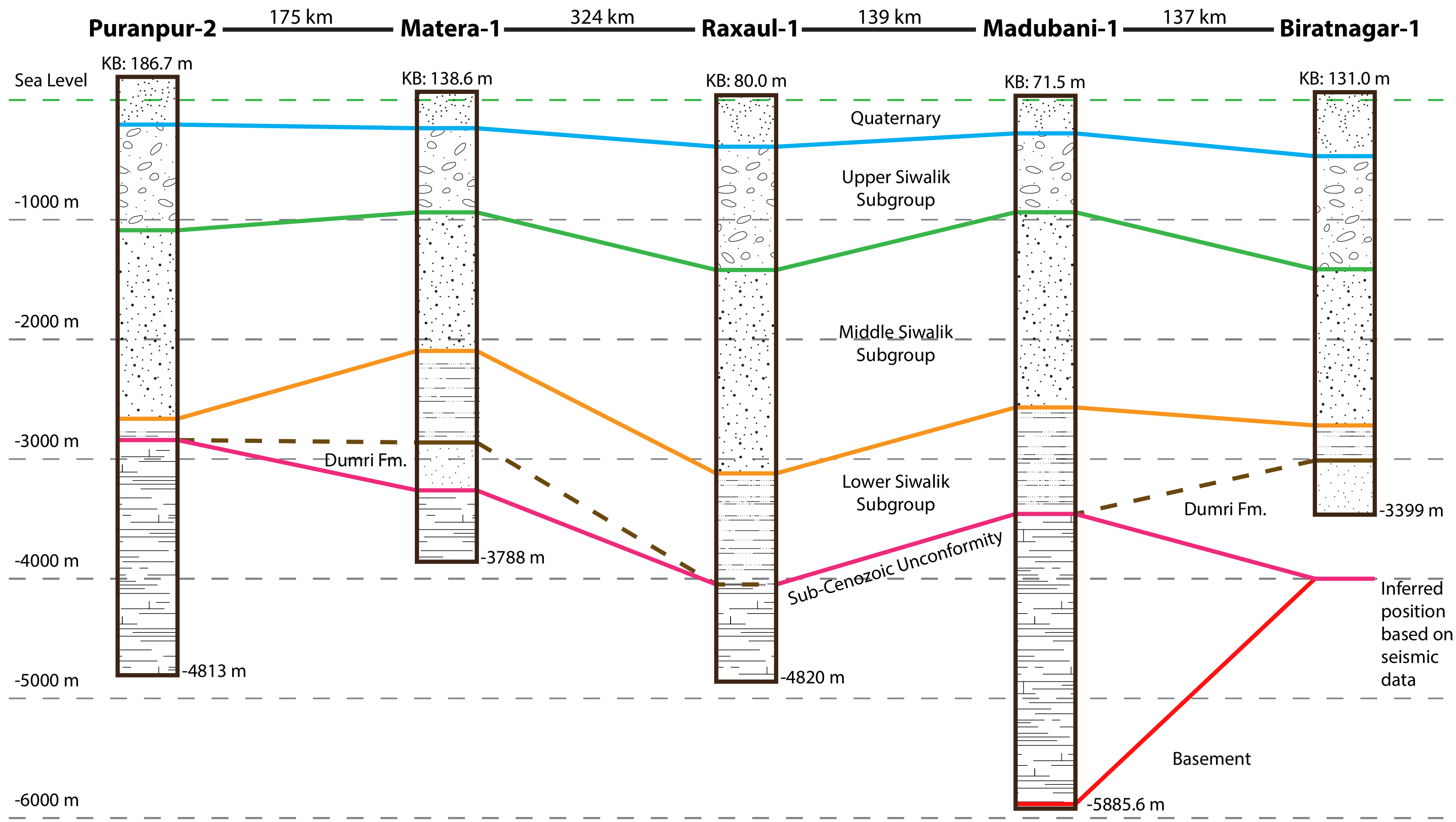

Fig. 1-7. Regional structural correlation of selected wells in the Ganga Basin

Depths based on Hartsink and Pradhan (1989), Fuloria (1996), and Srinivasan and Khar (1996). Locations shown in Fig. 1-6. KB: Elevation of kelly bushing. Datum used is sea level.

poor vertical or phase correlations were bulk-shifted up or down. This process ensured that each block of data was correctly levelled to the seismic datum, and that the same reflection on one line was always the same reflection on the intersecting lines. The bulk shifting done in this process was relatively small (~50 ms TWT maximum).

Well data also had to be prepared before significant interpretations were made. Checkshot data were analyzed to ensure that interval velocities were plausible for the lithologies observed in the wells. No issues were identified in the checkshot data. Well tops were cross-referenced with driller's logs to ensure that a consistent lithological boundary was picked as a given well top.

1.6.2 Seismic interpretation

Four regional horizons (Figs. 1-5, 1-8) were picked after the above quality control measures were taken: the top of the acoustic basement (also referred to as the 'blue horizon'), the Sub-Cenozoic angular unconformity (or 'pink horizon'), a horizon near the top of the Lower Siwalik Subgroup (the 'orange' horizon), and a horizon near the top Middle Siwalik Subgroup (the 'green' horizon). These horizons were picked due to their prominence in the seismic data, their lateral continuity, and their usefulness in determining the geometry of the foreland basin through time (Fig. 1-8).

The well Biratnagar-1 was used to tie lithostratigraphic boundaries to the seismic data. No sonic log was available; therefore a synthetic seismic profile could not be constructed. Two well tops were tied using the checkshot data. The Near-top Lower Siwalik Subgroup reflection is picked as a prominent trough at the top of a thinly banded interval in the seismic data. This corresponds to the transition from predominantly sandstone facies (higher acoustic impedance) of the Middle Siwalik Subgroup, to the predominantly mudstone facies (lower acoustic impedance) of the Lower Siwalik Subgroup in Biratnagar-1 at 2850 m measured depth (MD). The Near-top Middle Siwalik Subgroup was picked as a prominent peak in the seismic data, representing a change in lithology in the well from lower-density conglomeratic facies to higher density sandstone facies at 1545 m MD. Both horizons are 'near-top' horizons, because the most prominent seismic reflection did not tie perfectly with the lithostratigraphic contact that was picked in the well. The two remaining horizons were picked based on their seismic character (see Chapter 2). The top of the acoustic basement horizon was picked at the deepest laterally extensive peak in the seismic data, representing the transition from sedimentary strata to igneous/metamorphic basement. Below this horizon, no coherent reflections were visible. The Sub-

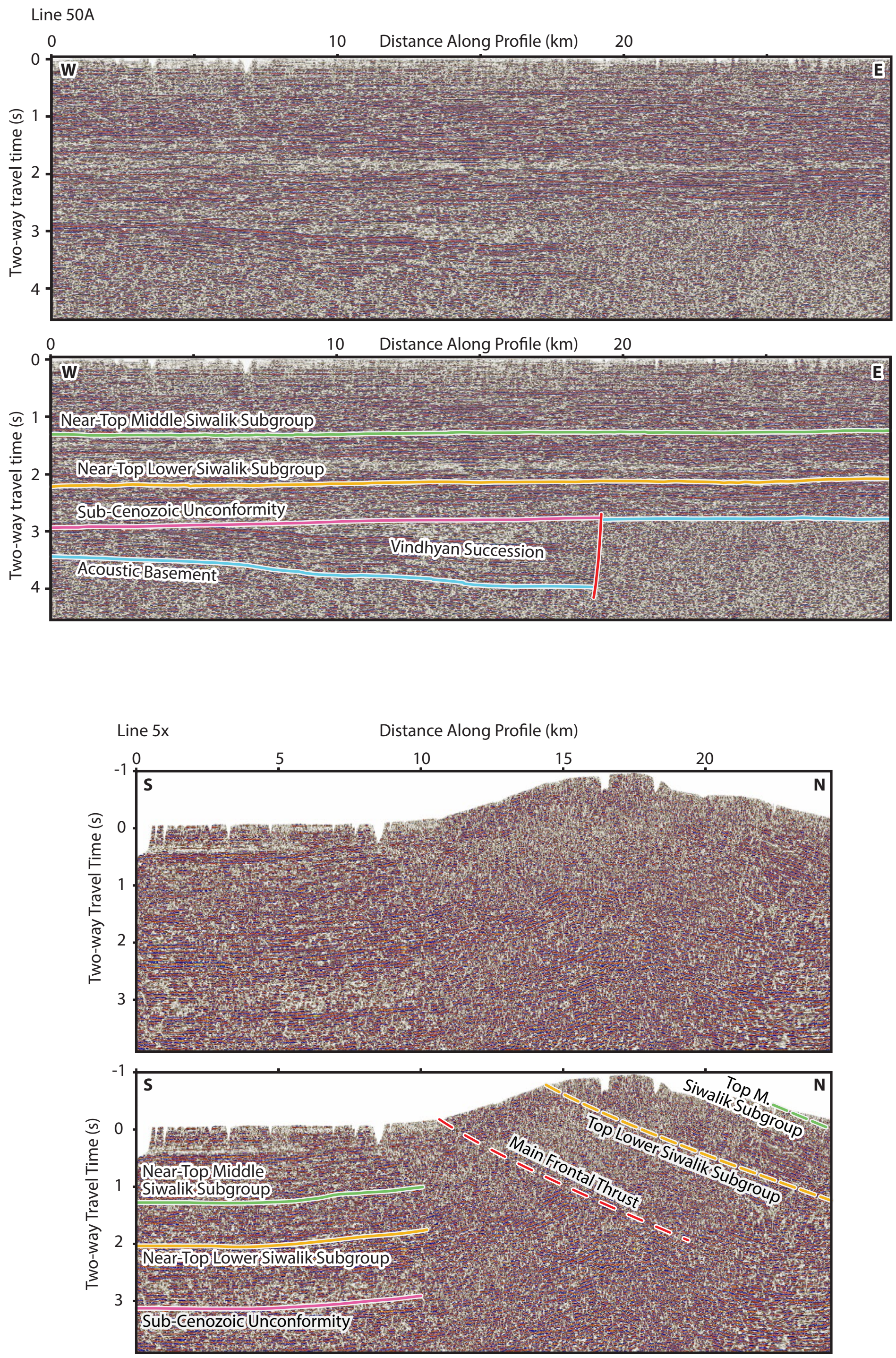

Fig. 1-8. Examples of seismic profiles interpreted in the Ganga Basin

Typical east-west and north-south seismic profiles. Line 50A (top) crosses a fault showing ~2600 m dip separation in pre-foreland basin strata (vertical exaggeration is ~2.5). Line 5x (bottom) shows a subtle upwarp of foreland basin strata south of the interpreted Main Frontal Thrust (natural scale). Line locations shown in Fig. 1-1c.

Cenozoic angular unconformity was recognized due to the change in dip in reflections above and below. A more detailed summary of each seismic horizon is given in Chapter 2.

The marker horizons were picked starting from Biratnagar-1 in Block 10, working west. Gaps between seismic surveys were crossed by creating a seismic ghost of the data on the interpreted side of the gap, and then comparing the ghost to the uninterpreted side. This allowed us to pick the same reflectors across data gaps.

1.6.3 Depth conversion

Seismic data were converted from the time domain to the depth domain using a time-depth relationship derived from the checkshots of three wells: Shahjahanpur-1, Havidih-1z, and Biratnagar-1. To model the foreland basin fill, we derived an empirical linear velocity function from the checkshot data. A detailed summary of the depth conversion used is given in Chapter 2.

1.7 Organization

This thesis is presented in paper format. Chapter 2 will lead to a paper under the authorship Duvall, M.D., Waldron, J.W.F., Godin, L., and Najman, Y. It has a regional focus, discussing the geometry of the Ganga Basin of Nepal. Four regional seismic horizons are used to determine sedimentation patterns in the basin fill and pre-foreland-basin strata. Along-strike changes within the foreland basin are compared with basement structures, and inheritance of basement structure is interpreted to be the driving force of along-strike accommodation.

Chapter 3 has been prepared for publication in a tectonics journal under the authorship Duvall, M.D., Waldron, J.W.F., Godin, L., and Najman, Y. Chapter 3 has a focus restricted to Eastern Nepal, and explores how faults and folds are forming within the foreland basin as the Main Himalayan thrust propagates southward. The structures observed in the basin indicate that there is active slip, interpreted as movement along a series of tear and thrust faults. The amount of slip accumulated on these faults is quantified, and their role in the context of modern Himalayan seismicity is discussed.

Chapter 4 summarizes the main findings of the thesis, and the main questions that have surfaced because of this work.

1.8 References

Aditya, S., Raju, A.T.R., and Shukla, S.N., 1979, Assessment of hydrocarbon prospects of the sub-Himalayan, Punjab and Ganga basins-India, *in* Himalayan Geology Seminar New Delhi 1976: Section 3 - Oil and Natural Gas Resources, Geological Survey of India Miscellaneous Publications, v. 41, p. 127–140.

Anders, A.M., Roe, G.H., Hallet, B., Montgomery, D.R., Finnegan, N.J., and Putkonen, J., 2006, Spatial patterns of precipitation and topography in the Himalaya, *in* Willett, S.D., Hovius, N., Brandon, M.T., and Fisher, D.M. eds., Tectonics, Climate, and Landscape Evolution, Geological Society of America Special Paper, v. 398, p. 39–53, doi:10.1130/2006.2398(03).

Avouac, J.-P., 2003, Mountain Building, Erosion, and the Seismic Cycle in the Nepal Himalaya: Amster, Elsevier, Advances in Geophysics, v. 46, 80 p., doi:10.1016/S0065-2687(03)46001-9.

Bashyal, R.P., 1998, Petroleum exploration in Nepal: Journal of Nepal Geological Society, v. 18, p. 19–24.

Basuyau, C., Diament, M., Tiberi, C., Hetényi, G., Vergne, J., and Peyrefitte, A., 2013, Joint inversion of teleseismic and GOCE gravity data: application to the Himalayas: Geophysical Journal International, v. 193, p. 149–160, doi:10.1093/gji/ggs110.

van der Beek, P., Litty, C., Baudin, M., Mercier, J., Robert, X., and Hardwick, E., 2016, Contrasting tectonically driven exhumation and incision patterns, western versus central Nepal Himalaya: Geology, v. 44, p. 327–330, doi:10.1130/G37579.1.

Bose, P.K., Sarkar, S., Das, N.G., Banerjee, S., Mandal, A., and Chakraborty, N., 2015, Proterozoic Vindhyan Basin: configuration and evolution, *in* Mazumder, R. and Eriksson, P.G. eds., Precambrian Basins of India: Stratigraphic and Tectonic Context, Geological Society of London Memoir, v. 43, p. 85–102, http://mem.lyellcollection.org/lookup/doi/10.1144/M43.6 (accessed February 2018).

Bouilhol, P., Jagoutz, O., Hanchar, J.M., and Dudas, F.O., 2013, Dating the India–Eurasia collision through arc magmatic records: Earth and Planetary Science Letters, v. 366, p. 163–175, doi:10.1016/j.epsl.2013.01.023.

Brown, L.D., Zhao, W., Nelson, K.D., Hauck, M., Alsdorf, D., Ross, A., Cogan, M., Clark, M., Liu, X., and Che, J., 1996, Bright Spots, Structure, and Magmatism in Southern Tibet from INDEPTH Seismic Reflection Profiling: Science, v. 274, p. 1688–1690, doi:10.1126/science.274.5293.1688.

Burbank, D.W., Beck, R.A., and Mulder, T., 1996, The Himalayan foreland basin, *in* Yin, A. and

Harrison, T.M. eds., The Tectonic Evolution of Asia, Cambridge, Cambridge University Press, p. 149–188.

Burchfiel, B.C., Zhiliang, C., Hodges, K.V., Yuping, L., Royden, L.H., and Changrong, D., 1992, *in* The South Tibetan detachment system, Himalayan orogen: Extension contemporaneous with and parallel to shortening in a collisional mountain belt, Geological Society of America - Special Paper, v. 269.

Burgess, W., Yin, A., Dubey, C.S., Shen, Z.-K., and Kelty, T.K., 2012, Holocene shortening across the Main Frontal Thrust zone in the eastern Himalaya: Earth and Planetary Science Letters, v. 357–358, p. 152–167, doi:10.1016/j.epsl.2012.09.040.

Cairn Energy, 2006, Seismic Interpretation - Nepal: Cairn UK Internal Report.

Casshyap, S.M., and Khan, A., 2000, Basin of central India: evidence of pre-Trap doming, rifting and palaeoslope reversal: Journal of African Earth Sciences, v. 31, p. 65–76.

Dasgupta, S., 1993, Tectono-geologic framework of the eastern Gangetic foredeep, *in* Bihar Nepal Earthquake (August 20, 1988), Geological Survey of India Special Publication, v. 31, p. 61–69.

Dasgupta, S., Mukhopadhyay, B., Mukhopadhyay, M., and Nandy, D.R., 2013, Role of transverse tectonics in the Himalayan collision: Further evidences from two contemporary earthquakes: Journal of the Geological Society of India, v. 81, p. 241–247, doi:10.1007/s12594-013-0027-5.

DeCelles, P.G., Gehrels, G.E., Najman, Y., Martin, A.J., Carter, A., and Garzanti, E., 2004, Detrital geochronology and geochemistry of Cretaceous–Early Miocene strata of Nepal: implications for timing and diachroneity of initial Himalayan orogenesis: Earth and Planetary Science Letters, v. 227, p. 313–330, doi:10.1016/j.epsl.2004.08.019.

DeCelles, P.G., Gehrels, G.E., Quade, J., LaReau, B., and Spurlin, M., 2000, Tectonic implications of U-Pb zircon ages of the Himalayan orogenic belt in Nepal: Science, v. 288, p. 497–499.

DeCelles, P.G., Gehrels, G.E., Quade, J., and Ojha, T.P., 1998a, Eocene-early Miocene foreland basin development and the history of Himalayan thrusting, western and central Nepal: Tectonics, v. 17, p. 741–765.

DeCelles, P.G., Gehrels, G.E., Quade, J., Ojha, T.P., Kapp, P.A., and Upreti, B.N., 1998b, Neogene foreland basin deposits, erosional unroofing, and the kinematic history of the Himalayan fold-thrust belt, western Nepal: Geological Society of America Bulletin, v. 110, p. 2–21, doi:10.1130/0016-7606(1998)110<0002:NFBDEU>2.3.CO;2.

DeCelles, P.G., Robinson, D.M., Quade, J., Ojha, T.P., Garzione, C.N., Copeland, P., and Upreti, B.N., 2001, Stratigraphy, structure, and tectonic evolution of the Himalayan fold-thrust belt in western Nepal: Tectonics, v. 20, p. 487–509.

Duncan, C., Masek, J., and Fielding, E., 2003, How steep are the Himalaya? Characteristics and implications of along-strike topographic variations: Geology, v. 31, p. 75–78.

Fuloria, R.C., 1996, Geology and hydrocarbon prospects of the Vindhyan sediments in Ganga valley (A. Bhattacharyya, Ed.): Memoirs of the Geological Society of India, v. 36, p. 235–256.

Gahalaut, V.K., and Kundu, B., 2012, Possible influence of subducting ridges on the Himalayan arc and on the ruptures of great and major Himalayan earthquakes: Gondwana Research, v. 21, p. 1080–1088, doi:10.1016/j.gr.2011.07.021.

Gansser, A., 1964, Geology of the Himalayas: London, New York, Interscience Publishers, 289 p.

Garzanti, E., 2019, The Himalayan Foreland Basin from collision onset to the present: a sedimentary–petrology perspective, *in* Treloar, P.J. and Searle, M.P. eds., Himalayan Tectonics: A Modern Synthesis, Geological Society of London Special Publications, v. 483.

Godin, L., and Harris, L.B., 2014, Tracking basement cross-strike discontinuities in the Indian crust beneath the Himalayan orogen using gravity data – relationship to upper crustal faults: Geophysical Journal International, v. 198, p. 198–215, doi:10.1093/gji/ggu131.

Godin, L., Soucy La Roche, R., Waffle, L., and Harris, L.B., 2019, Influence of inherited Indian basement faults on the evolution of the Himalayan Orogen, *in* Sharma, R., Villa, I., and Kumar, S. eds., Crustal Architecture and Evolution of the Himalaya–Karakoram–Tibet Orogen, Geological Society of London Special Publication, v. 481.

Gopalan, K., Kumar, A., Kumar, S., and Vijayagopal, B., 2013, Depositional history of the Upper Vindhyan succession, central India: Time constraints from Pb–Pb isochron ages of its carbonate components: Precambrian Research, v. 233, p. 108–117, doi:10.1016/j.precamres.2013.04.014.

Goscombe, B., Gray, D., and Foster, D.A., 2018, Metamorphic response to collision in the Central Himalayan Orogen: Gondwana Research, v. 57, p. 191–265, doi:10.1016/j.gr.2018.02.002.

Hartsink, J., and Pradhan, U.M.S., 1989, Well Completion Report - Biratnagar 1: Kathmandu, Shell Nepal B.V.

Hauck, M.L., Nelson, K.D., Brown, L.D., Zhao, W., and Ross, A.R., 1998, Crustal structure of the Himalayan orogen at ~ 90 east longitude from Project INDEPTH deep reflection profiles: Tectonics, v. 17, p. 481–500.

Heim, A., and Gansser, A., 1939, Central Himalaya - Geological Observations of the Swiss Expedition 1936: Hindustan Publishing; Delhi, 246 p.

Hu, X., Wang, J., BouDagher-Fadel, M., Garzanti, E., and An, W., 2016, New insights into the timing of the India – Asia collision from the Paleogene Quxia and Jialazi formations of the Xigaze forearc basin, South Tibet: Gondwana Research, v. 32, p. 76–92, doi:10.1016/j.gr.2015.02.007.

Karunakaran, C., and Rao, A.R., 1979, Status of exploration for hydrocarbons in the Himalayan region-contributions to stratigraphy and structure, *in* Himalayan Geology Seminar New Delhi 1976: Section 3 - Oil and Natural Gas Resources, Geological Survey of India Miscellaneous Publications, v. 41 (5), p. 1–66.

Kellett, D.A., and Grujic, D., 2012, New insight into the South Tibetan detachment system: Not a single progressive deformation: South Tibetan Detachment System: Tectonics, v. 31, p. n/a-n/a, doi:10.1029/2011TC002957.

Lyon-Caen, H., and Molnar, P., 1985, Gravity anomalies, flexure of the Indian plate, and the structure, support and evolution of the Himalaya and Ganga Basin: Tectonics, v. 4, p. 513–538.

Martin, A.J., Burgy, K.D., Kaufman, A.J., and Gehrels, G.E., 2011, Stratigraphic and tectonic implications of field and isotopic constraints on depositional ages of Proterozoic Lesser Himalayan rocks in central Nepal: Precambrian Research, v. 185, p. 1–17, doi:10.1016/j.precamres.2010.11.003.

McKenzie, N.R., Hughes, N.C., Myrow, P.M., Xiao, S., and Sharma, M., 2011, Correlation of Precambrian–Cambrian sedimentary successions across northern India and the utility of isotopic signatures of Himalayan lithotectonic zones: Earth and Planetary Science Letters, v. 312, p. 471–483, doi:10.1016/j.epsl.2011.10.027.

McQuarrie, N., Tobgay, T., Long, S.P., Reiners, P.W., and Cosca, M.A., 2014, Variable exhumation rates and variable displacement rates: Documenting recent slowing of Himalayan shortening in western Bhutan: Earth and Planetary Science Letters, v. 386, p. 161–174, doi:10.1016/j.epsl.2013.10.045.

Mohanty, S., 2012, Spatio-temporal evolution of the Satpura Mountain Belt of India: A comparison with the Capricorn Orogen of Western Australia and implication for evolution of the supercontinent Columbia: Geoscience Frontiers, v. 3, p. 241–267, doi:10.1016/j.gsf.2011.10.005.

Monsalve, G., Sheehan, A., Schulte-Pelkum, V., Rajaure, S., Pandey, M.R., and Wu, F., 2006, Seismicity and one-dimensional velocity structure of the Himalayan collision zone: Earthquakes in the crust and upper mantle: Journal of Geophysical Research, v. 111, doi:10.1029/2005JB004062.

Najman, Y., Burley, S.D., Copley, A., Kelly, M.J., Pander, K., and Mishra, P., 2018, The Late Eocene-Early Miocene Unconformities of the NW Indian Intraplate Basins and Himalayan Foreland: A Record of Tectonics or Mantle Dynamics? Tectonics, v. 37, p. 3970–3985, doi:10.1029/2018TC005286.

Najman, Y., Carter, A., Oliver, G., and Garzanti, E., 2005, Provenance of Eocene foreland basin sediments, Nepal: Constraints to the timing and diachroneity of early Himalayan orogenesis: Geology, v. 33, p. 309–312.

Najman, Y., Jenks, D., Godin, L., Boudagher-Fadel, M., Millar, I., Garzanti, E., Horstwood, M., and Bracciali, L., 2017, The Tethyan Himalayan detrital record shows that India–Asia terminal collision occurred by 54 Ma in the Western Himalaya: Earth and Planetary Science Letters, v. 459, p. 301–310, doi:10.1016/j.epsl.2016.11.036.

Najman, Y., Johnson, K., White, N., and Oliver, G., 2004, Evolution of the Himalayan foreland basin, NW India: Basin Research, v. 16, p. 1–24, doi:10.1111/j.1365-2117.2004.00223.x.

Nelson, K.D. et al., 1996, Partially Molten Middle Crust Beneath Southern Tibet: Synthesis of Project INDEPTH Results: Science, v. 274, p. 1684–1688, doi:10.1126/science.274.5293.1684.

Ojha, P.S., 2012, Precambrian sedimentary basins of India: an appraisal of their petroleum potential, *in* Geology and Hydrocarbon Potential of Neoproterozoic–Cambrian Basins in Asia, Geological Society of London Special Publications, v. 366, p. 19–58, http://sp.lyellcollection.org/lookup/doi/10.1144/SP366.11 (accessed June 2018).

Ojha, T.P., Butler, R.F., DeCelles, P.G., and Quade, J., 2009, Magnetic polarity stratigraphy of the Neogene foreland basin deposits of Nepal: Basin Research, v. 21, p. 61–90, doi:10.1111/j.1365-2117.2008.00374.x.

Prasad, B., and Asher, R., 2001, Acritarch biostratigraphy and lithostratigraphic classification of Proterozoic and Lower Paleozoic sediments (Pre-unconformity sequence) of Ganga Basin, India: Dehra Dun, Geoscience Research Group, Keshava Deva Malaviya Institute of Petroleum Exploration, Oil and Natural Gas Corporation.

Prasad, B., and Pundir, B.S., 2017, Gondwana biostratigraphy of the Purnea Basin (eastern Bihar, India), and its correlation with Rajmahal and Bengal Gondwana basins: Journal of the Geological Society of India, v. 90, p. 405–427, doi:10.1007/s12594-017-0735-3.

Raiverman, V., 1983, Basin geometry, Cenozoic sedimentation and hydrocarbon prospects in north western Himalaya and Indo-Gangetic plains: Petroleum Asia Journal, v. 6, p. 67–92.

Raiverman, V., 2002, Foreland sedimentation in Himalayan tectonic regime: a relook at the orogenic process: Dehra Dun, Bishen Singh Mahendra Pal Singh.

Raiverman, V., Chugh, M.L., Srivastava, A.K., Prasad, D.N., and Das, S.K., 1994, Cenozoic Tectonics of the Fold Belt of Himalaya and the Indo-Gangetic Fordeep with Pointers towards Hydrocarbon Prospects, *in* Biswas, S.K., Dave, A., Garg, P., Pandey, J., Maithani, A., and Thomas, N.J. eds., Proceedings of the Second Seminar on Petroliferous Basins of India: Himalayan foothills, Vindhyan and Gondwana basins, geoscientific studies and hydrocarbon exploration techniques, Dehra Dun, v. 3, p. 25–54.

Rao, M.R., 1973, The subsurface geology of the Indo-Gangetic plains: Journal of the Geological Society of India, v. 14, p. 217–242.

Rasmussen, B., Bose, P.K., Sarkar, S., Banerjee, S., Fletcher, I.R., and McNaughton, N.J., 2002, 1.6 Ga U-Pb zircon age for the Chorhat Sandstone, lower Vindhyan, India: Possible implications for early evolution of animals: Geology, v. 30, p. 103–106.

Ratschbacher, L., Frisch, W., Liu, G., and Chen, C., 1994, Distributed deformation in southern and western Tibet during and after the India-Asia collision: Journal of Geophysical Research: Solid Earth, v. 99, p. 19917–19945.

Sakai, H., 1983, Geology of the Tansen Group of the Lesser Himalaya in Nepal.: Memoirs of the Faculty of Science, Kyushu University, v. 25, p. 27–74.

Sakai, H., 1989, Rifting of the Gondwanaland and uplifting of the Himalayas recorded in Mesozoic and Tertiary fluvial sediments in the Nepal Himalayas, *in* Taira, A. and Masuda, F. eds., Sedimentary facies in the active plate margin, Tokyo, Terra Scientific Publishing Company, p. 723–732.

Sakai, H., 1991, The Gondwanas in the Nepal Himalaya, *in* Tandon, S.K., Pant, C.C., and Casshyap, S.M. eds., Sedimentary Basins of India: Tectonic Context: Proceedings of the seminar held at Department of Geology, Kumaun University, Nainital, Nainital : Gyanodaya Prakashan, p. 202–217.

Sastri, V.V., Bhandari, L.L., Raju, A.T.R., and Datta, A.K., 1971, Tectonic framework and subsurface stratigraphy of the Ganga basin: Jornal of the Geological Society of India, v. 12, p. 222–233.

Searle, M.P., Law, R.D., Godin, L., Larson, K.P., Streule, M.J., Cottle, J.M., and Jessup, M.J., 2008, Defining the Himalayan main central thrust in Nepal: Journal of the Geological Society, v. 165, p. 523–534.

Sengupta, S.N., 1962, Basement configuration of the Indo-Gangetic plains shown by aeromagnetic surveys, *in* Proceedings of the Seminar on Oil Prospects in the Ganga Valley, Oil and Natural Gas Corporation Technical Publications, v. 1, p. 52–54.

Sitaula, R.P., 2009, Petrofacies and Paleotectonic Evolution of Gondwanan and Post-Gondwanan Sequences of Nepal [MSc thesis]: Auburn University, 206 p.

Soucy La Roche, R., Godin, L., Cottle, J.M., and Kellett, D.A., 2018, Preservation of the Early Evolution of the Himalayan Middle Crust in Foreland Klippen: Insights from the Karnali Klippe, West Nepal: Tectonics, v. 37, p. 1161–1193, doi:10.1002/2017TC004847.

Srinivasan, S., and Khar, B.M., 1996, Status of Hydrocarbon Exploration in Northwest Himalaya and Foredeep - Contributions to Stratigraphy and Structure, *in* Proceedings of the Symposium on NW Himalaya and Foredeep, Feb 1995, Geological Survey of India Special Publications, v. 21, p. 295–405.

de la Torre, T.L., Monsalve, G., Sheehan, A.F., Sapkota, S., and Wu, F., 2007, Earthquake processes of the Himalayan collision zone in eastern Nepal and the southern Tibetan Plateau: Geophysical Journal International, v. 171, p. 718–738, doi:10.1111/j.1365-246X.2007.03537.x.

Tripathy, G.R., and Singh, S.K., 2015, Re–Os depositional age for black shales from the Kaimur Group, Upper Vindhyan, India: Chemical Geology, v. 413, p. 63–72, doi:10.1016/j.chemgeo.2015.08.011.

Upreti, B.N., 1999, An overview of the stratigraphy and tectonics of the Nepal Himalaya: Journal of Asian Earth Sciences, v. 17, p. 577–606, doi:10.1016/S1367-9120(99)00047-4.

Valdiya, K.S., 1980, Geology of Kumaun Lesser Himalaya: Dehra Dun, Wadia Institute of Himalayan Geology.

Valdiya, K.S., 1997, Himalaya, the Northern Frontier of East Gondwanaland: Gondwana Research, v. 1, p. 3–9, doi:10.1016/S1342-937X(05)70002-2.

Valdiya, K.S., 1976, Himalayan transverse faults and folds and their parallelism with subsurface structures of north Indian plains: Tectonophysics, v. 32, p. 353–386.

Veevers, J.J., and Tewari, R.C., 1995, Gondwana master basin of Peninsular India between Tethys and the interior of the Gondwanaland Province of Pangea: Colorado, Geological Society of America, Geological Society of America Memoir, v. 187, 67 p., doi:10.1130/0-8137-1187-8.1.

Vögeli, N., Najman, Y., van der Beek, P., Huyghe, P., Wynn, P.M., Govin, G., van der Veen, I., and Sachse, D., 2017, Lateral variations in vegetation in the Himalaya since the Miocene and implications for climate evolution: Earth and Planetary Science Letters, v. 471, p. 1–9, doi:10.1016/j.epsl.2017.04.037.

Wadia, D.N., 1919, Geology of India: London, United Kingdom, Macmillan and Co Ltd, 536 p.

Xiao, S., Tang, Q., Hughes, N.C., McKenzie, N.R., and Myrow, P.M., 2016, Biostratigraphic and detrital zircon age constraints on the basement of the Himalayan Foreland Basin: Implications for a Proterozoic link to the Lesser Himalaya and cratonic India: Terra Nova, v. 28, p. 419–426, doi:10.1111/ter.12235.

Yin, A., 2006, Cenozoic tectonic evolution of the Himalayan orogen as constrained by along-strike variation of structural geometry, exhumation history, and foreland sedimentation: Earth-Science Reviews, v. 76, p. 1–131, doi:10.1016/j.earscirev.2005.05.004.

Zhao, W., Nelson, K.D., Che, J., Quo, J., Lu, D., Wu, C., and Liu, X., 1993, Deep seismic reflection evidence for continental underthrusting beneath southern Tibet: Nature, v. 366, p. 557–559, doi:10.1038/366557a0.

Chapter 2: Influence of Indian plate structural inheritance on the Himalayan foreland basin, Nepal

Foreland basin sediments of the Ganga Basin in northern India and southern Nepal were deposited during Himalayan orogensis above older strata and structures preserved in the Indian plate. 2D seismic data across the Nepali lowlands allow mapping of several regional subsurface markers in time. The geometry of these markers, when depth converted, highlights the interplay between basement structure and longitudinal variations in sedimentary rock thickness, structural elevations, and faulting within the Ganga Basin. Several basement structural highs and depressions, tens to hundreds of kilometres wide, at high angles to the orogenic front, can be correlated with similarly oriented lineaments in the Bouguer gravity anomaly pattern. These features influenced deposition of Precambrian Vindhyan Succession and overlying Cenozoic successions. Gradual cross-strike thickness variations in the Cenozoic succession provide evidence of active differential subsidence during foreland basin development, controlled by the basement ridge/fault systems. Local thickness changes at different stratigraphic levels suggest differential subsidence at different times during Neogene basin development. The subsidence history of the basin likely reflects variations in the flexural rigidity of the Indian plate as it was translated northward beneath the Himalayan orogen.

2.1 Introduction

The Himalayan orogen is the product of an ongoing continent-continent collision between the Indian and Eurasian plates that initiated between 60 and 40 Ma (Bouilhol et al., 2013; Hu et al., 2016; Najman et al., 2017). South of the orogen is the Ganga Foreland Basin, a collisional foreland basin that stretches east-west along the length of the orogen from Pakistan through India to Nepal, formed in response to tectonic loading during the rise of the Himalaya (Fig. 2-1) (Lyon-Caen and Molnar, 1985; Burbank et al., 1996).

The Ganga Basin is commonly subdivided into longitudinally continuous units. The apparent longitudinal continuity contrasts with along-strike changes summarized by Godin et al. (2019); these affect Himalayan topography (Duncan et al., 2003), incision patterns (van der Beek et al., 2016), crustal density (Basuyau et al., 2013), structure (Yin, 2006), rates of convergence and exhumation (Burgess et al., 2012; McQuarrie et al., 2014), seismicity (Monsalve et al., 2006;

de la Torre et al., 2007; Gahalaut and Kundu, 2012), and climate (Anders et al., 2006; Vögeli et al., 2017). Regional-scale crustal lineaments on the Indian plate interpreted as transverse crustal-scale basement faults have potentially played a role in the segmentation of the orogen and the Ganga Basin (Bollinger et al., 2004; Godin & Harris, 2014; Godin et al., 2019).

The modern Ganga alluvial plain is the upper surface of the Ganga foreland basin, formed by flexural subsidence in response to the load of the Himalayan orogen on the Indian plate. The Ganga foreland basin is filled with Cenozoic sedimentary rocks that were deposited on top of late Carboniferous to Cretaceous sedimentary strata from the margin of Gondwana (the Gondwana succession), and Paleo- to Neoproterozoic rocks of the intracratonic Vindhyan basin (Krishnan, 1949; Gansser, 1964; Veevers and Tewari, 1995; Rasmussen et al., 2002; Ray et al., 2002; Ray, 2006) (Fig. 2-2). Through correlations with surficial mapping, gravity anomaly studies, and rare boreholes, several basement highs or 'spurs' have been interpreted at regional scale under the Ganga foreland basin (Sengupta, 1962; Rao, 1973; Valdiya, 1976; Karunakaran and Rao, 1979; Raiverman et al., 1994; Shukla and Chakraborty, 1994; Godin and Harris, 2014). They are oriented NE-SW, at a high angle to the orogen, and include the Delhi-Haridwar, Faizabad, and Munger-Saharsa ridges (Fig. 2-1). Steeply-dipping lineaments that coincide with the ridge edges have been interpreted to continue underneath the orogen to the northern edge of the subducted Indian lithosphere under Tibet (Godin and Harris, 2014). These ridge systems have been invoked to explain the spatial distribution and thickness variation of Gondwanan and Cenozoic successions (Rao, 1973; Raiverman, 1983; Raiverman et al., 1994). Recent work has suggested that the deep crustal faults associated with each ridge may have been reactivated through time, presenting a mechanism to explain the longitudinal variation in the Ganga foreland basin (Godin and Harris, 2014; Godin et al., 2019; Soucy La Roche and Godin, 2019). We seek to examine the effects of these ridges and their associated faults on the foreland basin strata in Nepal.

We assess the geometry of the Nepali segment of the Ganga foreland basin through 2D seismic interpretation. Our study compares variations in thickness and basin geometry with the spatial distribution of subsurface ridges and associated deep-seated crustal faults. We assess the role that these Indian plate basement features have played in the subsidence history of the Ganga Basin.

2.2 Tectonic setting

2.2.1 Himalayan Orogen

Four lithotectonic Himalayan domains (Avouac, 2003) are bounded by a series of north-dipping continental-scale faults, which record the successive southward migration of the deformation front (Fig. 2-1). The faults root into a geophysically-imaged shallow dipping regional décollement, the Main Himalayan Thrust (MHT; Zhao et al. 1993; Brown et al. 1996; Nelson et al. 1996; Hauck et al. 1998). The northernmost lithotectonic domain is the sedimentary Tethyan Himalaya formerly deposited on the northern continental margin of northern India, bounded to the north by the Indus-Tsangpo Suture Zone (ITSZ), and to the south by the South Tibet Detachment system (STD; Burchfiel et al., 1992; Ratschbacher et al., 1994; Kellett et al., 2019). High-metamorphic grade rocks of the Greater Himalaya occur between the STD and the Main Central Thrust (MCT; Heim and Gansser, 1939; Searle et al., 2008) to the south. Lower-grade metasedimentary and metavolcanic rocks of the Lesser Himalaya are bounded by the MCT and the Main Boundary Thrust (MBT; Heim and Gansser, 1939; Gansser, 1964). Finally, Cenozoic sedimentary rocks of the Sub-Himalaya lie between the MBT and the active Main Frontal Thrust (MFT); they represent uplifted foreland basin deposits, formed during later stages of the rise of the Himalaya (Burbank et al., 1996). Foreland basin sediments and sedimentary rocks south of the MFT underlie the Indo-Gangetic Alluvial Plain. Our study focuses on the least deformed of these, the Indo-Gangetic Plain and the Sub-Himalaya, and examines the record of deformation and subsidence of the Indian Plate as it entered the orogen.

Flexural subsidence driven by the weight of the Himalaya has produced the Indo-Gangetic depression along the southern flank of the orogen (Lyon-Caen and Molnar, 1985; DeCelles et al., 1998a), which has been viewed as a classic example of an active collisional foreland basin (Burbank et al., 1996). Foredeep deposits stretch ~400-450 km south of the Sub-Himalaya, and comprise sediment derived from the erosional unroofing of the orogen (Gansser, 1964). The depression is dominantly filled by the Neogene to Pleistocene Siwalik Group (also known in Nepal as the Churia Group) and underlying Paleogene deposits. However, active alluvial and fluvial sedimentation has continued to the present day (Upreti, 1999). The modern basin has been divided (Rao, 1973), reflecting present-day topography and drainage divides: the Indus basin mainly in Pakistan, the Ganga Basin in northern India and Nepal, and the Bengal Basin in NE India and Bangladesh (Fig. 2-1a).

2.2.2 Basement structure

The foreland basin deposits overlie strata of continental India and numerous Precambrian basement domains of the Indian shield (Valdiya, 1976). Three subsurface Indian basement ridges strike at high angles to the Himalayan orogen: The Delhi-Haridwar ridge, which manifests as a ~50 km wide horst containing the Proterozoic Aravalli mobile belt at surface; the Faizabad ridge, which correlates with the granite and gneiss-dominated Bundelkhand Craton; and the Munger-Saharsa ridge, the subsurface expression of the Satpura fold belt (Fig. 2-1) (Valdiya, 1976). Numerous smaller basement highs or 'spurs' correspond to crustal-scale lineaments, mainly in the western portion of the Ganga Basin (Raiverman, 1983; Raiverman et al., 1994). Depressions between the ridges and spurs accommodate significant deposits of Proterozoic and Paleozoic sedimentary strata, and subdivide the Ganga basin (Sastri et al., 1971; Raiverman, 1983; Raiverman et al., 1994). The Gandak and Sarda Depressions (Fig. 2-1c) occur east and west of the Faizabad ridge, respectively. Raiverman (1983, 2002) interpreted a small basement high trending E-W within the Sarda depression, lacking correlation to shield features, termed the Dudwa ridge (Fig. 2-1).

Heterogeneities in the Indian plate beneath the Ganga basin produce aeromagnetic and gravity anomalies (Sengupta, 1962; Sastri et al., 1971; Rao, 1973; Valdiya, 1976; Karunakaran and Rao, 1979). Several crustal-scale faults, also at high angles to the Himalayan Orogen, have been identified under the Ganga Basin, including (from east to west) the Kishangang basement fault, the Munger-Saharsa Ridge fault, the West and East Patna faults, the Lucknow fault, and the Great Boundary fault (Fig. 2-1b) (Sastri et al., 1971; Rao, 1973; Aditya et al., 1979; Karunakaran and Rao, 1979; Dasgupta, 1993; Raiverman et al., 1994; Dasgupta et al., 2013; Godin and Harris, 2014). These faults predominantly strike NE-SW, transverse to the orogen (Fig. 2-1b). They are deep-seated, and typically show normal offsets below the foreland basin strata, without disrupting Cenozoic foreland strata (Raiverman et al., 1994). Many of these faults coincide with the edges of basement ridges and spurs (Godin & Harris, 2014; Godin et al., 2019). The ridge-bounding faults dip steeply, and in the case of the Faizabad and Delhi-Haridwar ridges show opposing senses of dip on either side of the ridges (Godin and Harris, 2014). These ridge/fault systems are interpreted as horsts (Godin and Harris, 2014; Godin et al., 2019). Raiverman (1983; Raiverman et al., 1994) have suggested that reactivation of their bounding faults may have influenced along-strike sediment distributions in the Ganga Basin.

Faults at the scale of seismic reflection profiles occur in Nahan-Dehradun-Haridwar area (Fig. 2-1b) of the Ganga basin, where they are grouped into two trends (Raiverman et al., 1994): a predominantly NW-SE population of normal faults, and a N-S set interpreted by Raiverman et al. (1994) as predominantly showing dextral strike slip. Both sets of faults cut only pre-Cenozoic strata in the foreland basin, suggesting movement is pre-Cenozoic. However, the N-S population cuts Miocene strata in the thrust belt; Raiverman et al. (1994) interpreted this difference of fault timing to indicate reactivation of basement faults in the thrust belt.

2.2.3 Stratigraphy of the Ganga foreland basin

The stratigraphy of the Ganga foreland basin and its basement south of the MFT has been largely defined by a series of exploration wells drilled in India (Sastri et al., 1971; Karunakaran and Rao, 1979; Fuloria, 1996; Srinivasan and Khar, 1996). Only a single well (Biratnagar-1; Fig. 2-1c), which did not penetrate the basement, has been drilled on the Nepali side of the basin. Four subsurface sedimentary successions or megasequences have been recognized (Srinivasan and Khar, 1996). Formation names vary along strike; here we use the Nepalese stratigraphy; along-strike equivalents are shown in Fig. 2-2. From base to top, the successions are: the Proterozoic to possibly Cambrian Vindhyan succession, related to deposition in the intracratonic Vindhyan Basin; the Late Carboniferous/Permian to Paleogene Gondwanan succession, deposited on the northern margin of continental India; the Paleocene to lower middle Eocene Bhainskati Formation (equivalent to the Subathu sequence in India; Srinivasan and Khar, 1996), representing the earliest deposits of the Himalayan foreland basin system; and the Neogene to Quaternary Dumri–Siwalik succession, deposited as continental deposits within the Ganga foreland basin (DeCelles et al., 1998a).

2.2.3.1 Basement units

At its southern boundary (Fig. 2-1b), the Ganga Basin oversteps Archean and Proterozoic basement provinces and mobile belts (Sastri et al., 1971; Valdiya, 1976; Balakrishnan et al., 2009; Mitra et al., 2011). From east to west, the Ganga basin onlaps: the ~2300 – 1000 Ma Chotanagpur Gneissic Complex (Chatterjee and Ghose, 2011; Mohanty, 2012); the Proterozoic Satpura Mobile Belt (Meert et al., 2010; Mohanty, 2012); the Vindhyan succession (Meert et al., 2010) in the Gandak depression; the Bundelkhand Craton, primarily Archean granite (Sharma and Rahman, 2000); the Vindhyan succession in the Sarda depression; and the Proterozoic Aravalli-Delhi fold belt (Sastri et al., 1971; Valdiya, 1976) (Fig. 2-1b).

Fig. 2-1. Regional maps
a) Regional political map of south central Asia and major sedimentary basins underneath the Ganga Alluvial Plain, with the Ganga Basin highlighted after Rao (1973). (b) Generalized geology map of Northern India, Nepal, and adjacent areas after Yin (2006), Goscombe et al., (2018), Kellett & Grujic (2012), Soucy la Roche et al., (2018), Mohanty (2012), Casshyap & Khan (2000), and USGS public data. Approximate traces of basement ridges after Godin & Harris (2014). ITSZ: Indus-Tsangpo Suture Zone; STD: South Tibet Detachment system; MCT: Main Central Thrust; MBT: Main Boundary Thrust; MFT: Main Frontal Thrust; KF: Kishangang Fault; MSF Munger-Saharsa Ridge fault, WPF West Patna Fault; EPF: East Patna Fault; LF: Lucknow fault; GBF: Great Boundary Fault; NSNF: North Son-Narmada Fault. (c) Detailed map of seismic lines and wells within the study area (location shown in (a). Seismic surveys used in this study are highlighted, and were shot in four blocks: the Western Block, the Eastern Block, the Central Block, and 'Block 10.' Gaps between the blocks range from 60 km to 9 km. The well Biratnagar-1 (bold) acted as the sole well tie, while the Madhubani-1 and Raxaul-1, and Matera -1 wells (underlined) were used as supplementary controls on stratigraphy in the Eastern and Western Blocks. A-A' marks line of section in Figure 2-10. Highlighted lines are shown in (i) Fig. 2-5 and (ii) Fig. 2-6.

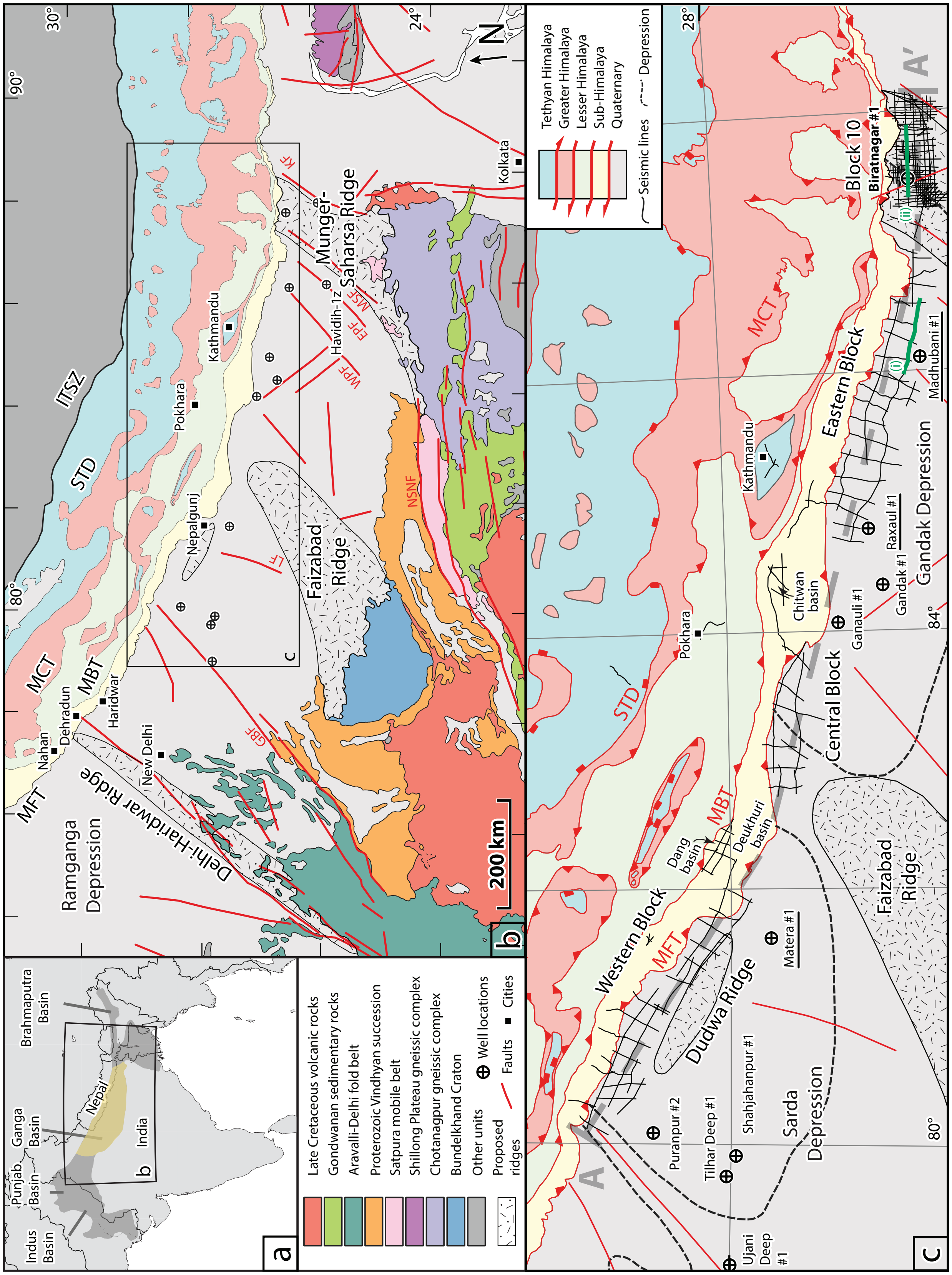

a
Indus Basin
Punjab Basin
Ganga Basin
Brahmaputra Basin
Nepal
India
b
Late Cretaceous volcanic rocks
Gondwanan sedimentary rocks
Aravalli-Delhi fold belt
Proterozoic Vindhyan succession
Satpura mobile belt
Shillong Plateau gneissic complex
Chotanagpur gneissic complex
Bundelkhand Craton
Other units
Proposed ridges
Well locations
Faults
Cities
Ramganga Depression
Delhi-Haridwar Ridge
MFT
MCT
MBT
STD
ITSZ
Nahan
Dehradun
Haridwar
New Delhi
Nepalgunj
Pokhara
Kathmandu
Kolkata
Faizabad Ridge
Munger-Saharsa Ridge
Havidih-1z
GBF
LF
WPF
EPF
MSF
KF
NSNF
200 km
N
80°
90°
30°
24°
c
Tethyan Himalaya
Greater Himalaya
Lesser Himalaya
Sub-Himalaya
Quaternary
Seismic lines
Depression
A
A'
Western Block
Central Block
Eastern Block
Block 10
Dudwa Ridge
Faizabad Ridge
Sarda Depression
Gandak Depression
Dang basin
Deukhuri basin
Chitwan basin
Ujani Deep #1
Tilhar Deep #1
Puranpur #2
Shahjahanpur #1
Matera #1
Ganauli #1
Gandak #1
Raxaul #1
Madhubani #1
Biratnagar #1
80°
84°
28°

2.2.3.2 Vindhyan Succession

To the south of the Ganga Plain, the Bundelkhand craton is flanked by deposits of the intracratonic Vindhyan basin, which contains Proterozoic Vindhyan succession sedimentary rocks (Fig. 2-1b). The Vindhyan basin is bounded to the west by the Aravalli Mountains, and to the southeast by the North Son-Narmada Fault (Shukla and Chakraborty, 1994). It contains relatively undeformed and unmetamorphosed sandstone, mudstone, and carbonate units, with subordinate conglomerate and volcaniclastic horizons (Bhattacharyya, 1996). A regional unconformity divides the succession into the upper and lower Vindhyan successions (Ray, 2006).

The Vindhyan succession extends underneath the Ganga Basin and has been intersected by many deep exploration wells in India (Shukla and Chakraborty, 1994), where some authors have distinguished the subsurface Vindhyan deposits as Ganga Supergroup (Fuloria, 1996; Prasad and Asher, 2001). We use the term Vindhyan succession for both the exposed and subsurface units. The succession was preferentially deposited between the main basement ridges (Negi and Eremenko, 1968; Karunakaran and Rao, 1979) and along their flanks, and it has been suggested that movement of the crustal-scale bounding faults played a role in accommodation and localization of Vindhyan strata (Raiverman et al., 1994; Gahalaut and Kundu, 2012; Godin and Harris, 2014). An angular unconformity separates the Vindhyan succession from overlying strata (Rao, 1973).

2.2.3.3 Gondwanan Succession

Gondwanan (Late Carboniferous/Permian to earliest Paleogene) strata on the Indian subcontinent are largely restricted to basins coinciding with suture zones between Archean cratons, and show graben or half-graben geometries (Veevers and Tewari, 1995; Biswas, 1999; Mukhopadhyay et al., 2010). These basins have been interpreted as rift basins associated with the breakup of the supercontinent Gondwana (Biswas, 1999).

In the Lesser Himalaya of Nepal, Gondwanan strata have a broad spatial distribution (Sakai, 1983; Sitaula, 2009). In western Nepal, they (Fig. 2-2; Sakai, 1983) have been interpreted as representing the northern continental margin of India, deposited before Himalayan orogenesis (DeCelles et al., 2004; Sitaula, 2009).

In the Ganga Basin subsurface, it is possible that Gondwanan strata may be preserved in the area covered by the seismic data interpreted here (Fuloria, 1996; Bashyal, 1998). However, Mesozoic strata previously reported (Sastri et al., 1971) in the Tilhar-1, Ujani-1 and Puranpur-2 wells (Fig. 2-1c) have been reinterpreted as Proterozoic, to possibly Cambrian (McKenzie et al., 2011; Xiao et al., 2016). In the seismic data interpreted in this study, we have not distinguished Gondwanan strata, if present, from the underlying Vindhyan succession.

2.2.3.4 Paleogene Bhainskati Formation – early foreland basin deposits

The Bhainskati Formation (Fig. 2-2) conformably overlies the Gondwanan deposits that predate the Himalayan orogeny (Sakai, 1983; DeCelles et al., 1998a). The basal contact is concordant in outcrop (Sakai, 1989; Sakai et al., 1992), and represents the transition from quartzose sandstone beds of the Cretaceous Amile Formation to marine shale beds of the Bhainskati Formation (DeCelles et al., 2004). This contact is interpreted to be at least as young as 60 ± 8 Ma (Najman et al., 2005) based on detrital zircon fission track analyses, and signifies a shift in provenance from continental India to the combined influences of the Himalaya and Indian continent (DeCelles et al., 2004; Ravikant et al., 2011; Garzanti, 2019). The Bhainskati Formation, >90 m thick in outcrop in the Lesser Himalaya, is predominantly fossiliferous organic-rich black shale, with infrequent quartz-rich sandstone and oolitic ironstone layers characteristic of a shallow marine environment (Sakai, 1983; DeCelles et al., 2004). The uppermost Bhainskati Formation is a lateritic paleosol, interpreted as a residual deposit produced by weathering at an overlying unconformity surface (DeCelles et al., 1998a). The upper contact is constrained to be younger than 45 Ma based on fission track detrital zircon analysis (Najman et al., 2005). Overall, the Bhainskati Formation has been interpreted as representing deposition in a shallow marine seaway, possibly corresponding with the back-bulge portion of the early Ganga foreland basin (DeCelles et al., 2004), although the existence of this back-bulge is disputed (Garzanti, 2019).

2.2.3.5 Neogene to Quaternary Dumri Formation and Siwalik Group

The Dumri Formation, approximately equivalent to the Dagshai/Kasauli and Dharamasala Formations in India (Fig. 2-2), is a fluvial unit that ranges in thickness from 700 m to 1200 m (DeCelles et al., 1998a). The regional unconformity at the base of the Dumri Formation is interpreted as a peripheral bulge unconformity relating to the load of the Himalaya (DeCelles et al., 1998a), or as a product of redistribution of the load (Najman et al., 2004), or mantle processes such as slab break-off (Najman et al., 2018; Garzanti, 2019). In the seismic stratigraphic framework, this boundary separates the Eocene Bhainskati succession from the Neogene Dumri Formation and overlying Siwalik Group. The Dumri Formation (and correlative units) represent the earliest continental deposits of the Himalayan foredeep (Sakai,

Fig. 2-2. Generalized lithostratigraphic chart of the Ganga Basin and Sub-Himalaya Group names shown as uppercase text. Timescale after Cohen et al., (2013). b) Seismic stratigraphy column after Srinivasan & Khar (1996). c) Lithostratigraphy of the Sub- and Lesser Himalaya of India after Mathur (1978), Valdiya (1980), Najman et al., (1997), White et al., (2002), Hughes et al., (2005). d) Lithostratigraphy of the Sub- and Lesser Himalaya of Western Nepal, based on Sakai (1983), Upreti (1999), Najman et al., (2005), and Ojha et al. (2009). e) Idealized stratigraphic column representing units potentially present in the Ganga basin. Alluvium and Siwalik Group thicknesses represent those in the Biratnagar-1 well; outcrop thicknesses from Sakai (1983) were used for older strata.

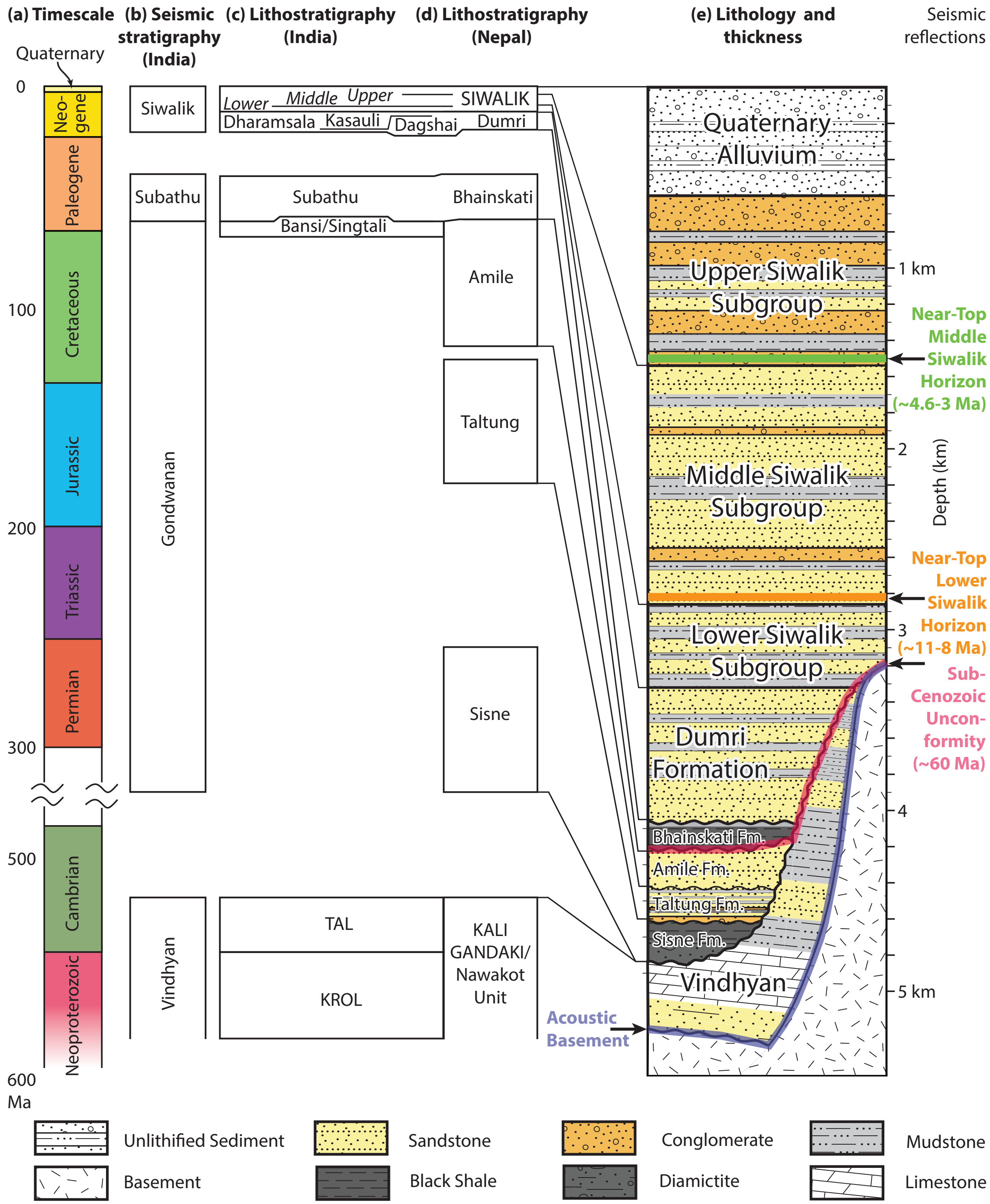
(a) Timescale
(b) Seismic stratigraphy (India)
(c) Lithostratigraphy (India)
(d) Lithostratigraphy (Nepal)
(e) Lithology and thickness
Seismic reflections
Quaternary
0
100
200
300
500
600 Ma
Neo-gene
Paleogene
Cretaceous
Jurassic
Triassic
Permian
Cambrian
Neoproterozoic
Siwalik
Subathu
Gondwanan
Vindhyan
Lower Middle Upper
SIWALIK
Dharamsala Kasauli Dagshai Dumri
Subathu
Bhainskati
Bansi/Singtali
Amile
Taltung
Sisne
TAL
KROL
KALI GANDAKI/ Nawakot Unit
Quaternary Alluvium
Upper Siwalik Subgroup
Middle Siwalik Subgroup
Lower Siwalik Subgroup
Dumri Formation
Bhainskati Fm.
Amile Fm.
Taltung Fm.
Sisne Fm.
Vindhyan
Acoustic Basement
1 km
2
3
4
5 km
Depth (km)
Near-Top Middle Siwalik Horizon (~4.6-3 Ma)
Near-Top Lower Siwalik Horizon (~11-8 Ma)
Sub-Cenozoic Uncon-formity (~60 Ma)
Unlithified Sediment
Sandstone
Conglomerate
Mudstone
Basement
Black Shale
Diamictite
Limestone

1983; DeCelles et al., 1998b). The Dumri Formation is dominated by trough cross-stratified sandstone and planar silty sandstone beds that represent three main lithofacies associations: channel fill, crevasse splays, and paleosols (DeCelles et al., 1998a). The Dumri Formation has a maximum depositional age determined by fission track detrital zircon analysis of 32-30 Ma (Najman et al., 2005). However, in western Nepal it has been dated between ~19.9 to 15.1 Ma via magnetostratigraphy (Ojha et al., 2009). These data suggest a long hiatus between deposition of the Bhainskati Formation and the Dumri Formation. The Bhainskati and Dumri Formations are restricted to the Lesser Himalaya of Nepal and to the deeper parts of the Ganga basin, along its northern margin (Raiverman et al., 1994; Fuloria, 1996). These deposits onlap on to pre-Cenozoic strata at their southern extremity, and were presumably controlled by foreland basin subsidence at the time of deposition (Raiverman, 1983; Raiverman et al., 1994).

2.2.3.6 Miocene to Quaternary Siwalik Group

The Siwalik Group represents the thickest accumulation of detritus derived from the Himalaya in the Ganga Basin (Sahni and Mathur, 1964). It consists of fluvial mudstone, sandstone, and conglomerate, deposited in a similar style to that of the modern Indo-Gangetic Plains (Parkash et al., 1980). The Siwalik Group was deposited between 16 Ma and 0.5 Ma, as determined by magnetostratigraphy (Appel et al., 1991; Harrison et al., 1993; Rösler et al., 1997; Ojha et al., 2000, 2009; Gautam and Fujiwara, 2000). A tripartite division into the Lower, Middle, and Upper Siwalik Subgroups has long existed, first based on vertebrate markers (Pilgrim, 1913), but later refined to reflect lithological contrasts from mudstone-dominated, to sandstone-dominated, and conglomerate-dominated facies, respectively (Sahni and Mathur, 1964; Karunakaran and Rao, 1979). Although the Siwalik Group has been further subdivided into formations (Kumar and Tandon, 1985; Nakayama and Ulak, 1999; e.g. Corvinus and Rimal, 2001; Dhital, 2015), the tripartite division is used in this study. A magnetostratigraphic boundary near the base of the Siwalik Group constrains its base to >15.5 Ma in Nepal (Gautam and Fujiwara, 2000). Magnetostratigraphic studies at several localities throughout Nepal have placed the Lower to Middle Siwalik contact between 11.05 and 8.0 Ma, and the Middle to Upper Siwalik contact between 4.6 and 3.0 Ma (Rösler et al., 1997; Ojha et al., 2000, 2009). However, magnetostratigraphic correlation of the major intra-Siwalik boundaries across Nepal also suggests that they are diachronous, spanning ~2 Ma (Ojha et al., 2009).

The middle Miocene Lower Siwalik Subgroup reaches thicknesses >850 m and consists of fluvial and paleosol deposits (Quade et al., 1995; DeCelles et al., 1998b). Typical outcrops are shown in Figure 2-3. Sandstone lenses are typically 2-5 m thick and intercalated with bedded floodplain deposits on a scale of <1 m to 10 m (Quade et al., 1995). The basal contact of the Lower Siwalik Subgroup is not exposed in Nepal but is documented in India (Figure 3 of White et al., 2001).

The upper Miocene – Pliocene Middle Siwalik Subgroup (Fig. 2-3) is dominated by thick sandstone beds punctuated by thin siltstone horizons, deposited in a fluvial/floodplain environment (Quade et al., 1995; Bernet et al., 2006). Channel-fills are up to 20 m thick. Both the upper and basal contacts are conformable.

The Pliocene – Quaternary Upper Siwalik Subgroup is the coarsest of the Siwalik deposits, composed of mainly conglomerate, together with sandstone and siltstone beds - diagnostic of a proximal fluvial, braided stream, or alluvial deposit (Kumar and Tandon, 1985). The contact between the Middle Siwalik and the Upper Siwalik Subgroups is typically defined based on the first major (>1m) influx of conglomerate (Fig. 2-3).

The Siwalik Group thus displays a coarsening-upward trend of megasequences, grading from predominantly floodplain fines in the Lower Subgroup, to braided river conglomerate that dominates the Upper Subgroup. This coarsening upward trend has been attributed to cratonward migration of the thrust front through time (DeCelles et al., 1998a).

The Siwalik Group in the Sub-Himalaya (north of the MFT) forms a tectonic wedge, dominated by a series of north-dipping thrusts, that have folded and displaced strata southward (Mugnier et al., 1999). Fault propagation folds (blind and emergent), duplexes, north-dipping monoclines, and south dipping backthrusts have all been documented within the Sub-Himalaya (Gill, 1951; Banks and Warburton, 1986; Mugnier et al., 1999; Husson and Mugnier, 2003; Hirschmiller et al., 2014; Almeida et al., 2018). Immediately north of the MFT, in the southern Sub-Himalaya, a zone of open folds is commonly observed (Gill, 1951). Small intermontane basins exist within the thrust belt, including the Deukhuri, Dang, and Chitwan basins (Fig. 2-1c). Central parts of the Sub-Himalaya are characterized by large-displacement reverse faults and intervening open folds. Towards the MBT, at the north edge of the Sub-Himalaya, imbricated horses are documented (Mugnier et al., 1999). The seismic lines of our study predominantly cover the area that was considered as relatively undeformed the south of the MFT, with some coverage between the MFT and the MBT (Fig. 2-1c).

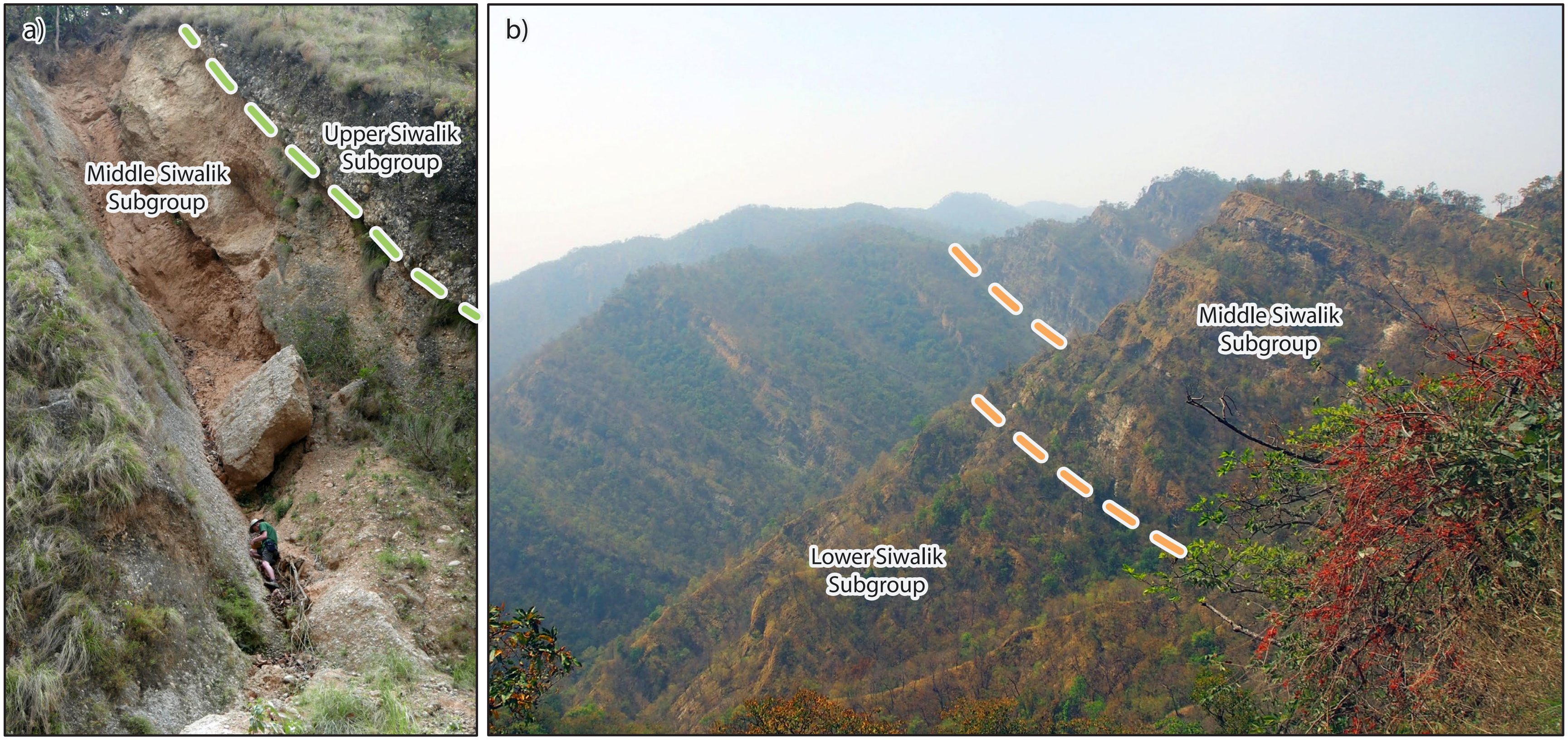

Fig. 2-3. Field photographs

a) Contact between the Middle and Upper Siwalik Subgroups as observed in the Sub-Himalaya near Nepalgunj, geologist for scale: 1.78 m. b) View of the contact between the Lower and Middle Siwalik Subgroups, north of Nepalgunj, in the Sub-Himalaya. The contact between the predominantly mudstone facies of the Lower Siwalik Subgroup and the predominantly sandstone facies of the Middle Siwalik Subgroup corresponds to a break in slope in the far ridgeline. Topographic relief visible on the far ridgeline is approximately 300 m.

2.3 Methods

2.3.1 Data

The geometry of the Ganga Basin is here assessed through interpretation of 181 2D seismic profiles that span the Himalayan foothills in Nepal (Fig. 2-1c). The seismic data were acquired from 1982-1984 by Compagnie Général de Géophysique, Shell, and Petro-Canada International Assistance Corporation, to evaluate the hydrocarbon potential of the Nepal Sub-Himalaya and Ganga Basin deposits. Four blocks of data were acquired, termed the 'Western Block', 'Central Block', 'Eastern Block', and 'Block 10' (Fig. 2-1c). Data gaps exist between several blocks. Seismic line spacing is typically 15 km between N-S lines, and 20 km between E-W lines for the Western, Central, and Eastern Blocks, while Block 10 has a substantially closer profile spacing of approximately 8 km between N-S lines, and 5 km between E-W lines. The total length of the interpreted seismic lines is 5134 km. The majority of these lines lie south of the MFT. However, there are two areas where seismic lines were shot north of the MFT: five lines in the central Block, corresponding to the Chitwan basin, and eight lines in the Western Block, located in the Deukhuri and Dang intermontane basins. These Sub-Himalayan profiles were interpreted as well. The vertical resolution of the data in two-way travel time (TWT) is estimated at 10 ms near the surface, increasing to 20 ms at depth, representing a depth range of roughly 20-50 m. The seismic datum is 50 m above sea level (ASL).

The original data were processed and underwent 2D migration. Sepia film copies of the profiles were scanned, vectorized, migrated, and prepared for workstation interpretation by Fugro-Robertson in 2005 (Cairn Energy, 2006). These data are not shared to the reader due to a confidentiality agreement. Interpretation work by Cairn Energy in 2006 led to the mapping of six regional reflectors, and fifteen localized subordinate horizons (Cairn Energy, 2006). For this study, four of these regional reflector interpretations were reinterpreted to ensure consistent interpretation across the region.

Within the southern Nepal seismic coverage, only a single well is located within the 2D seismic grid: Biratnagar-1 (Fig. 2-1c). This dry vertical well was drilled on an anticline to a total depth of 3530 m below drilling floor (BDF), corresponding to 3409 m below sea level (BSL), and intersected two of the regional reflectors (Figs. 2-4, 2-5). The datum for the well was the drill rig floor, at an elevation of 121 m ASL. The contact at the top of the Middle Siwalik Subgroup is expressed as a 3 m interval of 'limey dolomite' (possibly a caliche unit) capping the sandstone and mudstone interbeds characteristic of the unit (Hartsink and Pradhan, 1989). This contact occurs 1545 m BDF. The top of the Lower Siwalik Subgroup is intersected at 2850 m BDF, where a >50 m sandstone interval overlies interbeds of mudstone and sandstone. Below 3323 m, the basal 207 m of the well penetrated interbedded sandstone and mudstone, initially interpreted to be 'Gondwanan or Vindhyan' rocks (Hartsink and Pradhan, 1989). Palynological data from cuttings and sidewall core analyzed after drilling constrained the age of the 'Vindhyan or Gondwanan' strata to late Eocene or younger, with several palynomorphs more diagnostic of Middle to Late Miocene age, consistent with the Dumri Formation (Hartsink and Pradhan, 1989) The Biratnagar-1 well is too shallow to penetrate the base Miocene unconformity, the Sub-Cenozoic unconformity, or the Precambrian basement.

Indian wells Madhubani-1, Raxaul-1 and Matera-1 were drilled within 9 km, 2 km, and 29 km respectively of the seismic grid (Fig. 2-1c). Data from these wells were projected down-dip onto the closest seismic lines as an independent check on the consistency of our horizon picks across southern Nepal.

2.3.2 Velocity information

To derive the time-depth relationship, we compiled checkshot data from the Biratnagar-1, Havidih-1z, and Shajahanpur-1 wells (e.g. Fig. 2-4), which show an approximately linear increase in velocity with depth in the Cenozoic strata. Wells that penetrated strata below the Cenozoic showed a sharp increase in velocity but a near linear time-depth relationship, so a constant velocity of 5000 m/s was used for all sub-Cenozoic strata. Seismic data were depth-converted using a simple linear relationship that increases velocity as a function of depth within the Cenozoic, and a fixed velocity below the Cenozoic package:

$$v = -0.9102\, z + 1586.1 \qquad \text{where } v = \text{seismic velocity and } z = \text{elevation}$$

We then used the regional 90 m Shuttle Radar Topography Mission (SRTM) Digital Elevation Model (DEM) to position the topographic surface, which ranges from ~40 to ~250 m ASL in the Ganga Basin, rising to ~1300 m in the Sub-Himalaya. We coarsened the DEM to a 200 x 200 m grid to better match the much lower resolution seismic horizon surfaces and converted the horizons from time to depth using the relationship described above.

Because of the uncertainties in these estimates, time to depth conversions are subject to significant uncertainties. Based on the observed variations between the wells for which time-depth data exist, it is estimated that the predicted depths may differ from true depths by ± 10%.

2.3.3 Description/picking methodology

Four regional reflectors are mapped across the 900 km wide study area: the top of the acoustic basement (also referred to as the 'blue horizon'), the Sub-Cenozoic angular unconformity (or 'pink horizon'), a horizon near the top of the Lower Siwalik Subgroup (the 'orange' horizon), and a horizon near the top Middle Siwalik Subgroup (the 'green' horizon). In the absence of appropriate well-log velocity data, these correlations must be regarded as approximate.

The 'top of acoustic basement' marks the nonconformity between sedimentary basin fill and the igneous/metamorphic basement; it is picked along the lowest coherent and laterally extensive positive reflection. The horizon typically occurs below several laterally continuous, high-amplitude reflections at the base of the sedimentary package. Below this contact, no strong reflectors are present inside the rock package, and there are no laterally continuous reflections, suggesting rocks without strong internal acoustic impedance contrasts or layering. This top of acoustic basement horizon is interpreted to be the upper boundary of the Proterozoic basement, and represents the transition from igneous and metamorphic basement rocks into overlying mainly siliciclastic sedimentary strata.

The Sub-Cenozoic angular unconformity is recognized, where present, in seismic data via a change in stratigraphic dip and resulting truncation of reflections below the flat-lying Cenozoic successions. The underlying layers, representing the Gondwanan and Vindhyan successions show apparent dip angles on the seismic profiles that vary from horizontal to a maximum of 25°.

The package between the pink and orange horizons, representing the Bhainskati and Dumri Formations and the Lower Siwalik Subgroup, is manifested by closely spaced peaks and troughs, with much more consistent, higher amplitudes and greater lateral continuity than the overlying Middle Siwalik Subgroup. Reflectors have an average wavelength of ~30 ms. This is consistent with aforementioned descriptions that the Lower Siwalik Subgroup records lower-energy fluvial environments, with more laterally continuous strata (DeCelles et al., 1998b). The Near-top Lower Siwalik Subgroup (orange) horizon was defined in the Biratnagar-1 well, and

Fig. 2-4. Biratnagar-1 lithology log and regional checkshot data
a) Lithostratigraphic column representing strata intersected by the Biratnagar-1 well. Corresponding horizons picks are indicated in time. Neither the acoustic basement nor the Sub-Cenozoic unconformity were intersected by this well. Calculated interval velocities are derived from check shot data (Hartsink and Pradhan, 1989). b) Checkshot data compiled from the Biratnagar-1, Havidih-1z, and Shajahanpur-1 wells, used for calculating a regional time-depth relationship. Well locations shown in figure 2-1.

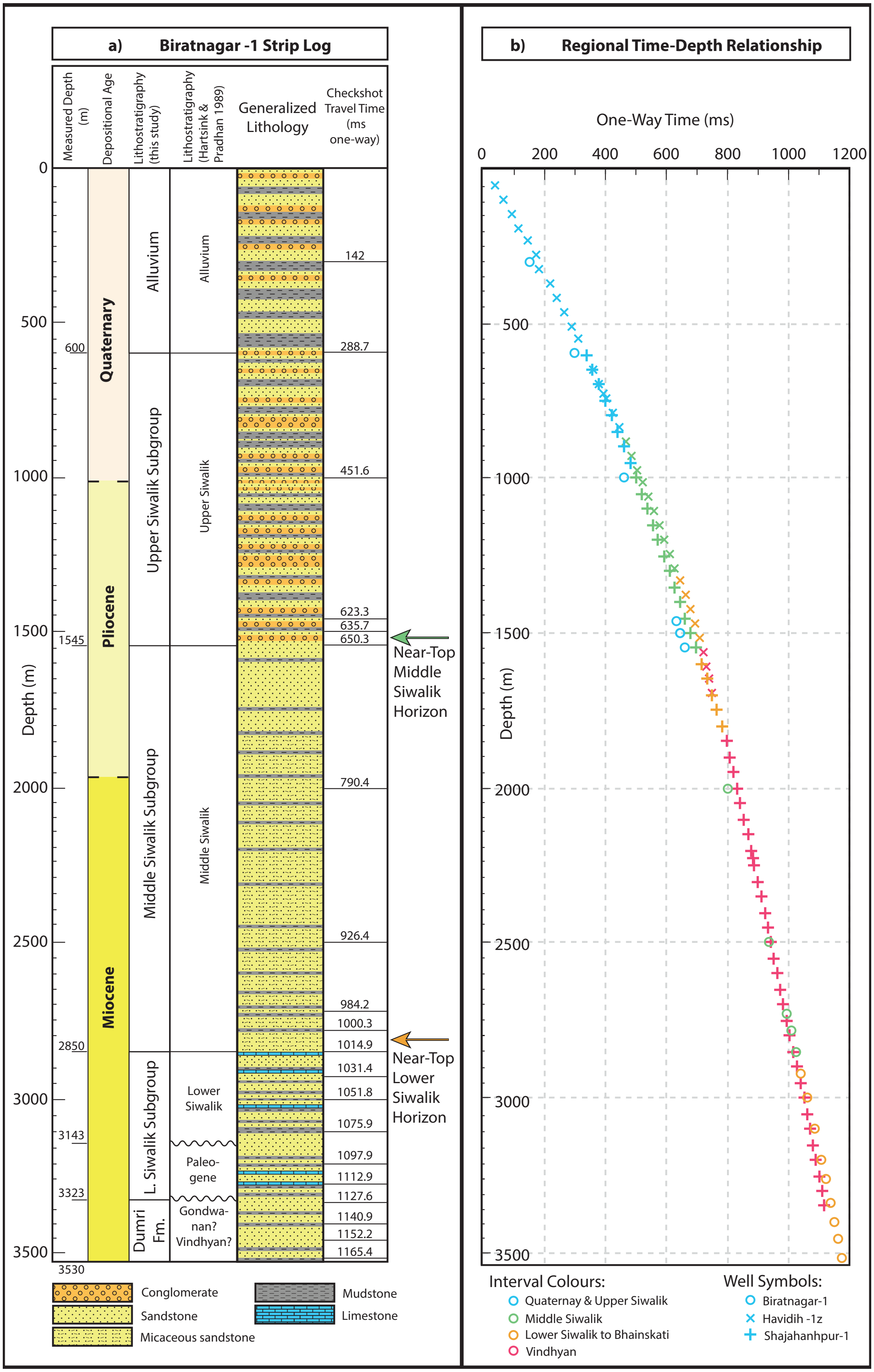
a) Biratnagar -1 Strip Log
Measured Depth (m)
Depositional Age
Lithostratigraphy (this study)
Lithostratigraphy (Hartsink & Pradhan 1989)
Generalized Lithology
Checkshot Travel Time (ms one-way)
Depth (m)
Quaternary
Pliocene
Miocene
Alluvium
Upper Siwalik Subgroup
Middle Siwalik Subgroup
L. Siwalik Subgroup
Dumri Fm.
Upper Siwalik
Middle Siwalik
Lower Siwalik
Paleo-gene
Gondwa-nan? Vindhyan?
Near-Top Middle Siwalik Horizon
Near-Top Lower Siwalik Horizon
Conglomerate
Sandstone
Micaceous sandstone
Mudstone
Limestone
b) Regional Time-Depth Relationship
One-Way Time (ms)
Depth (m)
Interval Colours:
Quaternay & Upper Siwalik
Middle Siwalik
Lower Siwalik to Bhainskati
Vindhyan
Well Symbols:
Biratnagar-1
Havidih -1z
Shajahanhpur-1

is correlated across the study area. It was tied to Biratnagar-1 at the shallowest high-amplitude trough found below the Middle Siwalik subgroup.

The internal stratigraphy of the Middle Siwalik Subgroup is imaged as a tightly packed interval of positive and negative moderate amplitudes with dominant wavelengths ranging from 20 to 70 ms. Reflections merge and diverge laterally over distances of 200 to 500 m, consistent with equivalent exposed strata that are channelized fluvial facies (Corvinus and Rimal, 2001). The near-top Middle-Siwalik reflector (green) is picked as a thin laterally continuous peak. This seismic character was established in Biratnagar-1, and interpreted throughout the Ganga basin.

Sedimentary strata in the upper part of the seismic section, above the near-top Middle-Siwalik reflector, are attributed to the Upper Siwalik Subgroup and the overlying Quaternary alluvium. In seismic profiles, these strata are represented by a mix of medium amplitude, laterally continuous reflections, and highly discontinuous, low amplitude reflections. Some reflections are continuous over more than 15 km, while others rapidly change character over distances of a few hundred metres. The wavelengths of reflections range from 20 to 40 ms. These observations are consistent with a proximal fluvial environment (Kumar and Tandon, 1985), where floodplains manifest themselves as laterally extensive reflectors, and channel deposits are expressed as closely spaced changes in seismic character.

As the seismic data consist of four independent surveys, there are gaps between the blocks of seismic data. These gaps create uncertainty in the longitudinal continuity of several picks. These gaps range in width from 9 to 60 km (Fig. 2-1c). One gap partially coincides with the previously mapped location of the Faizabad ridge, restricting our ability to make interpretations directly above it. To reduce uncertainty across each gap, uninterpreted dip- and strike- profiles were compared to their cross-gap counterparts. Prominent reflections were aligned, and once a satisfactory match was found, seismic horizons were visualized and interpreted across each gap. The top-of-basement nonconformity is easily tracked across each gap due to the lack of lateral continuity of reflections in the basement, and the Sub-Cenozoic unconformity is also confidently identified via discordances and changes in dip. The near-top Middle Siwalik and Lower Siwalik horizons are interpreted via less obvious seismic signatures and stratigraphic correlation; their location relative to stronger reflections was used to correlate across gaps.

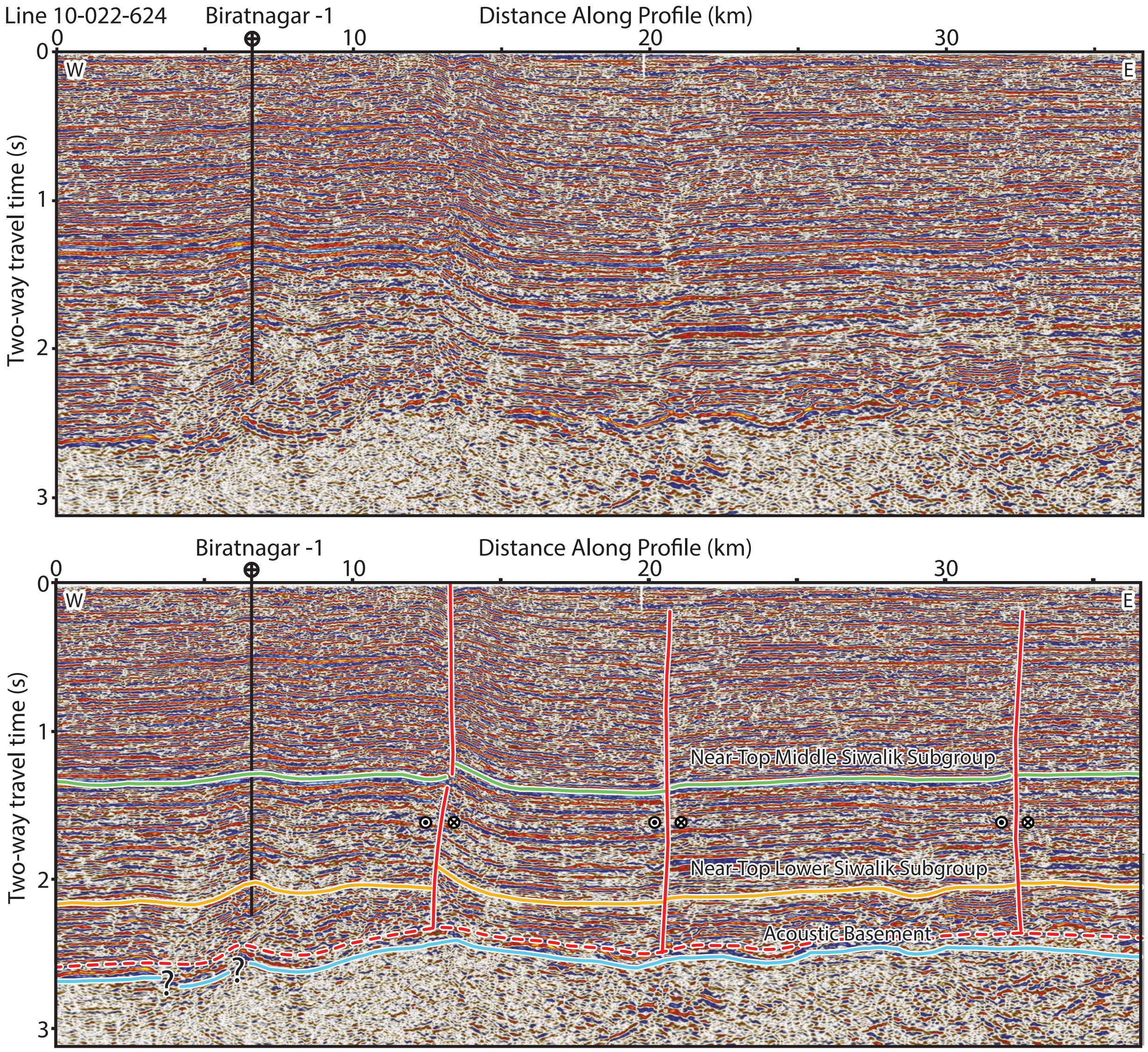

Fig. 2-5. Illustration of well tie, seismic character of the foreland basin fill, and tear faults Uninterpreted (top) and interpreted (bottom) along-strike seismic profile line 10-022-624 in Block 10 above the Munger-Saharsa ridge. Correlation to Biratnagar-1 well is shown. Three steep vertical faults are observed, accompanied by damage zones. Damage zones of the various faults are bordered by contractional and extensional folds. Faults influence Cenozoic strata as shallow as 100 m depth, and are interpreted as strike-slip tear faults. Both sinistral and dextral senses of movement are interpreted in the area. The Sub-Cenozoic unconformity is interpreted to coincide with the acoustic basement along this profile. Line location seen in Figure 2-1c. This scale is equivalent to an approximate vertical exaggeration of 2.5 assuming an average velocity of 4 km/s.

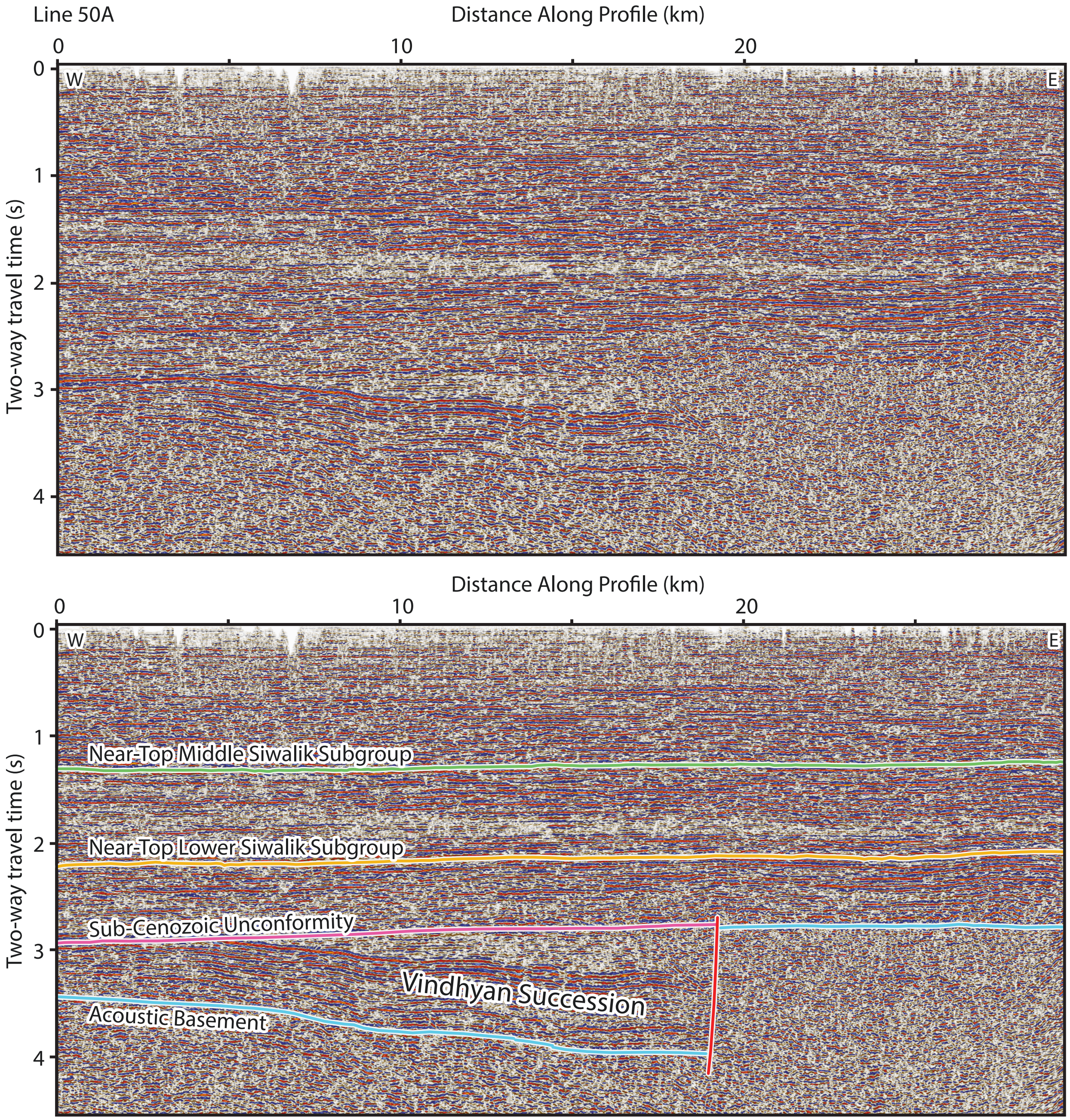

Fig. 2-6. Typical seismic character of the foreland basin fill, above the East Patna half graben Uninterpreted (top) and interpreted (bottom) along-strike seismic profile of line 50A in the Eastern Block showing the typical character of reflections in the study. Red line marks Sub-Cenozoic normal fault that spatially correlates with the East Patna fault. Basement strata show ~2600 m dip separation, producing a Vindhyan filled half-graben. Faulting predates overlying Cenozoic strata. Line location shown in Figure 2-1c. This scale is equivalent to an approximate vertical exaggeration of 2.5 assuming an average velocity of 4 km/s.

To supplement the seismic and well data, we examined key outcrop sections described previously in the fold-thrust belt of Central Nepal (Fig. 2-3; Appel et al., 1991; Quade et al., 1995; Rösler et al., 1997; DeCelles et al., 1998b; Mugnier et al., 1999; Szulc et al., 2006; Ojha et al., 2009; Regumi et al., 2011). Two of the main seismic reflectors were observed (the top of the Lower and Middle Siwalik Subgroups), and showed strong prominence and lateral continuity at outcrop and mountainside scale (Fig. 2-3).

2.3.4 Faults

Faults and folds at seismic scale within the sedimentary package are relatively uncommon, except close to the trace of the MFT, with the result that most strata lie flat and undisturbed (e.g. Fig. 2-6 from 0 to 2.8 s TWT). Interpreted faults in the seismic data coincide with areas of low signal coherence across which reflections are offset. Most faults are only identified on single lines, but within the area of closely spaced lines in Block 10, steep faults striking NNW-SSE and NNE-SSW, interpreted as tear faults above a new frontal thrust can be correlated between lines; these will be discussed in Chapter 3.

2.3.5 Subsurface structure and isopach maps

Subsurface structure and isopach maps were constructed from horizon picks on seismic profiles, and form the basis for our interpretation of regional structure and stratigraphic distributions (Figs. 2-8, 2-9). All maps and observations portray elevations above sea level unless otherwise stated; hence the majority of elevations are negative in the subsurface. Our maps are built exclusively from depth-converted horizon picks on seismic profiles, which correspond approximately to unit boundaries in the Biratnagar-1 well. All maps are generated using a convergent interpolation algorithm in PetrelTM software. Because of the large area covered, the small scale of the maps, and the wide line spacing, fault polygons were not separately outlined prior to gridding; faults therefore show as localized steep gradients. Initial maps using isotropic gridding produced 'bulls-eye' artefacts, due to variable data densities and gradients along and across strike. These artefacts were mitigated by using a rectangular gridding interval of 600 x 200 m. The long axis of this contouring grid is oriented at an azimuth of 110°, approximately parallel to the orogen. This rectangular grid smooths artefacts where the widely spaced dip lines encounter local highs that are restricted to single lines, and more effectively approximates the results of hand contouring. The anisotropic grid also better accounts for the overall effects of flexure of the Indian plate on foreland basin geometry (Lyon-Caen and Molnar, 1985).

2.4 Observations and results

2.4.1 Features of the structure maps

Figure 2-8 shows the structural elevation of the depth-converted horizons representing near-top Middle Siwalik Subgroup (green horizon), near-top Lower Siwalik Subgroup (orange horizon), Sub-Cenozoic unconformity (pink horizon), and acoustic basement (blue horizon). Figure 2-10 shows an along-strike cross section built from the structural elevation maps (line of section shown on Fig. 2-1).

Figure 2-8d shows the elevation structure of the nonconformity between the igneous and metamorphic rocks of the Indian basement (acoustic basement; pink horizon) and the overlying sedimentary deposits. In Block 10, the Munger-Saharsa ridge is recognizable on this surface as a feature that peaks at -3000 m to -4000 m. This regional high extends northwards to the MFT, and is locally cut by smaller-scale features interpreted as normal faults of ~275 to 950 m separation that may have been active during deposition of the overlying Vindhyan to Gondwanan successions. The western edge of the ridge is marked by the East Patna fault, a normal fault with ~2500 m dip separation that offsets the acoustic basement (Figs. 2-1c, 2-6). West of the East Patna fault, the basement gradually shallows, and then deepens into the Gandak depression (Fig. 2-8d). The Gandak depression is characterized by seismic reflections beyond the maximum survey depth (6 s TWT), corresponding to depths of at least 12 km; hence the top-of-basement unconformity was not interpreted in this area, and the mapped elevations result from interpolation between the eastern and western blocks. Along the western margin of the Gandak basin, a gradational shallowing of the basement nonconformity is observed towards the eastern flank of the Faizabad ridge. West of the inferred Faizabad ridge (where data are lacking), the acoustic basement displays depths typically between -6200 and -6700 m, with local basement highs between -5000 m and -5100 m in the easternmost portion of the Western Block. Directly west of the eastern edge of the western block, the basement undulates to form a small trough fluctuating from -8600 m to -5800 m, suggesting a more complex topography than the Dudwa ridge interpreted in this region (e.g. by Raiverman, 2002). At the west end of the Western Block, the basement gently dips north at elevations of ~ -5500 to -6500 m. North of the MFT, acoustic basement depth was too difficult to interpret because of general incoherency in the profiles probably due to the deformation in the subsurface or difficult data acquisition conditions in the more rugged topography.

The Sub-Cenozoic unconformity (pink horizon) structure map shows much more gradational changes in slope throughout, except in some parts of Block 10 where it coincides with the top of acoustic basement (Fig. 2-8c). A northward-deepening trend continues north of the MFT beneath the Deukhuri, Dang, and Chitwan intermontane basins. However, in Block 10 and the Western Block, the unconformity locally shallows northward within ~10 km of the surface trace of the MFT, here interpreted as the result of deformation close to the MFT. A prominent structural high correlating with the Munger-Saharsa ridge occurs in Block 10, where the elevation of the unconformity ranges between -2800 m to -4000 m below sea level. The unconformity is at its deepest in a wide basin in the Eastern and Central Blocks, corresponding to the Gandak depression, where elevations range from -4700 m to -5700 m below sea level. To the west, a shallowing of the Sub-Cenozoic unconformity corresponds to the interpreted location of the Faizabad Ridge. Two discrete depressions, with depths -5500 m to -5800 m occupy the Western Block: a small structural high exists in the southwest extremity of this block, to the west of the inferred Dudwa ridge of Raiverman (2002). This boundary separates low-density foreland basin strata (2150 – 2250 kgm^{-3} in the Havidh-1z well) from higher density Vindhyan strata (Gaur, 2009). The depth ranges estimated here are broadly consistent with the Bouguer gravity anomaly shown by Godin and Harris (2014).

The near-top Lower Siwalik (orange) horizon shows comparable morphology to the Sub-Cenozoic unconformity, though the surface is much shallower. Regionally, dramatic gradients in slope of the near-top Lower Siwalik reflection are rare. The surface displays regional northward deepening, progressing from southern highs between -2000 and -2700 m (Fig. 2-8b) to northern depths of -2800 to -3800 m. However, this gradient is noticeably steeper in Block 10 and the Eastern Block, where the surface shallows 1000 m over a distance of 35 – 40 km (corresponding to a dip of ~1.6°). In the Western and Central Blocks ~500 m shallowing is seen over 26 km (dip ~1.1°). Similar to the Sub-Cenozoic unconformity, a regional depression (-3700 m) is observed in the Eastern Block, and two smaller troughs are seen in the Western Block (-3100 m; Fig. 2-8b). The Western and Central Blocks are bridged longitudinally by a gently sloped structural high, which shallows to -2200 m and spatially correlates with the Faizabad ridge. The near-top Lower Siwalik horizon also shallows in Block 10, reaching elevations of -2600 to -2300 m coinciding with the Munger-Saharsa ridge. The near-top Lower Siwalik reflection also shallows locally near the MFT. Elevations in the Deukhuri and Chitwan basins are comparable with those south of the MFT. However, the near-top Lower Siwalik reflection is significantly shallower in the Dang basin, suggesting that it has been elevated by Sub-Himalayan thrust faulting. At the extreme southeast extremity of Block 10, a gentle fold in near-top Lower Siwalik surface extends between two steep strike-slip faults (Figs. 2-7, 2-11). We interpret this feature as a

Fig. 2-7. Map of subsurface structures interpreted above the Munger-Saharsa Ridge
Map of Block 10, showing faults identified by seismic interpretation, supplemented with field mapping by the Nepal Department of Mines and Geology (Pradhan et al., 2006). The near-top Middle Siwalik elevation surface is shown, highlighting sharp elevation changes along tear faults, and an anticline located in the Southeast corner of Block 10. A marks the location of line 10-022-624 shown in Figure 2-5. B and C mark locations of profiles 10-073-565-2 and 10-21-195 respectively, shown in Figure 2-11. MCT = Main Central Thrust. MBT = Main Boundary Thrust. MFT = Main Frontal Thrust. NFT = New Frontal Thrust.

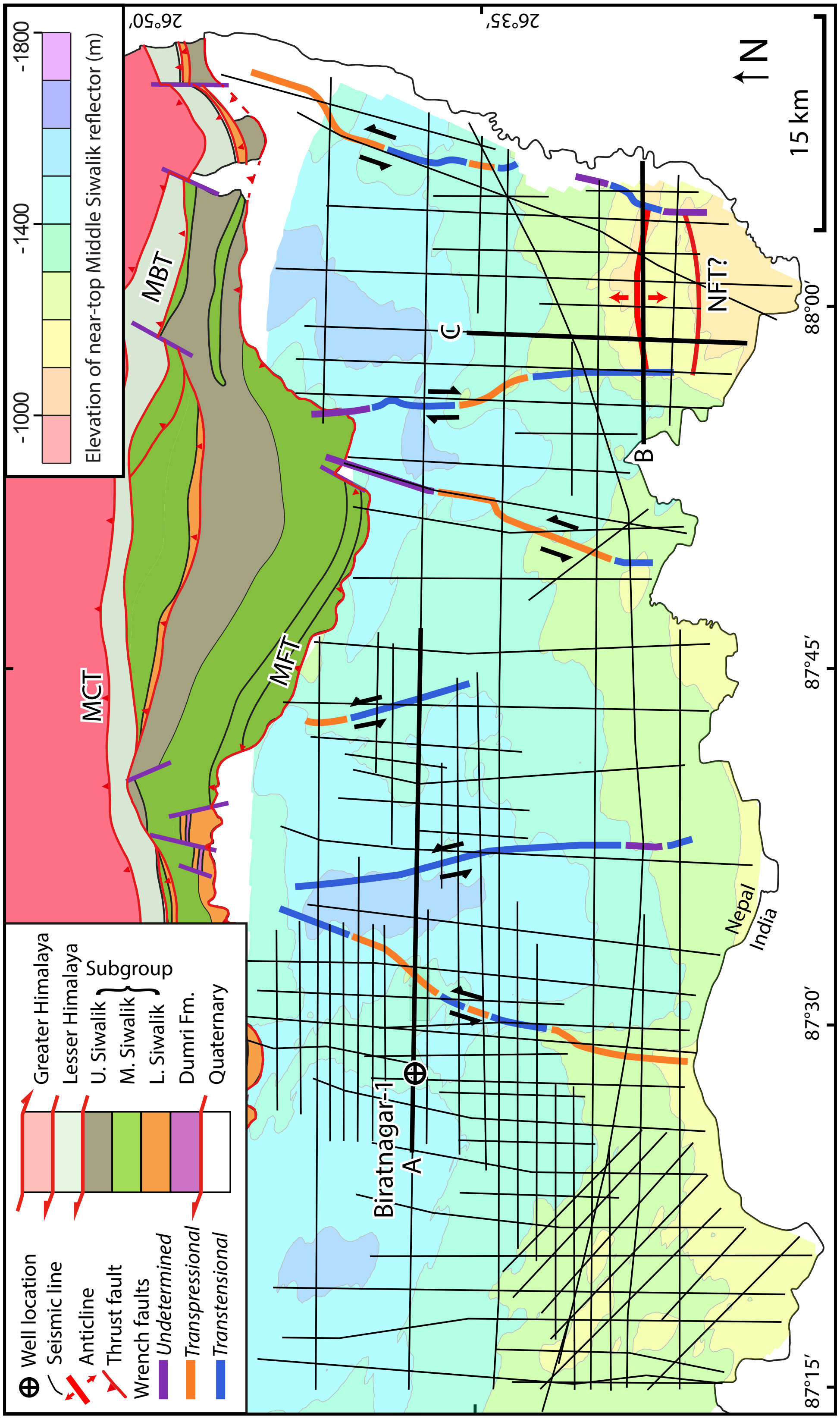
Well location
Seismic line
Anticline
Thrust fault
Wrench faults
Undetermined
Transpressional
Transtensional
Greater Himalaya
Lesser Himalaya
U. Siwalik
M. Siwalik
L. Siwalik
Subgroup
Dumri Fm.
Quaternary
Elevation of near-top Middle Siwalik reflector (m)
-1000
-1400
-1800
MCT
MBT
MFT
NFT?
Biratnagar-1
A
B
C
Nepal
India
N
15 km
87°15′
87°30′
87°45′
88°00′
26°50′
26°35′

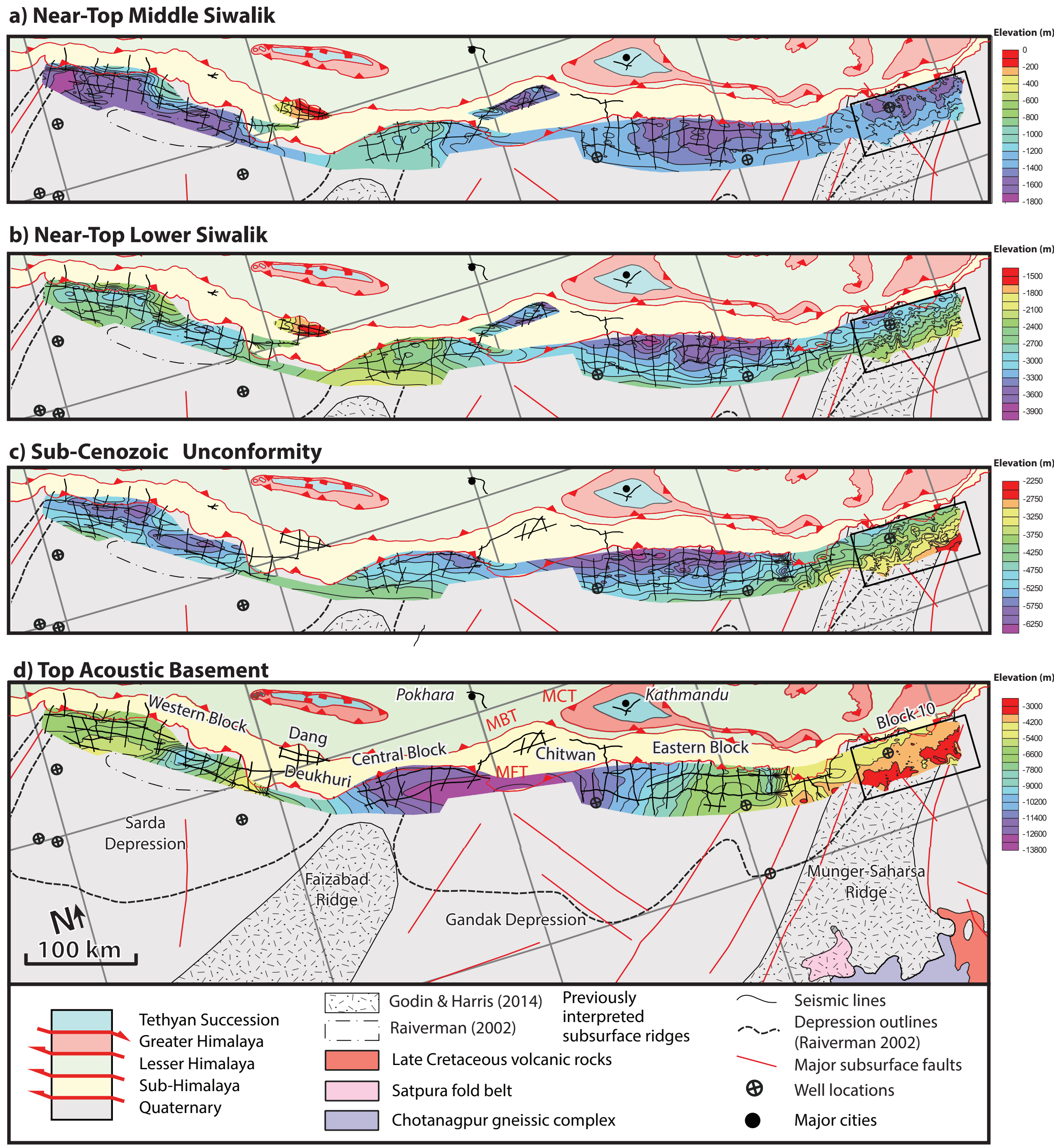

Fig. 2-8. Structural maps of regional marker horizons

Structural maps of the: (a) near-top Middle Siwalik Subgroup, (b) near-top Lower Siwalik, (c) Sub-Cenozoic unconformity, and (d) acoustic basement. Elevations are relative to sea level. Note that the colour scale represents different elevation ranges in each map. Major structural features have been included, from Godin & Harris (2014) and Raiverman (2002).

fault-propagation fold above a blind thrust, here termed the New Frontal Thrust (NFT) that has propagated into the basin from the MFT, described in more detail in chapter 3.

Figure 2-8a shows the elevation of the near-top Middle Siwalik (green) reflector. The surface varies regionally from -1000 to -1700 m. In comparison to underlying horizons, the near-top Middle Siwalik is relatively uniform, reaching similar depths in all blocks. Regional northward deepening at 1-2° is again observed. A localized high in Block 10 coincides with an interpreted blind NFT at depth (Figs. 2-7, 2-11). Close to the MFT, in the Central and Western Blocks, this horizon shallows abruptly northward at steeper angles (dips 5°-11°), probably due to deformation associated with the thrust front (Fig. 1-8). Deformation is also probably responsible for the higher elevation of this reflector in the Deukhuri and Dang intermontane basins; the elevation of this reflector in the Chitwan basin is comparable to that in the Central Block to the south of the MFT. Regional high points at approximately -1200 to -900 m are observed in portions of the Western Block. Along strike, regional low points (-1600 to -1700 m) occur in the centre of the Eastern, Central and Western Blocks. Local highs are seen at the eastern edge of the Western Block, corresponding to the western flank of the Faizabad ridge; and between the Eastern and Central Blocks. A gentle high corresponds to the western portion of the Munger-Saharsa ridge.

2.4.2 Isopach map features

True stratigraphic thicknesses were calculated from the depth-converted structural surfaces discussed in the previous section, and converted into isopach maps (Fig. 2-9). The isopach intervals range: (1) from the acoustic basement to the Sub-Cenozoic unconformity (Fig. 2-9d); (2) from the Sub-Cenozoic unconformity to the near-top Lower Siwalik (Fig. 2-9c); (3) from the near-top Lower Siwalik to the near-top Middle Siwalik (Fig. 2-9b); and (4) from the near-top Middle Siwalik to the topographic DEM surface (Fig. 2-9a). The maps represent progressively shorter time intervals from Proterozoic to present.

Figure 2-9d shows the stratigraphic thickness of the rock units between the acoustic basement and the Sub-Cenozoic unconformity, consisting mainly of Vindhyan strata, and possible Gondwanan strata. The thickness of this interval varies dramatically, from 0 to > 7000 m. The thickness is highly variable in Block 10, related to the presence of normal faults, and onlap onto the basement (Fig. 2-11). The Vindhyan succession is absent in some portions of Block 10, and less than 1 km thick elsewhere. The interval is also less than 1 km thick at the

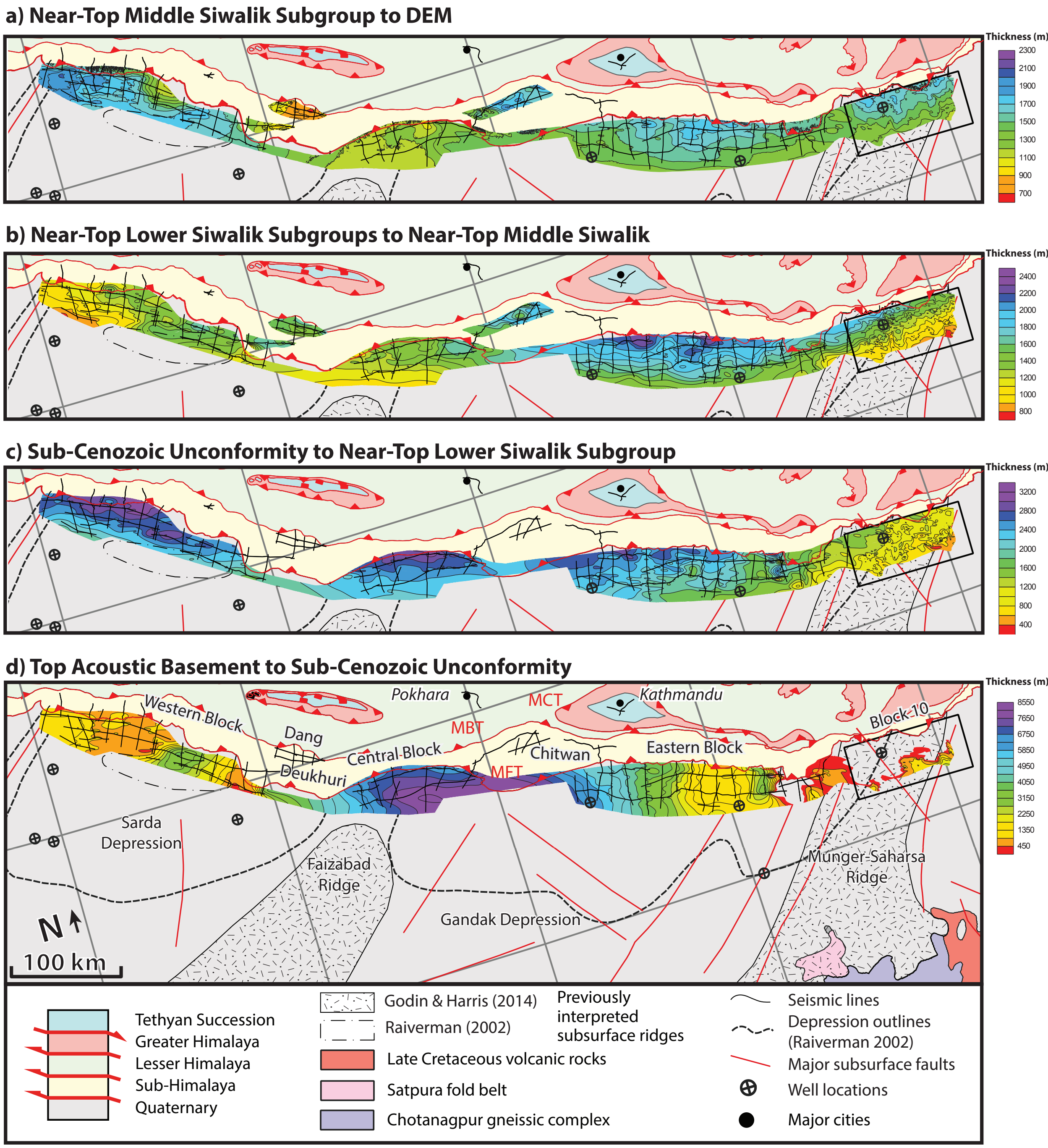

Fig. 2-9. Isopach maps of regional marker horizons

Isopach maps of the: (a) Surface to near-top Middle Siwalik, (b) near-top Middle Siwalik to near-top Lower Siwalik, (c) near-top Lower Siwalik to Sub-Cenozoic unconformity, and (d) Sub-Cenozoic unconformity to acoustic basement. Note that the colour scale represents different elevation ranges in each map. Major structural features have been included, from Godin & Harris (2014) and Raiverman (2002).

east and west ends of the Western Block. This interval is appreciably thicker in the Gandak depression, and in a small trough in the centre of the Western Block.

The stratigraphic thickness between the Pre-Cenozoic unconformity horizon and the near-top Lower Siwalik horizon encompasses the Lower Siwalik Subgroup, the Dumri Formation, and the Bhainskati Formation (and equivalents; Fig. 2-2e). The thickness of this interval ranges from ~2800 m in the foredeep of the Western and Central Blocks, to < 800 m in block 10 (Fig. 2-9c). The interval appears to thicken both from south to north and from east to west (Fig. 2-9c). Local thin areas occur at the eastern edge of the Western Block and in Block 10 (Fig. 2-9c).

The thickness of the near-top Lower Siwalik to the near-top Middle Siwalik interval ranges from ~700 m to 2200 m (Fig. 2-9b). The interval thickens in the order of 600 to 1000 m from south to north. The interval also increases in thickness from east to west (Fig. 2-9b). Three regional thin areas are seen: a thinning to >800 m in the westernmost part of the study area, thinning to >750 m in the western part of the Central Block, and an overall thinning along strike from the Eastern Block to Block 10 (Fig. 2-9b). The Block 10 area shows thinning over a 145 km wide swath, directly over the Munger-Saharsa ridge. A subtler thickness gradient is seen in the Central Block, where ~500 m of thinning occurs over 45 km. Thickness reaches a maximum in the foredeep of the Eastern Block, correlating with the Gandak depression (Srinivasan and Khar, 1996).

The thickness between the near-top Middle Siwalik and the surface (DEM), encompassing the unlithified Quaternary alluvium and the Upper Siwalik Formation, ranges from ~1100 m to ~ 2000 m (Fig. 2-9a). The Western Block contains the thickest and thinnest areas, the thinnest areas occurring close to the MFT. Elsewhere, the interval generally thickens northward, but notably shows a thickness minimum near the postulated Faizabad ridge (Fig. 2-9a).

2.5 Discussion

2.5.1 Geometry and development of the Ganga Basin

Isopach and structural maps generated from the seismic data display a regional geometry consistent with a classic foreland basin (Figs. 2-8, 2-9). A gentle northward deepening/thickening of Cenozoic horizons/intervals reflects a gentle slope from the southern edge of the study area towards the foredeep. The Siwalik horizons are locally shallower along the northern extremities of the basin, reflecting the local influence of thrust faults and related folds near the MFT (Fig. 2-8a, b).

Our data show that the geometry of the crystalline basement is highly irregular, and partly controlled by normal faults (e.g. Figs. 2-6, 2-8d). Much of this basement topography is filled by Vindhyan/Gondwanan sedimentary successions. However, three highs in the Sub-Cenozoic unconformity – roughly consistent with the location of the Munger-Saharsa & Faizabad ridges, and a third local high at the west end of the Western Block – act as major controls on accommodation across the basin. The Vindhyan/Gondwanan successions are regionally thinned above these ridges, or, in the case of the Munger-Saharsa ridge, longitudinally discontinuous (Fig. 2-9d). The western edge of the Munger-Saharsa ridge best spatially correlates to the East Patna Fault, while the Lucknow fault is the western boundary of a half graben to the west of the Faizabad ridge (Fig. 2-10). Both these faults coincide with crustal-scale lineaments mapped by Godin and Harris (2014), and do not cut the Cenozoic strata. The majority of the sub-Cenozoic strata are restricted to the intervening Gandak and Sarda depressions, where Vindhyan/Gondwanan successions occur in distinct basins while the Sub-Cenozoic unconformity marks their upper boundary (Fig. 2-9d). Small half-grabens of Vindhyan or Gondwanan strata occur on and around the flanks of the Munger-Saharsa ridge (e.g. Fig. 2-6). The major ridges and depressions continue south into India, and maintain a consistent geometry (Valdiya, 1976; Raiverman, 1983; Raiverman et al., 1994; Shukla and Chakraborty, 1994; Srinivasan and Khar, 1996).

The Sub-Cenozoic unconformity is a discrete horizon showing up to 15° of discordance. Above the unconformity, the youngest foreland basin deposits gently undulate from NW to SE, relatively unperturbed by faults except around the two basement highs and close to the MFT (Figs. 2-8ab, 2-10, 2-11). None of the major faults that control the basement ridges and the distribution of Vindhyan to Gondwanan strata appear to cut this surface, suggesting that the structural features in the overlying Ganga Basin were dominantly controlled by flexure of the basement, and not by fault reactivation.

The overall structural geometry of the Ganga Basin highlighted by our regional markers suggests that differential subsidence has played (and likely continues to play) a significant role in generating accommodation. All basement lows correspond to thick successions in the Cenozoic strata, whereas all basement highs also correspond with thinner overlying strata. Structural lows correlate with those seen in Indian seismic data (Raiverman et al., 1994). Thus the Gandak and

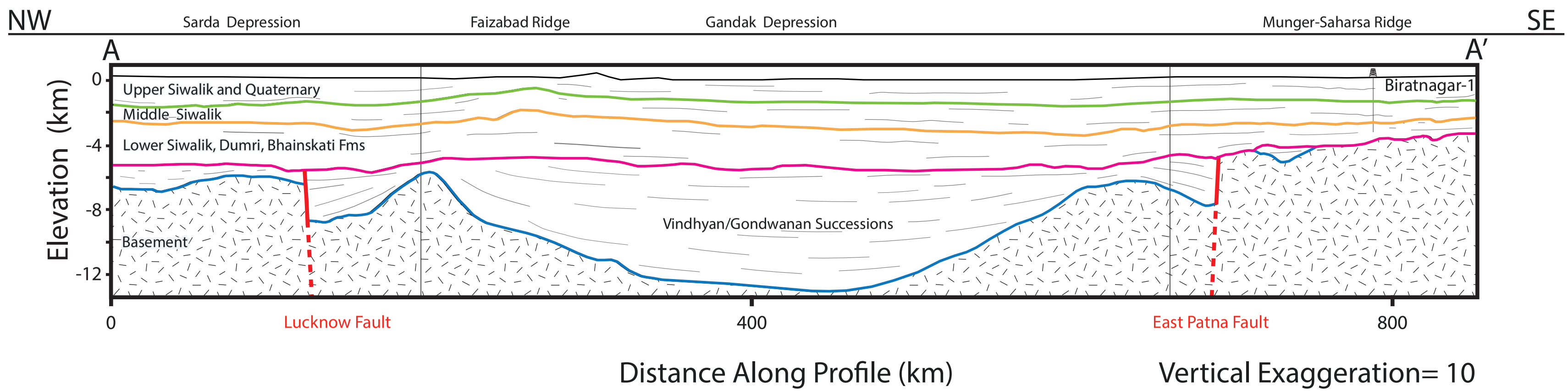

Fig. 2-10. Cross-section of the Ganga foreland basin derived from depth-converted seismic data
Longitudinal profile A-A' spanning the Ganga Basin of Nepal from west to east. Vertical lines represent changes of profile direction. Basement faults from Godin and Harris (2014) have been projected on the profile. Line of section shown on Figure 2-1.

Sarda depressions probably extend from the Indian continental interior up to (and likely beyond) the Main Frontal Thrust to the north (Raiverman et al., 1994).

Isopach maps representing the thicknesses of the foreland basin strata shed light on the timing of basement-influenced subsidence. The two deepest Cenozoic intervals (between the Sub-Cenozoic unconformity and the near-top Middle Siwalik surface) show the most substantial changes along-strike (Fig. 2-9b). They are thickest in the Gandak and Sarda depressions, where thicknesses approach three times that above the Munger-Saharsa ridge. These intervals also thin above local highs of the Western Block. We infer that the Cenozoic successions are similarly thin above the Faizabad ridge, although the data density is low in this region. These thickness trends are gradual; none of the faults that cut the Gondwanan/Vindhyan successions appear to cut the Cenozoic succession. Overall, the thickness variation in the foreland basin strata suggests these depressions were subsiding at least as recently as Middle Siwalik deposition, but this differential subsidence likely continues to the present day.

The spatial distribution of basement ridges and depressions identified in this study can be compared with those postulated by previous works (Raiverman et al., 1994; Godin and Harris, 2014). In Block 10 and the Eastern Block, the Munger-Saharsa ridge correlates well with previous estimates of its position (e.g. Godin & Harris 2014). However, Figure 2-8 shows that the western edge of this ridge closely correlates to the East Patna fault, farther west than the position shown by Godin & Harris (Fig. 2-10; 2014). As illustrated in the isopach maps (Figure 2-9) the effect of this ridge declines up section, suggesting that control by the Munger-Saharsa ridge was most important during early stages of foreland basin subsidence.

A dramatic depression in the western half of the Eastern Block corresponds to the Gandak depression (e.g. Raiverman, 2002). A portion of this depression is also preserved beneath the Chitwan Dun basin, north of the MFT within the thrust belt (Fig. 2-8c, d). The western margin of the Gandak depression, marking the eastern edge of the postulated Faizabad ridge and associated lineaments (Godin and Harris, 2014; Godin et al., 2019) is complex. A thick Vindhyan basin, centred under the western part of the Central Block, thins westward towards a prominent positive feature near the eastern edge of the Western Block, approximately ~100 km west of the approximated ridge trace and associated lineaments (Godin and Harris, 2014; Godin et al., 2019). The Sub-Cenozoic unconformity shows at most a minor positive feature centered slightly west of the Godin & Harris (2014) position. However, higher Siwalik surfaces suggest distinct upwarp across the postulated ridge. Isopach maps and the regional cross section (Figs. 2-9, 2-10)

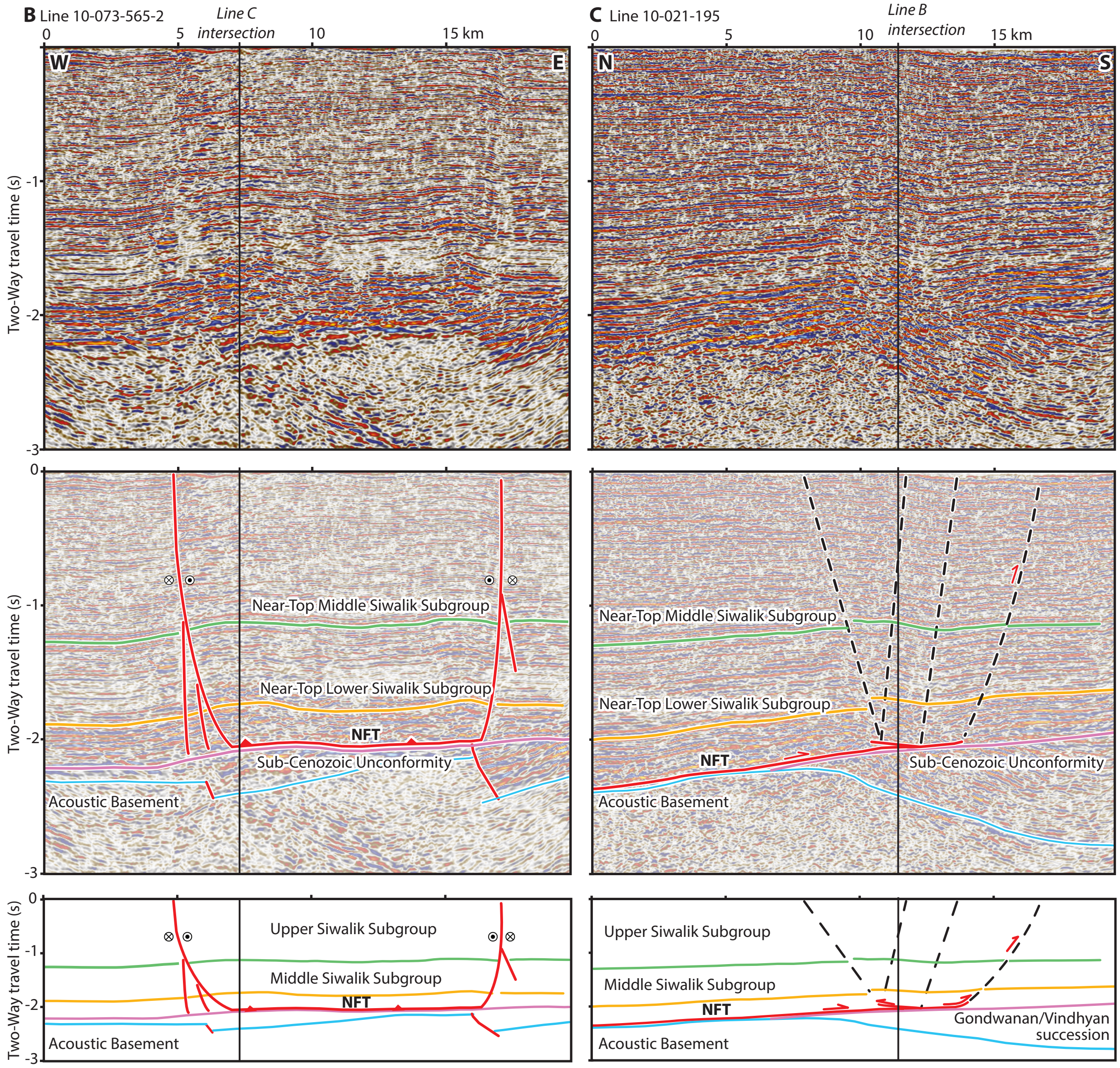

Fig. 2-11. Subsurface thrusting and folding below the Bhadrapur High
Uninterpreted (top), interpreted (middle), and natural scale interpretations of seismic profiles (B) 10-073-565-2 and (C) 10-21-195 in Block 10. Line locations shown in Fig. 2-7. Red lines denote faults. Axial traces related to thrust propagation shown with dashed lines. NFT = New frontal thrust. Lower sections shown at natural scale (1:1) for a velocity of 4 km/s.

show that most of the upwarp was acquired during deposition of the Upper Siwalik Subgroup. This leads us to infer that the influence of the Faizabad Ridge (and ridge bounding faults) on subsidence has increased over time.

2.5.2 Basin dynamics

Several studies have scrutinized the development of along-strike heterogeneities in the Ganga basin, invoking mechanisms such as basement composition, pre-deformation basin thicknesses, and basement faulting to explain the pattern of spurs and depressions on the Indian plate (Raiverman et al., 1994; Prasad et al., 2011; Mitra et al., 2011; Godin and Harris, 2014). Significant variation in crustal seismic velocity ratios are seen along-strike (Mitra et al., 2011). This reflects changes from granitic to mafic compositions as the foreland basin oversteps from east to west the Shillong plateau, Chotanagpur gneissic complex, Bundelkhand craton, and Rajasthan craton (Fig. 2-1b). Contrasts from this change in bulk chemistry may play a role in the subsidence pattern observed, such as longitudinal thermal heterogeneities produced by changes in radiogenic heat production (Kumar et al., 2009).

How have these basement heterogeneities controlled subsidence in the Ganga Basin? The basin and spur geometry of the Ganga foreland basin has been rationalized as a series of horsts and grabens, driven by movement along deep, multiply reactivated crustal scale basement faults (Godin and Harris, 2014; Godin et al., 2019). Lineaments identified by Bouguer anomalies parallel to the edges of the Delhi-Haridwar, Faizabad, and Munger-Saharsa ridges represent surfaces that extend as deep as the base of the Indian lithosphere (Godin and Harris, 2014), and in the case of several ridges, appear to show opposing senses of dip. Several mapped basement faults align with these lineaments, including the Great Boundary, Lucknow, Kishangang, and West/East Patna faults (Valdiya, 1976; Godin and Harris, 2014; Rao et al., 2015). Some of these faults have been interpreted to be active based on observations of recent soft sediment deformation structures (e.g. Verma et al., 2017). Slip along these basement faults could provide a mechanism for the subsidence seen in the intervening basins. However, no obvious faults cut the Cenozoic package along ridge margins, where the Cenozoic succession of the foreland basin smoothly tapers into neighboring basins. Therefore, any slip would have to occur at sub-seismic resolutions. A more likely hypothesis is therefore that the basement lineaments mark longitudinal changes in the flexural rigidity of the Indian lithosphere, which have resulted in the differential accommodation pattern seen in this study (Fig. 2-12).

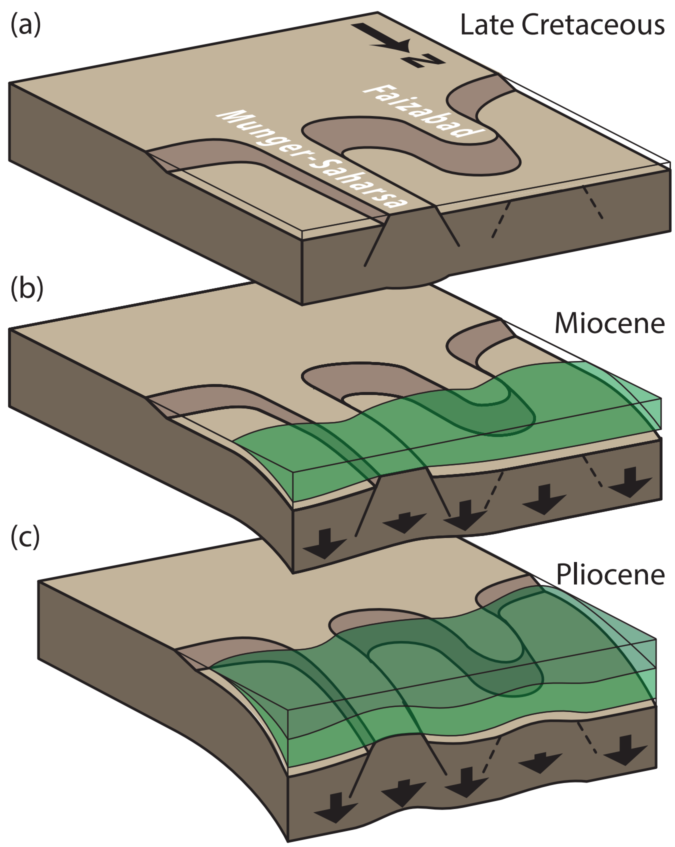

Fig. 2-12. Cartoon showing along-strike thickness variations in the Ganga Basin
Not to scale. Foreland basin fill shown in green. (a) Ridges and basins in the Indian plate prior to Himalayan collision. (b) Flexure of plate under loading by orogen (not shown) leads to progressive differential subsidence of basin. During deposition of the Bhainskati and Dumri Formations, and the Lower Siwalik Subgroup, the Munger-Saharsa ridge acts as an upwarp, and restricts deposition above. (c) During deposition of the Middle and Upper Siwalik Subgroups, the Faizabad ridge shows increasing upwarp, while the Munger-Saharsa ridge shows less influence on subsidence.

2.5.3 Influence of basement structures on the thrust front

Several near-vertical faults are correlated between seismic lines in Block 10, striking NNE-SSW and NNW-SSE. The adjacent strata are offset by local contractional and extensional folds (e.g. Fig. 2-5), particularly where the faults show subtle changes in strike, suggesting that the folds mark restraining and releasing bends on tear faults at high angles to the thrust front allowing the sense of slip to be inferred (Fig. 2-7). In the southeast corner of Block 10 fault-related folds above the fault plane (Figs. 2-7, 2-11) suggest the presence of a detachment surface within or below the Lower Siwalik Subgroup (the NFT). There is no evidence that the thrust crosscuts the tear faults (Fig. 2-7), and the tear faults do not appear to extend deeper than the thrust. This indicates that the tear faults and blind thrust developed simultaneously, and the tear faults sole on the thrust, accommodating forward displacement along the detachment. This geometry is interpreted as a system of tear faults linked to an incipient tectonic wedge above the basement high, that developed as thrusting propagated south of the MFT (Fig. 2-11), as further discussed in Chapter 3.

Similar N-S tear faults in Cenozoic strata, spatially associated with the Delhi-Haridwar ridge (Fig. 2-1b) have been interpreted to be the result of basement fault reactivation (Raiverman et al., 1994). However, the limited data from earthquakes at basement depths beneath Block 10 (Dasgupta et al., 2013) suggest dip-slip movement. Although these tear fault systems are located preferentially above basement ridges, their orientations differ from the basement features (see Chapter 3); it is therefore unlikely that they result directly from basement fault reactivation. We suggest that the basement highs provide indirect control on the nucleation of wrench and thrust faults in the overlying foreland basin, by controlling longitudinal variations in the topography of the sub-Cenozoic unconformity, the thickness of the overlying sedimentary basin, or facies that affect basal friction in the thrust wedge. These parameters have been shown to control thrust propagation and transfer-zone development in analogue models (Calassou et al., 1993).

2.6 Conclusions

Mapping of several regional seismic reflectors has allowed us to evaluate longitudinal changes in geometry and thicknesses of sedimentary successions within the Ganga foreland basin. Cenozoic deposition has been influenced by several fault-bounded crustal-scale structures, oriented at a high angle to the strike of the Himalaya. We show that basement highs, such as the Faizabad and Munger-Saharsa ridges, spatially correlate with depositional minima in overlying strata. In intervening depressions, significant Vindhyan and Cenozoic strata have been accommodated in structural lows. Thickness variations in the sedimentary package above suggest that these structures were active through much of the Cenozoic and that basement structure and/or composition affected the flexural properties of the Indian lithosphere, leading to along-strike segmentation of the foreland basin. This segmentation has not only controlled the thickness and geometry of sedimentary sequences deposited, but also the localization of wrench and thrust faults associated with the Himalayan thrust front. The Munger-Saharsa ridge shows declining influence through time, from the Lower Siwalik to the Upper Siwalik Subgroup. In contrast, the Faizabad ridge area was most prominent during Middle Siwalk deposition. Taken together, these observations are interpreted to show differential subsidence active at different times along the strike of the Ganga Basin. Tear faults, at high angles to the thrust front, have previously been interpreted as the result of reactivation of ridge-bounding faults at depth. Our interpretation of the seismic data suggests that this is not the case. Their localization is related to thrust propagation over the basement ridges and reflects indirect controls by the ridges on the mechanical properties of the overlying foreland basin sedimentary strata.

Acknowledgements

We thank John Clayburn and Cairn Energy for their contribution to the project. Schlumberger's Petrel software licenses donated to the University of Alberta assisted data analysis. Participation by JWFW and LG was supported by National Sciences and Engineering Research Council of Canada Discovery Grants. We acknowledge the use of public geological data from the United States Geological Survey database, accessed from: fttps://catalog.data.gov/dataset/geologic-map-of-south-asia-geo8ag.

2.7 References

Aditya, S., Raju, A.T.R., and Shukla, S.N., 1979, Assessment of hydrocarbon prospects of the sub-Himalayan, Punjab and Ganga basins-India, in Himalayan Geology Seminar New Delhi 1976: Section 3 - Oil and Natural Gas Resources, Geological Survey of India Miscellaneous Publications, v. 41, p. 127–140.

Almeida, R.V., Hubbard, J., Liberty, L., Foster, A., and Sapkota, S.N., 2018, Seismic imaging of the Main Frontal Thrust in Nepal reveals a shallow décollement and blind thrusting: Earth and Planetary Science Letters, v. 494, p. 216–225, doi:10.1016/j.epsl.2018.04.045.

Anders, A.M., Roe, G.H., Hallet, B., Montgomery, D.R., Finnegan, N.J., and Putkonen, J., 2006, Spatial patterns of precipitation and topography in the Himalaya, in Willett, S.D., Hovius, N., Brandon, M.T., and Fisher, D.M. eds., Tectonics, Climate, and Landscape Evolution, Geological Society of America Special Paper, v. 398, p. 39–53, doi:10.1130/2006.2398(03).

Appel, E., Rösler, W., and Corvinus, G., 1991, Magnetostratigraphy of the Miocene-Pleistocene Surai Khola Siwaliks in West Nepal: Geophysical Journal International, v. 105, p. 191–198, doi:10.1111/j.1365-246X.1991.tb03455.x.

Avouac, J.-P., 2003, Mountain Building, Erosion, and the Seismic Cycle in the Nepal Himalaya: Amster, Elsevier, Advances in Geophysics, v. 46, 80 p., doi:10.1016/S0065-2687(03)46001-9.

Balakrishnan, T.S., Unnikrishnan, P., and Murty, A.V.S., 2009, The tectonic map of India and contiguous areas: Journal of the Geological Society of India, v. 74, p. 158–168.

Banks, C.J., and Warburton, J., 1986, 'Passive-roof' duplex geometry in the frontal structures of the Kirthar and Sulaiman mountain belts, Pakistan: Journal of Structural Geology, v. 8, p. 229–237, doi:10.1016/0191-8141(86)90045-3.

Bashyal, R.P., 1998, Petroleum exploration in Nepal: Journal of Nepal Geological Society, v. 18, p. 19–24.

Basuyau, C., Diament, M., Tiberi, C., Hetényi, G., Vergne, J., and Peyrefitte, A., 2013, Joint inversion of teleseismic and GOCE gravity data: application to the Himalayas: Geophysical Journal International, v. 193, p. 149–160, doi:10.1093/gji/ggs110.

van der Beek, P., Litty, C., Baudin, M., Mercier, J., Robert, X., and Hardwick, E., 2016, Contrasting tectonically driven exhumation and incision patterns, western versus central Nepal Himalaya: Geology, v. 44, p. 327–330, doi:10.1130/G37579.1.

Bernet, M., van der Beek, P., Pik, R., Huyghe, P., Mugnier, J.-L., Labrin, E., and Szulc, A., 2006, Miocene to Recent exhumation of the central Himalaya determined from combined detrital zircon fission-track and U/Pb analysis of Siwalik sediments, western Nepal: Miocene to Recent exhumation of the central Himalaya: Basin Research, v. 18, p. 393–412, doi:10.1111/j.1365-2117.2006.00303.x.

Bhattacharyya, A., 1996, Recent advances in Vindhyan geology: Geological Society of India Memoir, v. 36, 331 p.

Biswas, S.K., 1999, A review on the evolution of rift basins in India during Gondwana with special reference to western Indian basins and their hydrocarbon prospects: Proceedings of the Indian National Science Academy - Part A, v. 65, p. 261–284.

Bollinger, L., Avouac, J.P., Beyssac, O., Catlos, E.J., Harrison, T.M., Grove, M., Goffé, B., and Sapkota, S., 2004, Thermal structure and exhumation history of the Lesser Himalaya in central Nepal: Thermal Structure of the Lesser Himalaya: Tectonics, v. 23, p. n/a-n/a, doi:10.1029/2003TC001564.

Bouilhol, P., Jagoutz, O., Hanchar, J.M., and Dudas, F.O., 2013, Dating the India–Eurasia collision through arc magmatic records: Earth and Planetary Science Letters, v. 366, p. 163–175, doi:10.1016/j.epsl.2013.01.023.

Brown, L.D., Zhao, W., Nelson, K.D., Hauck, M., Alsdorf, D., Ross, A., Cogan, M., Clark, M., Liu, X., and Che, J., 1996, Bright Spots, Structure, and Magmatism in Southern Tibet from INDEPTH Seismic Reflection Profiling: Science, v. 274, p. 1688–1690, doi:10.1126/science.274.5293.1688.

Burbank, D.W., Beck, R.A., and Mulder, T., 1996, The Himalayan foreland basin, in Yin, A. and Harrison, T.M. eds., The Tectonic Evolution of Asia, Cambridge, Cambridge University Press, p. 149–188.

Burchfiel, B.C., Zhiliang, C., Hodges, K.V., Yuping, L., Royden, L.H., and Changrong, D., 1992, in The South Tibetan detachment system, Himalayan orogen: Extension contemporaneous with and parallel to shortening in a collisional mountain belt, Geological Society of America - Special Paper, v. 269.

Burgess, W., Yin, A., Dubey, C.S., Shen, Z.-K., and Kelty, T.K., 2012, Holocene shortening across the Main Frontal Thrust zone in the eastern Himalaya: Earth and Planetary Science Letters, v. 357–358, p. 152–167, doi:10.1016/j.epsl.2012.09.040.

Cairn Energy, 2006, Seismic Interpretation - Nepal: Cairn UK Internal Report.

Calassou, S., Larroque, C., and Malavieille, J., 1993, Transfer zones of deformation in thrust wedges: an experimental study: Tectonophysics, v. 221, p. 325–344.

Casshyap, S.M., and Khan, A., 2000, Basin of central India: evidence of pre-Trap doming, rifting and palaeoslope reversal: Journal of African Earth Sciences, v. 31, p. 65–76.

Chatterjee, N., and Ghose, N.C., 2011, Extensive Early Neoproterozoic high-grade metamorphism in North Chotanagpur Gneissic Complex of the Central Indian Tectonic Zone: Gondwana Research, v. 20, p. 362–379, doi:10.1016/j.gr.2010.12.003.

Cohen, K.M., Harper, D.A.T., Gibbard, P.L., and Fan, J.-X., 2013, The ICS International Chronostratigraphic Chart v2018/08: Episodes, v. 36, p. 119–204.

Corvinus, G., and Rimal, L.N., 2001, Biostratigraphy and geology of the Neogene Siwalik Group of the Surai Khola and Rato Khola areas in Nepal: Palaeogeography, Palaeoclimatology, Palaeoecology, v. 165, p. 251–279.

Dasgupta, S., 1993, Tectono-geologic framework of the eastern Gangetic foredeep, in Bihar Nepal Earthquake (August 20, 1988), Geological Survey of India Special Publication, v.

31, p. 61–69.

Dasgupta, S., Mukhopadhyay, B., Mukhopadhyay, M., and Nandy, D.R., 2013, Role of transverse tectonics in the Himalayan collision: Further evidences from two contemporary earthquakes: Journal of the Geological Society of India, v. 81, p. 241–247, doi:10.1007/s12594-013-0027-5.

DeCelles, P.G., Gehrels, G.E., Najman, Y., Martin, A.J., Carter, A., and Garzanti, E., 2004, Detrital geochronology and geochemistry of Cretaceous–Early Miocene strata of Nepal: implications for timing and diachroneity of initial Himalayan orogenesis: Earth and Planetary Science Letters, v. 227, p. 313–330, doi:10.1016/j.epsl.2004.08.019.

DeCelles, P.G., Gehrels, G.E., Quade, J., and Ojha, T.P., 1998a, Eocene-early Miocene foreland basin development and the history of Himalayan thrusting, western and central Nepal: Tectonics, v. 17, p. 741–765.

DeCelles, P.G., Gehrels, G.E., Quade, J., Ojha, T.P., Kapp, P.A., and Upreti, B.N., 1998b, Neogene foreland basin deposits, erosional unroofing, and the kinematic history of the Himalayan fold-thrust belt, western Nepal: Geological Society of America Bulletin, v. 110, p. 2–21, doi:10.1130/0016-7606(1998)110<0002:NFBDEU>2.3.CO;2.

Dhital, M.R., 2015, Geology of the Nepal Himalaya: Cham, Springer, Regional Geology Reviews, 498 p.

Duncan, C., Masek, J., and Fielding, E., 2003, How steep are the Himalaya? Characteristics and implications of along-strike topographic variations: Geology, v. 31, p. 75–78.

Fuloria, R.C., 1996, Geology and hydrocarbon prospects of the Vindhyan sediments in Ganga valley (A. Bhattacharyya, Ed.): Memoirs of the Geological Society of India, v. 36, p. 235–256.

Gahalaut, V.K., and Kundu, B., 2012, Possible influence of subducting ridges on the Himalayan arc and on the ruptures of great and major Himalayan earthquakes: Gondwana Research, v. 21, p. 1080–1088, doi:10.1016/j.gr.2011.07.021.

Gansser, A., 1964, Geology of the Himalayas: London, New York, Interscience Publishers, 289 p.

Garzanti, E., 2019, The Himalayan Foreland Basin from collision onset to the present: a sedimentary–petrology perspective, in Treloar, P.J. and Searle, M.P. eds., Himalayan Tectonics: A Modern Synthesis, Geological Society of London Special Publications, v. 483.

Gaur, M., 2009, Havidih-1 & 1z Well Completion Report: Gurgaon, India, Cairn, 64 p.

Gautam, P., and Fujiwara, Y., 2000, Magnetic polarity stratigraphy of Siwalik Group sediments of Karnali River section in western Nepal: Geophysical Journal International, v. 142, p. 812–824, doi:10.1046/j.1365-246x.2000.00185.x.

Gill, W.D., 1951, The tectonics of the Sub-Himalayan fault zone in the northern Potwar region and in the Kangra district of the Punjab: Quarterly Journal of the Geological Society, v. 107, p. 395–421.

Godin, L., and Harris, L.B., 2014, Tracking basement cross-strike discontinuities in the Indian crust beneath the Himalayan orogen using gravity data – relationship to upper crustal faults: Geophysical Journal International, v. 198, p. 198–215, doi:10.1093/gji/ggu131.

Godin, L., Soucy La Roche, R., Waffle, L., and Harris, L.B., 2019, Influence of inherited Indian basement faults on the evolution of the Himalayan Orogen, in Sharma, R., Villa, I., and Kumar, S. eds., Crustal Architecture and Evolution of the Himalaya–Karakoram–Tibet Orogen, Geological Society of London Special Publication, v. 481.

Goscombe, B., Gray, D., and Foster, D.A., 2018, Metamorphic response to collision in the Central Himalayan Orogen: Gondwana Research, v. 57, p. 191–265, doi:10.1016/j.gr.2018.02.002.

Harrison, T.M., Copeland, P., Hall, S.A., Quade, J., Burner, S., Ojha, T.P., and Kidd, W.S.F., 1993, Isotopic preservation of Himalayan/Tibetan uplift, denudation, and climatic histories of two molasse deposits: The Journal of Geology, v. 101, p. 157–175.

Hartsink, J., and Pradhan, U.M.S., 1989, Well Completion Report - Biratnagar 1: Kathmandu, Shell Nepal B.V.

Hauck, M.L., Nelson, K.D., Brown, L.D., Zhao, W., and Ross, A.R., 1998, Crustal structure of the Himalayan orogen at ~ 90 east longitude from Project INDEPTH deep reflection profiles: Tectonics, v. 17, p. 481–500.

Heim, A., and Gansser, A., 1939, Central Himalaya - Geological Observations of the Swiss Expedition 1936: Hindustan Publishing; Delhi, 246 p.

Hirschmiller, J., Grujic, D., Bookhagen, B., Coutand, I., Huyghe, P., Mugnier, J.-L., and Ojha, T., 2014, What controls the growth of the Himalayan foreland fold-and-thrust belt? Geology, v. 42, p. 247–250, doi:10.1130/G35057.1.

Hu, X., Wang, J., BouDagher-Fadel, M., Garzanti, E., and An, W., 2016, New insights into the timing of the India – Asia collision from the Paleogene Quxia and Jialazi formations of the Xigaze forearc basin, South Tibet: Gondwana Research, v. 32, p. 76–92, doi:10.1016/j.gr.2015.02.007.

Hughes, N.C., Peng, S., Bhargava, O.N., Ahluwalia, A.D., Walia, S., Myrow, P.M., and Parcha, S.K., 2005, Cambrian biostratigraphy of the Tal Group, Lesser Himalaya, India, and early

Tsanglangpuan (late early Cambrian) trilobites from the Nigali Dhar syncline: Geological Magazine, v. 142, p. 57–80, doi:10.1017/S0016756804000366.

Husson, L., and Mugnier, J.-L., 2003, Three-dimensional horizon reconstruction from outcrop structural data, restoration, and strain field of the Baisahi anticline, Western Nepal: Journal of Structural Geology, p. 79–90.

Karunakaran, C., and Rao, A.R., 1979, Status of exploration for hydrocarbons in the Himalayan region-contributions to stratigraphy and structure, in Himalayan Geology Seminar New Delhi 1976: Section 3 - Oil and Natural Gas Resources, Geological Survey of India Miscellaneous Publications, v. 41 (5), p. 1–66.

Kellett, D.A., Cottle, J.M., and Larson, K.P., 2019, The South Tibetan Detachment System: history, advances, definition and future directions, in Himalayan Tectonics: A Modern Synthesis, Geological Society London Special Publications, v. 483, http://sp.lyellcollection.org/lookup/doi/10.1144/SP483.2 (accessed August 2019).

Kellett, D.A., and Grujic, D., 2012, New insight into the South Tibetan detachment system: Not a single progressive deformation: South Tibetan Detachment System: Tectonics, v. 31, p. n/a-n/a, doi:10.1029/2011TC002957.

Krishnan, M.S., 1949, Geology of India and Burma: Madras Law Journal Office; Madras.

Kumar, P.S., Menon, R., and Reddy, G.K., 2009, Heat production heterogeneity of the Indian crust beneath the Himalaya: Insights from the northern Indian Shield: Earth and Planetary Science Letters, v. 283, p. 190–196, doi:10.1016/j.epsl.2009.04.015.

Kumar, R., and Tandon, S.K., 1985, Sedimentology of Plio-Pleistocene Late orogenic deposits associated with intraplate subduction—the Upper Siwalik Subgroup of a part of Panjab Sub-Himalaya, India: Sedimentary Geology, v. 42, p. 105–158.

Lyon-Caen, H., and Molnar, P., 1985, Gravity anomalies, flexure of the Indian plate, and the structure, support and evolution of the Himalaya and Ganga Basin: Tectonics, v. 4, p. 513–538.

Mathur, N.S., 1978, Biostratigraphical aspects of the Subathu Formation, Kumaun Himalaya: Recent Researches in Geology, v. 5, p. 96–112.

McKenzie, N.R., Hughes, N.C., Myrow, P.M., Xiao, S., and Sharma, M., 2011, Correlation of Precambrian–Cambrian sedimentary successions across northern India and the utility of isotopic signatures of Himalayan lithotectonic zones: Earth and Planetary Science Letters, v. 312, p. 471–483, doi:10.1016/j.epsl.2011.10.027.

McQuarrie, N., Tobgay, T., Long, S.P., Reiners, P.W., and Cosca, M.A., 2014, Variable exhumation rates and variable displacement rates: Documenting recent slowing of

Himalayan shortening in western Bhutan: Earth and Planetary Science Letters, v. 386, p. 161–174, doi:10.1016/j.epsl.2013.10.045.

Meert, J.G., Pandit, M.K., Pradhan, V.R., Banks, J., Sirianni, R., Stroud, M., Newstead, B., and Gifford, J., 2010, Precambrian crustal evolution of Peninsular India: A 3.0 billion year odyssey: Journal of Asian Earth Sciences, v. 39, p. 483–515, doi:10.1016/j.jseaes.2010.04.026.

Mitra, S., Kainkaryam, S.M., Padhi, A., Rai, S.S., and Bhattacharya, S.N., 2011, The Himalayan foreland basin crust and upper mantle: Physics of the Earth and Planetary Interiors, v. 184, p. 34–40, doi:10.1016/j.pepi.2010.10.009.

Mohanty, S., 2012, Spatio-temporal evolution of the Satpura Mountain Belt of India: A comparison with the Capricorn Orogen of Western Australia and implication for evolution of the supercontinent Columbia: Geoscience Frontiers, v. 3, p. 241–267, doi:10.1016/j.gsf.2011.10.005.

Monsalve, G., Sheehan, A., Schulte-Pelkum, V., Rajaure, S., Pandey, M.R., and Wu, F., 2006, Seismicity and one-dimensional velocity structure of the Himalayan collision zone: Earthquakes in the crust and upper mantle: Journal of Geophysical Research, v. 111, doi:10.1029/2005JB004062.

Mugnier, J.L., Leturmy, P., Mascle, G., Huyghe, P., Chalaron, E., Vidal, G., and Husson, L., 1999, The Siwaliks of western Nepal: I. Geometry and kinematics: Journal of Asian Earth Sciences, v. 17, p. 629–642.

Mukhopadhyay, G., Mukhopadhyay, S.K., Roychowdhury, M., and Parui, P.K., 2010, Stratigraphic correlation between different Gondwana Basins of India: Journal of the Geological Society of India, v. 76, p. 251–266, doi:10.1007/s12594-010-0097-6.

Najman, Y.M.R., 1997, Laser 40Ar/39Ar dating of single detrital muscovite grains from early foreland-basin sedimentary deposits in India: Implications for early Himalayan evolution: Geology, v. 25, p. 535–538.

Najman, Y., Burley, S.D., Copley, A., Kelly, M.J., Pander, K., and Mishra, P., 2018, The Late Eocene-Early Miocene Unconformities of the NW Indian Intraplate Basins and Himalayan Foreland: A Record of Tectonics or Mantle Dynamics? Tectonics, v. 37, p. 3970–3985, doi:10.1029/2018TC005286.

Najman, Y., Carter, A., Oliver, G., and Garzanti, E., 2005, Provenance of Eocene foreland basin sediments, Nepal: Constraints to the timing and diachroneity of early Himalayan orogenesis: Geology, v. 33, p. 309–312.

Najman, Y., Jenks, D., Godin, L., Boudagher-Fadel, M., Millar, I., Garzanti, E., Horstwood, M., and Bracciali, L., 2017, The Tethyan Himalayan detrital record shows that India–Asia terminal collision occurred by 54 Ma in the Western Himalaya: Earth and Planetary Science Letters, v. 459, p. 301–310, doi:10.1016/j.epsl.2016.11.036.

Najman, Y., Johnson, K., White, N., and Oliver, G., 2004, Evolution of the Himalayan foreland basin, NW India: Basin Research, v. 16, p. 1–24, doi:10.1111/j.1365-2117.2004.00223.x.

Nakayama, K., and Ulak, P.D., 1999, Evolution of fluvial style in the Siwalik Group in the foothills of the Nepal Himalaya: Sedimentary Geology, v. 125, p. 205–224.

Negi, B.S., and Eremenko, N.A., 1968, Tectonic Map of India: Oil and Natural Gas Commission.

Nelson, K.D. et al., 1996, Partially Molten Middle Crust Beneath Southern Tibet: Synthesis of Project INDEPTH Results: Science, v. 274, p. 1684–1688, doi:10.1126/science.274.5293.1684.

Ojha, T.P., Butler, R.F., DeCelles, P.G., and Quade, J., 2009, Magnetic polarity stratigraphy of the Neogene foreland basin deposits of Nepal: Basin Research, v. 21, p. 61–90, doi:10.1111/j.1365-2117.2008.00374.x.

Ojha, T.P., Butler, R.F., Quade, J., DeCelles, P.G., Richards, D., and Upreti, B.N., 2000, Magnetic polarity stratigraphy of the Neogene Siwalik Group at Khutia Khola, far western Nepal: Geological Society of America Bulletin, v. 112, p. 424–434.

Parkash, B., Sharma, R.P., and Roy, A.K., 1980, The Siwalik group (Molasse) — Sediments shed by collision of continental plates: Sedimentary Geology, v. 25, p. 127–159, doi:10.1016/0037-0738(80)90058-5.

Pilgrim, G.E., 1913, The correlation of the Siwaliks with mammal horizons of Europe: Records of the Geological Survey of India, v. 42, p. 264–326.

Pradhan, U.M.S., KC, S.B., Subedi, D.N., Sharma, S.R., Khanal, R.P., and Tripathi, G.N., 2006, Geological Map of Petroleum Exploration Block - 10: Biratnagar, Eastern Nepal: Petroleum Exploration Project, Department of Mines & Geology, Government of Nepal.

Prasad, B., and Asher, R., 2001, Acritarch biostratigraphy and lithostratigraphic classification of Proterozoic and Lower Paleozoic sediments (Pre-unconformity sequence) of Ganga Basin, India: Dehra Dun, Geoscience Research Group, Keshava Deva Malaviya Institute of Petroleum Exploration, Oil and Natural Gas Corporation.

Prasad, B.R., Klemperer, S.L., Rao, V.V., Tewari, H.C., and Khare, P., 2011, Crustal structure beneath the Sub-Himalayan fold–thrust belt, Kangra recess, northwest India, from seismic reflection profiling: Implications for Late Paleoproterozoic orogenesis and modern earthquake hazard: Earth and Planetary Science Letters, v. 308, p. 218–228.

Quade, J., Cater, J.M., Ojha, T.P., Adam, J., and Mark Harrison, T., 1995, Late Miocene environmental change in Nepal and the northern Indian subcontinent: Stable isotopic evidence from paleosols: Geological Society of America Bulletin, v. 107, p. 1381–1397.

Raiverman, V., 1983, Basin geometry, Cenozoic sedimentation and hydrocarbon prospects in north western Himalaya and Indo-Gangetic plains: Petroleum Asia Journal, v. 6, p. 67–92.

Raiverman, V., 2002, Foreland sedimentation in Himalayan tectonic regime: a relook at the orogenic process: Dehra Dun, Bishen Singh Mahendra Pal Singh.

Raiverman, V., Chugh, M.L., Srivastava, A.K., Prasad, D.N., and Das, S.K., 1994, Cenozoic Tectonics of the Fold Belt of Himalaya and the Indo-Gangetic Fordeep with Pointers towards Hydrocarbon Prospects, in Biswas, S.K., Dave, A., Garg, P., Pandey, J., Maithani, A., and Thomas, N.J. eds., Proceedings of the Second Seminar on Petroliferous Basins of India: Himalayan foothills, Vindhyan and Gondwana basins, geoscientific studies and hydrocarbon exploration techniques, Dehra Dun, v. 3, p. 25–54.

Rao, M.R., 1973, The subsurface geology of the Indo-Gangetic plains: Journal of the Geological Society of India, v. 14, p. 217–242.

Rao, N.P., Tiwari, V.M., Kumar, M.R., Hazarika, P., Saikia, D., Chadha, R.K., and Rao, Y.J.B., 2015, The M w 6.9 Sikkim–Nepal earthquake of September 2011: a perspective for wrench faulting in the Himalayan thrust zone: Natural Hazards, v. 77, p. 355–366, doi:10.1007/s11069-015-1588-y.

Rasmussen, B., Bose, P.K., Sarkar, S., Banerjee, S., Fletcher, I.R., and McNaughton, N.J., 2002, 1.6 Ga U-Pb zircon age for the Chorhat Sandstone, lower Vindhyan, India: Possible implications for early evolution of animals: Geology, v. 30, p. 103–106.

Ratschbacher, L., Frisch, W., Liu, G., and Chen, C., 1994, Distributed deformation in southern and western Tibet during and after the India-Asia collision: Journal of Geophysical Research: Solid Earth, v. 99, p. 19917–19945.

Ravikant, V., Wu, F.-Y., and Ji, W.-Q., 2011, U–Pb age and Hf isotopic constraints of detrital zircons from the Himalayan foreland Subathu sub-basin on the Tertiary palaeogeography of the Himalaya: Earth and Planetary Science Letters, v. 304, p. 356–368, doi:10.1016/j.epsl.2011.02.009.

Ray, J.S., 2006, Age of the Vindhyan Supergroup: a review of recent findings: Journal of Earth System Science, v. 115, p. 149–160.

Ray, J.S., Martin, M.W., Veizer, J., and Bowring, S.A., 2002, U-Pb zircon dating and Sr isotope systematics of the Vindhyan Supergroup, India: Geology, v. 30, p. 131–134.

Regumi, A., Dhital, M., Gadtaula, R., Tamrakar, N., and Yoshida, K., 2011, Lithostratigraphy and structures of the Siwaliks rocks in the southern part of Dang and its surrounding area, Southwestern Nepal: Journal of the Faculty of Science Shinshu University, v. 43, p. 1–42.

Rösler, W., Metzler, W., and Appel, E., 1997, Neogene magnetic polarity stratigraphy of some fluviatile Siwalik sections, Nepal: Geophysical Journal International, v. 130, p. 89–111, doi:10.1111/j.1365-246X.1997.tb00990.x.

Sahni, M.R., and Mathur, L.P., 1964, Stratigraphy of the Siwalik group: New Delhi, BC Roy, International Geological Congress, v. 7.

Sakai, H., 1983, Geology of the Tansen Group of the Lesser Himalaya in Nepal.: Memoirs of the Faculty of Science, Kyushu University, v. 25, p. 27–74.

Sakai, H., 1989, Rifting of the Gondwanaland and uplifting of the Himalayas recorded in Mesozoic and Tertiary fluvial sediments in the Nepal Himalayas, in Taira, A. and Masuda, F. eds., Sedimentary facies in the active plate margin, Tokyo, Terra Scientific Publishing Company, p. 723–732.

Sakai, H., Hamamoto, R., and Arita, K., 1992, Radiometric ages of alkaline volcanic rocks from the upper Gondwana of the Lesser Himalayas, western Central Nepal and their tectonic significance: Kathmandu: Bulletin of the Department of Geology, Tribhuvan University, v. 2, p. 65–74.

Sastri, V.V., Bhandari, L.L., Raju, A.T.R., and Datta, A.K., 1971, Tectonic framework and subsurface stratigraphy of the Ganga basin: Jornal of the Geological Society of India, v. 12, p. 222–233.

Searle, M.P., Law, R.D., Godin, L., Larson, K.P., Streule, M.J., Cottle, J.M., and Jessup, M.J., 2008, Defining the Himalayan main central thrust in Nepal: Journal of the Geological Society, v. 165, p. 523–534.

Sengupta, S.N., 1962, Basement configuration of the Indo-Gangetic plains shown by aeromagnetic surveys, in Proceedings of the Seminar on Oil Prospects in the Ganga Valley, Oil and Natural Gas Corporation Technical Publications, v. 1, p. 52–54.

Sharma, K.K., and Rahman, A., 2000, The Early Archaean–Paleoproterozoic crustal growth of the Bundelkhand craton, northern Indian shield, in Deb, M. ed., Crustal evolution and metallogeny in the northwestern Indian Shield: A festschrift for Asoke Mookherjee, Oxford, Alpha Science International Ltd, p. 51–72.

Shukla, S.N., and Chakraborty, D., 1994, Status of exploration and future programme of hydrocarbon exploration in Vindhyan and Gondwana basins, in Biswas, S.K., Dave, A., Garg, P., Pandey, J., Maithani, A., and Thomas, N.J. eds., Proceedings of the Second Seminar on Petroliferous Basins of India: Himalayan foothills, Vindhyan and Gondwana basins, geoscientific studies and hydrocarbon exploration techniques, Dehra Dun, Indian

Petroleum Publishers, v. 3, p. 63–100.

Sitaula, R.P., 2009, Petrofacies and Paleotectonic Evolution of Gondwanan and Post-Gondwanan Sequences of Nepal [MSc thesis]: Auburn University, 206 p.

Soucy La Roche, R., and Godin, L., 2019, Inherited Cross□Strike Faults and Oligocene□ Early Miocene Segmentation of the Main Himalayan Thrust, West Nepal: Journal of Geophysical Research: Solid Earth, v. 124, p. 7429–7444, doi:10.1029/2019JB017467.

Soucy La Roche, R., Godin, L., Cottle, J.M., and Kellett, D.A., 2018, Preservation of the Early Evolution of the Himalayan Middle Crust in Foreland Klippen: Insights from the Karnali Klippe, West Nepal: Tectonics, v. 37, p. 1161–1193, doi:10.1002/2017TC004847.

Srinivasan, S., and Khar, B.M., 1996, Status of Hydrocarbon Exploration in Northwest Himalaya and Foredeep - Contributions to Stratigraphy and Structure, in Proceedings of the Symposium on NW Himalaya and Foredeep, Feb 1995, Geological Survey of India Special Publications, v. 21, p. 295–405.

Szulc, A.G. et al., 2006, Tectonic evolution of the Himalaya constrained by detrital 40Ar-39Ar, Sm-Nd and petrographic data from the Siwalik foreland basin succession, SW Nepal: Tectonic evolution of the Himalaya: Basin Research, v. 18, p. 375–391, doi:10.1111/ j.1365-2117.2006.00307.x.

de la Torre, T.L., Monsalve, G., Sheehan, A.F., Sapkota, S., and Wu, F., 2007, Earthquake processes of the Himalayan collision zone in eastern Nepal and the southern Tibetan Plateau: Geophysical Journal International, v. 171, p. 718–738, doi:10.1111/j.1365-246X.2007.03537.x.

Upreti, B.N., 1999, An overview of the stratigraphy and tectonics of the Nepal Himalaya: Journal of Asian Earth Sciences, v. 17, p. 577–606, doi:10.1016/S1367-9120(99)00047-4.

Valdiya, K.S., 1980, Geology of Kumaun Lesser Himalaya: Dehra Dun, Wadia Institute of Himalayan Geology.

Valdiya, K.S., 1976, Himalayan transverse faults and folds and their parallelism with subsurface structures of north Indian plains: Tectonophysics, v. 32, p. 353–386.

Veevers, J.J., and Tewari, R.C., 1995, Gondwana master basin of Peninsular India between Tethys and the interior of the Gondwanaland Province of Pangea: Colorado, Geological Society of America, Geological Society of America Memoir, v. 187, 67 p., doi:10.1130/0-8137-1187-8.1.

Verma, A.K., Pati, P., and Sharma, V., 2017, Soft sediment deformation associated with the East Patna Fault south of the Ganga River, northern India: Influence of the Himalayan tectonics on the southern Ganga plain: Journal of Asian Earth Sciences, v. 143, p. 109–

121, doi:10.1016/j.jseaes.2017.04.016.

Vögeli, N., Najman, Y., van der Beek, P., Huyghe, P., Wynn, P.M., Govin, G., van der Veen, I., and Sachse, D., 2017, Lateral variations in vegetation in the Himalaya since the Miocene and implications for climate evolution: Earth and Planetary Science Letters, v. 471, p. 1–9, doi:10.1016/j.epsl.2017.04.037.

White, N.M., Parrish, R.R., Bickle, M.J., Najman, Y.M.R., Burbank, D., and Maithani, A., 2001, Metamorphism and exhumation of the NW Himalaya constrained by U–Th–Pb analyses of detrital monazite grains from early foreland basin sediments: Journal of the Geological Society, v. 158, p. 625–635, doi:10.1144/jgs.158.4.625.

White, N.M., Pringle, M., Garzanti, E., Bickle, M., Najman, Y., Chapman, H., and Friend, P., 2002, Constraints on the exhumation and erosion of the High Himalayan Slab, NW India, from foreland basin deposits: Earth and Planetary Science Letters, v. 195, p. 29–44, doi:10.1016/S0012-821X(01)00565-9.

Xiao, S., Tang, Q., Hughes, N.C., McKenzie, N.R., and Myrow, P.M., 2016, Biostratigraphic and detrital zircon age constraints on the basement of the Himalayan Foreland Basin: Implications for a Proterozoic link to the Lesser Himalaya and cratonic India: Terra Nova, v. 28, p. 419–426, doi:10.1111/ter.12235.

Yin, A., 2006, Cenozoic tectonic evolution of the Himalayan orogen as constrained by along-strike variation of structural geometry, exhumation history, and foreland sedimentation: Earth-Science Reviews, v. 76, p. 1–131, doi:10.1016/j.earscirev.2005.05.004.

Zhao, W., Nelson, K.D., Che, J., Quo, J., Lu, D., Wu, C., and Liu, X., 1993, Deep seismic reflection evidence for continental underthrusting beneath southern Tibet: Nature, v. 366, p. 557–559, doi:10.1038/366557a0.

Chapter 3: Incipient fault development in the Himalayan foreland basin: A New Frontal Thrust

The Himalayan foreland basin is often portrayed as having an undeformed, simple geometry. Using 2D seismic reflection data, we present evidence of recent deformation in the Ganga Basin of eastern Nepal, propagating over 37 km south from the southern edge of the Himalayan Main Frontal Thrust. A system of tear faults is observed at a high angle to the orogen that appear to be spatially localized above the Munger-Saharsa basement ridge. A blind thrust fault is interpreted in the subsurface, bounded by two tear faults, soling on a detachment surface below the top of the Lower Siwalik subgroup, near the Sub-Cenozoic unconformity and acoustic basement. We interpret the geometry of the fault system as a series of blocks soling on a basal décollement, with strike-slip movement on tear faults accommodating differential southward slip between the blocks. The faults represent the subsurface propagation of the Main Himalayan Thrust into the Ganga Basin as a New Frontal Thrust, and are probably localized by basement ridge influences on factors such as lithofacies, basin thickness, overpressure and/or the topography of the basin floor. We calculate that a cumulative slip between 42 and 124 m has accumulated on these faults over the last ~0.5 Ma. Present-day fault development in the Himalayan foreland basin may have implications for seismic hazard in eastern Nepal.

3.1 Introduction

In this Chapter we present observations of a system of strike-slip and thrust faults propagating into the Himalayan foreland basin, interpreted as a new salient in the Himalayan frontal thrust system, carrying an incipient piggyback basin. We calculate slip along the thrust system, and discuss the implications for seismicity in the region.

3.1.1 Himalayan Orogen

The Himalayan orogen is commonly subdivided into longitudinally extensive lithotectonic domains, bounded by continental-scale faults (Yin, 2006). From north to south, these rock domains are: the Tethyan Himalaya, composed of sediments deposited on the northern Indian paleocontinental shelf; the Greater Himalaya, containing igneous and metamorphic rocks that record Himalayan orogenesis; the sedimentary Lesser Himalaya; and the Sub-Himalaya, composed of uplifted sediments of the Himalayan foreland basin (Heim and Gansser, 1939; Gansser, 1964; Le Fort, 1975). These domains are linked by a series of faults, many of which root on the Main Himalayan Thrust, a crustal scale detachment (MHT; Zhao *et al.* 1993; Brown *et al.* 1996; Nelson *et al.* 1996; Hauck *et al.* 1998). The rise of the Himalaya resulted in lithospheric flexure of the Indian plate, producing a southward migrating foreland basin along its southern edge (Lyon-Caen and Molnar, 1985; Burbank et al., 1996).

3.1.2 Ganga Basin

The Ganga Basin (Fig. 3-1a) is part of the Himalayan foreland basin and has been filled by 3 km to > 12 km of mostly continental sediment (Burbank et al., 1996), that unconformably oversteps Proterozoic mobile belts, Proterozoic sedimentary basins, and an Archean Craton along its southern edge (Fig. 2-1). The foreland basin fill is divided by an Oligocene unconformity (DeCelles et al., 1998a; Najman et al., 2004). Paleogene strata below the unconformity consist of a thin (>90 m) succession dominated by marine mudstone (DeCelles et al., 2004); these outcrop in the Sub-Himalaya and Lesser Himalaya of Nepal. Miocene to Quaternary rocks above have been deposited as fluvial/continental deposits, filling the subsiding basin (Burbank et al., 1996). This thicker package comprises the Siwalik Group and the thinner, underlying, Dumri Formation. It outcrops in the Sub-Himalaya to the north (DeCelles et al., 1998b). The geometry of the foreland basin is commonly presented as a northward dipping depression, filled with the undeformed erosional detritus of the Himalaya (Burbank et al., 1996). This is despite the occurrence of earthquakes indicating fault movement within parts of the foreland basin (Seeber et al., 1981), and river migration patterns in the foreland basin that indicate active tectonic controls (Sahu et al., 2010).

3.2 Data and methods

Two-dimensional (2D) seismic reflection data from petroleum industry sources were used to assess basin geometry and identify faults within the foreland basin succession (Fig. 3-1b). The data were acquired from 1982-1984 by Compagnie Général de Géophysique (CGG), Shell, and Petro-Canada International Assistance Corporation (PCIAC), to evaluate the hydrocarbon potential of the Nepal Sub-Himalaya and Ganga Basin deposits. Four blocks of data were acquired, termed the 'Western Block', 'Central Block', 'Eastern Block', and 'Block 10'; the focus of this Chapter is on Block 10. Seismic line spacing is typically 8 km between N-S lines, and 5 km between E-W lines. The original data were processed, and underwent 2D migration.

Sepia film copies of the profiles were scanned and vectorized, and prepared for workstation interpretation by Fugro-Robertson in 2005 (Cairn Energy, 2006). The vertical resolution of the data in two-way travel time (TWT) is estimated at 10 ms near the surface, increasing to 20 ms at depth, representing a depth range of roughly 20-50 m using known seismic velocities of the basin fill. The data were imported using the seismic datum at 50 m above sea level (ASL). Interpretation work by Cairn Energy in 2006 led to the mapping of six regional reflectors, and fifteen localized subordinate horizons (Cairn Energy, 2006). For this study, four of these regional reflector interpretations were reinterpreted. These data were tied to a nearby well (Biratnagar-1; Figs. 3-1, 3-2), and depth-converted using a time-depth relationship established using the checkshot data from the well, in the absence of sonic logs. Further details are given in Chapter 1.

Four horizons have been interpreted throughout the dataset, to characterize the geometry of the basin. These are, from bottom to top:

- Top of acoustic basement, interpreted as the boundary between Archean to Proterozoic plutonic and metamorphic rocks (blue horizon)
- Sub-Cenozoic unconformity, representing the top of stratified Mesoproterozoic to Paleocene strata representing the sedimentary cover of the Indian craton (pink horizon). In locations without these strata, the Sub-Cenozoic is interpreted to coincide with the acoustic basement
- Near-top Lower Siwalik (orange) horizon, a strong negative reflector that lies close to the boundary between the Lower and Middle Siwalik subgroups, at ~11.05-8 Ma (Ojha et al., 2000, 2009)
- Near-top Middle Siwalik (green) horizon, a strong positive reflector close to the boundary between sandstone-dominated Middle Siwalik Subgroup and the conglomerate-dominated Upper Siwalik subgroup and overlying Quaternary alluvium at ~4.6-3 Ma.(Ojha et al., 2009)

Faults have been identified by noting areas with vertical separation of reflections and low signal coherence. Most faults are associated with wide (150-3000 m) zones of low reflection coherence, interpreted as damage zones.

Fig. 3-1: Satellite and elevation maps of Eastern Nepal
(a) Political map showing the location of the study area, and the spatial extent of the Ganga Basin. (b) Satellite map showing the location of the Biratnagar-1 well, as well as the 2D seismic profiles interpreted in this study. MFT: Main Frontal Thrust (c) Shuttle Radar and Topography Mission 1 arc second digital elevation model. Logarithmic scale. A series of topographic highs south of the MFT can be identified in the Ganga Alluvial Plains. The location of the Bhadrapur High is shown, here interpreted as an anticline formed due to fault bend folding above a blind thrust. Location of Fig. 3-5 shown. Elevations relative to mean sea level.

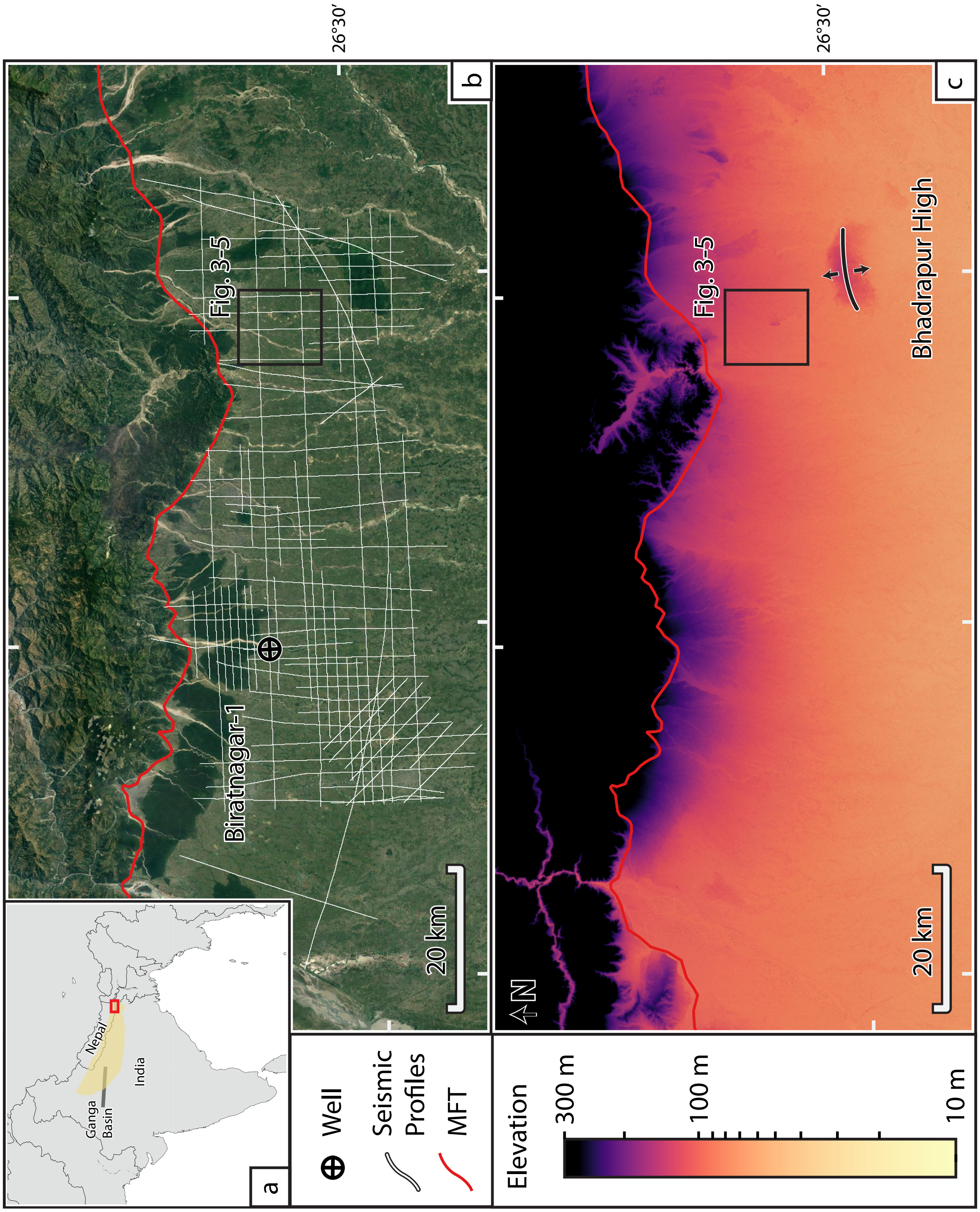
a
Nepal
India
Ganga
Basin
Well
Seismic
Profiles
MFT
Elevation
300 m
100 m
10 m
b
Biratnagar-1
Fig. 3-5
20 km
87°30′
88°
26°30′
c
Fig. 3-5
Bhadrapur High
20 km
N
26°30′

3.3 Observations and results

Faults and folds at seismic scale within the sedimentary package of the Ganga Basin are relatively uncommon, with the result that most strata lie flat and undisturbed. Faults are clustered in eastern Nepal, which is the focus of this Chapter. Two populations of structures have been identified within the study area.

3.3.1 Sub-vertical faults

The first population comprises near-vertical fault systems that appear to crosscut all or most of the resolvable Cenozoic strata (Figs. 3-2, 3-3). They are identified by near-vertical bands of low amplitude, low coherence reflectors, across which adjacent strata are typically offset and affected by gentle to open synclinal or anticlinal folds. Inside the low coherence areas, several smaller near-vertical faults can typically be inferred at discontinuities in the poorly coherent reflections. Some damage zones contain contractional and/or extensional folds, differentiated based on the upwarp/downwarp of mapped horizons relative to their regional structural level (e.g. Fig. 2-5).

Six instances of these faults and their associated folds have been mapped (Fig. 3-2). The fault planes cut strata from below the Lower Siwalik Subgroup, to the top of the seismic survey (most of the foreland basin succession). Correlated between profiles, these fault systems can be traced up to 33 km in length. Two main strike orientations are identified: approximately NNE-SSW and NNW-SSE. The faults show bends in strike when traced along their length (Fig. 3-2). As the damage zones are traced along the strike of the faults, the Siwalik maker horizons deflect above and below their regional elevations from line to line (e.g. Fig. 2-5). These damage zone folds switch between anticlines and synclines from profile to profile. Because the damage zone folds deform the marker horizons both above and below their regional structural elevation, we infer that both contraction and extension occurred adjacent to the same fault system (Fig. 3-2). These changes in many cases spatially coincide with the changes in fault strike.

Below the foreland basin fill several additional faults are interpreted, with an apparent normal sense of movement (Fig. 3-4). These faults form half-graben, here interpreted as Permian – Triassic Gondwanan half-graben due to their spatial proximity with the Gondwanan Purnea Basin (Prasad and Pundir, 2017). These faults are interpreted to cut strata from the Sub-Cenozoic unconformity to the acoustic basement. When correlated between lines, these near-basement faults strike WSW-ENE, a different orientation from the NNE-SSW striking foreland basin faults. Because of this, we infer the deeper WSW-ENE oriented faults formed prior to foreland basin development. The limited data from earthquakes at basement depths in eastern Nepal (Dasgupta et al., 2013) suggest dip-slip movement.

We interpret the foreland basin structures as a series of steep tear faults with predominant strike slip, linking thrust faults in the foreland basin strata. The strike changes of these faults produced bends, explaining the transitions from contraction to extension, causing uplift and subsidence of adjoining strata, respectively (Fig. 3-5). This allows us to identify bends in the fault traces as restraining (contractional) and releasing (extensional). Based on the distribution of the restraining and releasing bends and their correlated map traces, the kinematics (sinistral vs. dextral) of the faults can be characterized (Fig. 3-2). No single state of stress can explain both the strike-slip and contractional structures; the local state of stress is inferred to have been heterogeneous in space and time as the faults propagated in an overall environment of north-south shortening.

The best-imaged releasing bend shows a series of growth strata that onlap each other (Fig. 3-3). This indicates that strain occurred gradually, accommodating sediment progressively, in a pull-apart basin (Figs. 3-3, 3-5). The age of the pull-apart basin can be loosely estimated by extrapolating from the age of the near top Middle Siwalik horizon (nearest magnetostratigraphic date is 3.5 Ma; Ojha et al., 2009) and assuming a constant sedimentation rate. We estimate subsidence in the pull-apart basin started at ~0.5 Ma, and continues to the present.

3.3.2 Dipping reverse faults and folds

In the southeast corner of the study area, below a present-day topographic high known as the Bhadrapur High, we identified a zone of deformation ~2 km wide. The deformation zone displays a series of horizontal, upright, gentle synclines and anticlines (Figs. 3-4, 3-6). Four main axial surfaces can be identified where reflections change dip in the seismic section. These folds are interpreted as fault-bend folds, produced above changes in the dip of an underlying backthrust. The curvature of the fold hinge in map view, shown in Figure 3-1, may be related to the northward vergence of the backthrust. This curvature accounts for broad, gentle anticlines seen on line B, where the crest of a fault-bend fold ("F" in Fig. 3-4) passes obliquely through the seismic profile. Based on the changes in dip observed in overlying strata on line C, the thrust shows a maximum dip of ~5 degrees to the south (Fig. 3-6). The fault plane is inferred to be

Fig. 3-2: Map of faults interpreted in Block 10
Subsurface faults were identified by seismic interpretation, supplemented with field mapping by the Nepal Department of Mines and Geology (Pradhan et al., 2006). The near-top Middle Siwalik elevation surface is shown, highlighting sharp elevation changes along tear faults, and an anticline located in the Southeast corner of Block 10. Dots show localized uplift and subsidence associated with interpreted transpression and transtension, respectively. Colour bands mark inferred fault traces. A marks the location of Figures 3-3 and 3-5. B and C mark locations of profiles in Fig. 3-4. D marks the location of Fig. 3-6. MCT: Main Central Thrust. MBT:Main Boundary Thrust. MFT: Main Frontal Thrust. NFT: New Frontal Thrust. Grey shaded area represents area of inferred slip north of and beneath the Bhadrapur High.

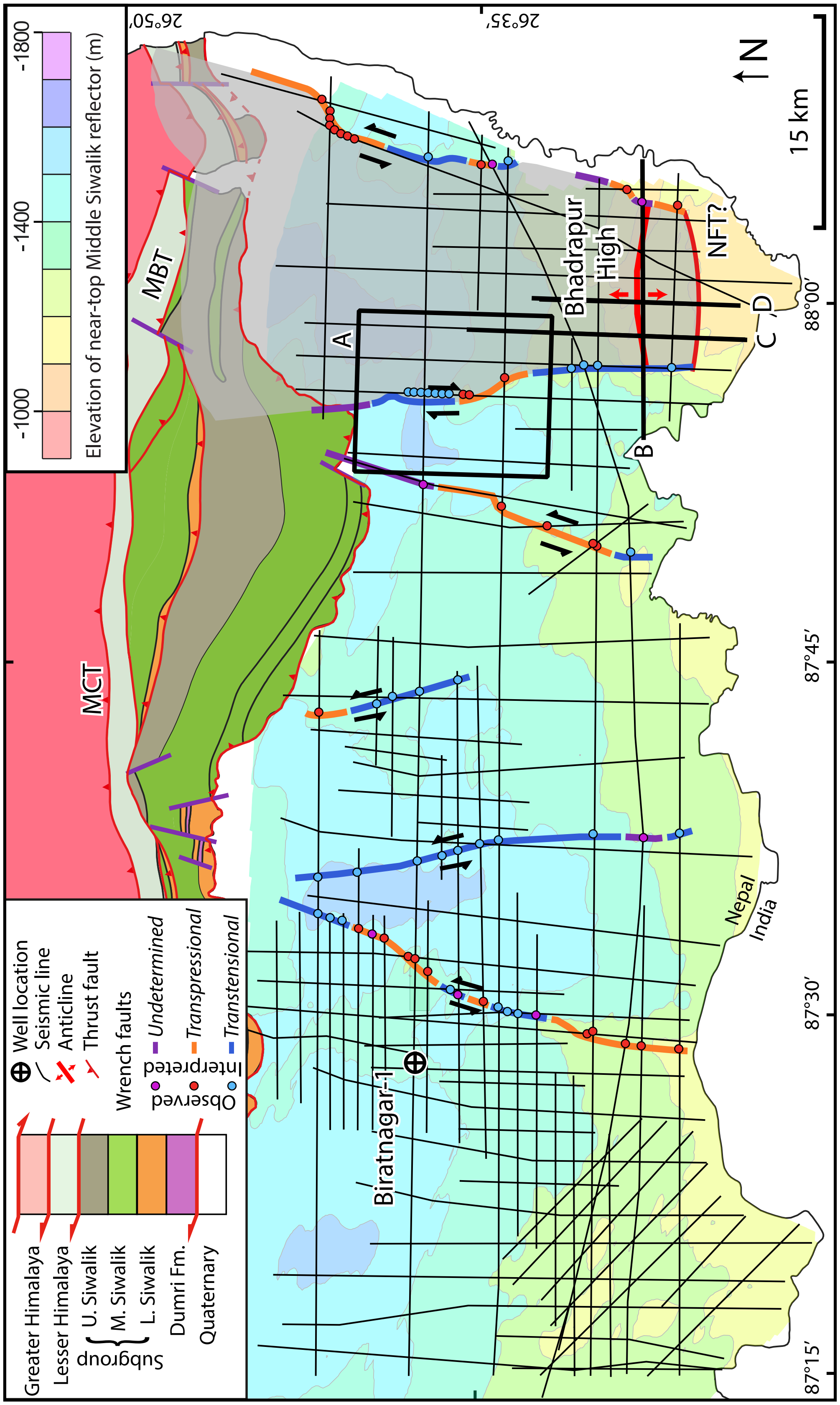
Greater Himalaya
Lesser Himalaya
U. Siwalik
M. Siwalik
L. Siwalik
Subgroup
Dumri Fm.
Quaternary
Well location
Seismic line
Anticline
Thrust fault
Wrench faults
Undetermined
Transpressional
Transtensional
Observed
Interpreted
Elevation of near-top Middle Siwalik reflector (m)
-1000
-1400
-1800
MCT
MBT
Biratnagar-1
Bhadrapur High
NFT?
A
B
C
D
Nepal
India
N
15 km
87°15′
87°30′
87°45′
88°00′
26°35′
26°50′

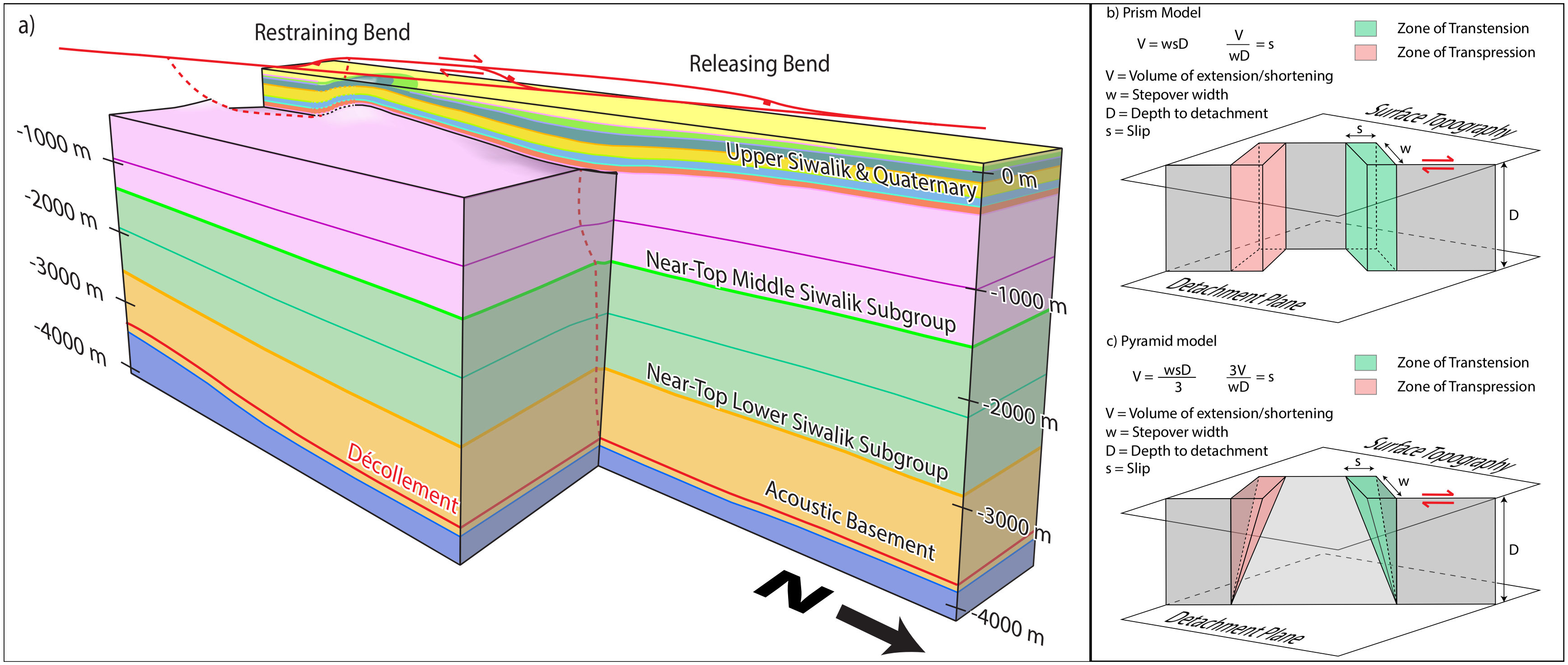

Fig. 3-3: Block diagrams showing deformation along the tear faults

a) 3D perspective of the restraining and releasing bends of a tear fault. Tear fault is at a low angle to the 2D profiles. Strata sag in the releasing bend, producing a pull apart basin. Strata are compressed in the releasing bend, creating an anticline that is interpreted to extend to the surface. The change in elevation relative to regional levels is used to calculate slip b) Slip calculation using a prism model. The volume of extension/structural relief observed in the pull apart basin should be equal to the volume of compression/structural relief observed in the restraining bend. Slip can be calculated using either knowing the width of the stepover, the depth to the detachment, and the volume of structural relief. c) Slip calculation using a pyramid model.

part of a detachment surface inside or below the Lower Siwalik Subgroup (Fig. 3-4). The thrust system appears to be blind, with the axial surfaces of the fault-bend folds extending through overlying strata to the surface, and likely producing the present-day topography. Overall, the geometry suggests an incipient tectonic wedge or triangle zone above a blind basal detachment (Figs. 3-4, 3-6).

Correlated between seismic profiles, the thrust fault, and overlying folds, can be traced at least 13 km along its east-west strike, corresponding approximately to the extent of the Bhadrapur High. Its lateral terminations coincide with the east and west margins of this topographic high, and with two of the six steep faults identified in the seismic data. The western fault shows inferred dextral offset, whereas the eastern fault shows inferred sinistral offset.

3.3.3 Inferred basal detachment

There is no evidence that the thrust crosscuts the tear faults (Fig. 3-4), and the tear faults do not appear to extend deeper than the thrust. This suggests that the tear faults and blind thrust developed simultaneously, and the tear faults sole on the thrust. This leads us to interpret the observed geometry as a system of blocks bounded laterally by tear faults and at their base by a décollement in the Lower Siwalik Subgroup. These blocks accommodated differential southward displacement along strike of the basin, and bound an incipient tectonic wedge beneath the Bhadrapur High. The basal décollement is therefore a subsurface extension of the Main Himalayan Thrust into the foreland basin. To distinguish it from the Main Frontal Thrust we refer to it as the New Frontal Thrust (NFT).

3.4 Discussion

3.4.1 Spatial localization of faults

The system of faults observed in our study spatially overly a basement high, the Munger-Saharsa Ridge (Rao, 1973). Similar N-S tear faults in Cenozoic strata spatially associated with the Delhi-Haridwar basement ridge (Fig. 2-1) have previously been interpreted as the result of basement fault reactivation (Raiverman et al., 1994). Strike-slip focal mechanisms have been observed in the Pakistani portion of the Himalayan foreland basin, above the Chenab spur (Seeber et al., 1981). These focal mechanisms have been interpreted as tear faults associated with a crustal detachment. The Himalayan foreland basin overlies at least eight basement structural

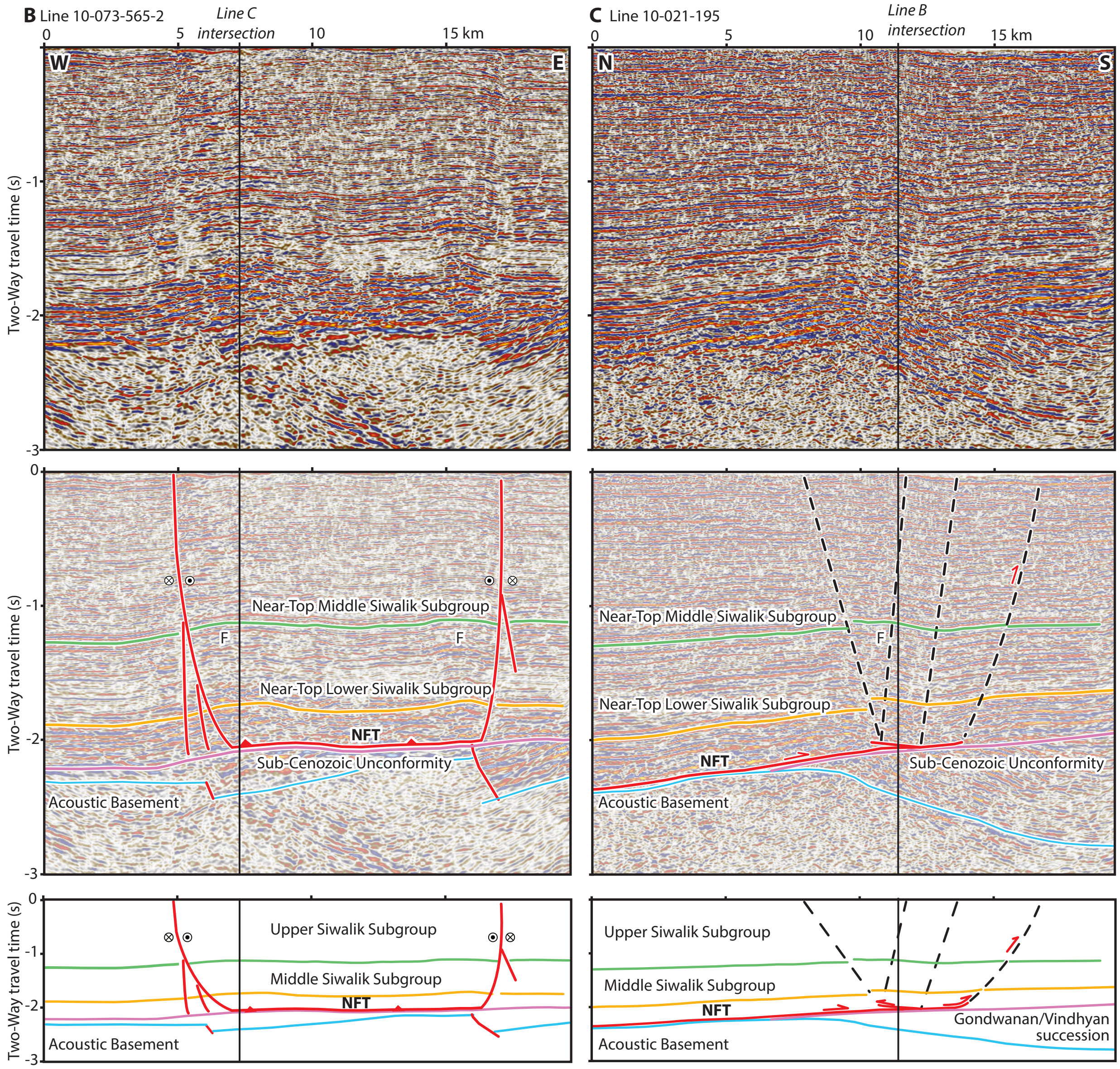

Fig. 3-4: Subsurface thrusting and folding interpreted below the Bhadrapur High Uninterpreted (top), interpreted (middle), and natural scale interpretations of seismic profiles (B) 10-073-565-2 and (C) 10-21-195 in Block 10. Line locations shown in Fig. 3-2. Red lines denote faults. Axial traces related to thrust propagation shown with dashed lines. NFT = New frontal thrust. “F” indicates the crest of fault bend fold anticlines as they pass obliquely through the profiles. Lower sections shown at natural scale for a velocity of 4 km/s.

highs (ridges or spurs), and strike-slip motion is now associated with three (Seeber et al., 1981; Raiverman, 1983).

We interpret the tear and thrust faults that cut the Cenozoic succession in eastern Nepal to be largely independent of basement faults; instead, we suggest that they formed during propagation of a basal detachment likely within or below the Lower Siwalik subgroup (Fig. 3-4). Although these tear fault systems are located preferentially above basement ridges, and are in many cases located above basement features (Fig. 3-4), it is unlikely that they result directly from basement fault reactivation. We suggest that the basement highs provide indirect control on the nucleation of tear and thrust faults in the overlying foreland basin, by controlling longitudinal variations in the topography of the sub-Cenozoic unconformity, the thickness of the overlying sedimentary basin, or facies, such as mudstone, that affect basal friction or fluid pressure in the thrust wedge. These parameters have been shown to control thrust propagation and transfer-zone development in analogue models (Calassou et al., 1993).

3.4.2 Slip estimates

Two estimates of slip are here calculated, from two separate deformed zones. The first estimate uses the “kink construction” to measure uplift and therefore constrain shortening in the subsurface fault-bend fold system above the NFT, below the Bhadrapur High. The second estimate determines accommodation generated in the pull-apart basin with the best-constrained geometry, and uses the volume of accommodation to solve for slip on a steep strike-slip fault. Both methods are subject to significant uncertainties, but give an order-or-magnitude estimate of possible slip on the NFT since its inferred initiation.

To estimate slip, we follow a 2D balancing method from Suppe (1983), (Fig. 3-6) but work, where necessary, with 3D volumes instead of 2D areas (Fig. 3-3). The main assumption and premise is that the volume of rock that is displaced (uplifted or subsided; volume of structural relief V_{sr}) from its regional elevation is equal to the volume of shortening (or extension; V_s). This assumption may not hold strictly true in our examples, as sediments undergo significant compaction in the first 1000 m of burial (Baldwin and Butler, 1985), and the volume of accommodation/uplift measured in the basin is a compacted volume, resulting in an underestimate of slip.

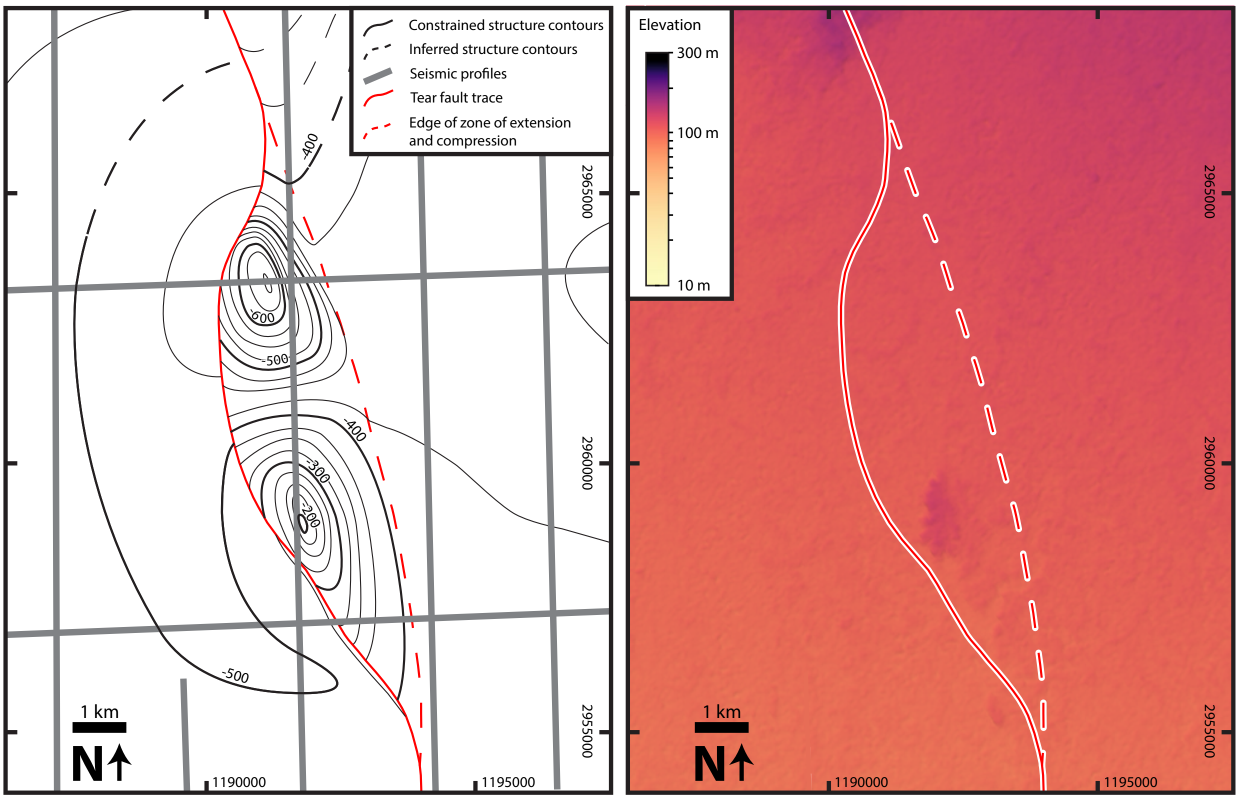

Fig. 3-5: Contour map of the releasing and restraining bends of a tear fault
Hand drawn structure contours (left) representing the elevation above sea level of a strong peak within the Upper Siwalik Subgroup/Quaternary of the Ganga Basin. Location of map shown in Figs. 3-1 and 3-2. In the releasing bend, the horizon curves down into a pull-apart basin. In the restraining bend, the horizon is thrusted above its regional structural level. Contour interval is 25 m. Surface topography map (right) generated from Shuttle Radar and Topography Mission 1 arc second digital elevation model.

3.4.3 Thrust slip estimated from uplift beneath the Bhadrapur High

The kink construction simplifies the geometry of cylindrically deformed rocks, creating a series of straight-line segments bisected by axial surfaces (Fig. 3-6). The methodology provides a satisfactory approximation even for rounded folds if they have parallel (class 2 of Ramsay, 1967) geometry, because any smooth parallel fold can be approximated by a series of straight line segments. Slip can be estimated by comparing the length of the deformed beds to strata that are undeformed and follow regional dip. Kink constructions were made for two profiles near the centre of the fold, to estimate the maximum slip. For the fault-bend fold resulting from the subsurface thrust, calculated slip was 97 m and 112 m, corresponding to a shortening of ~4% in both cases.

An equivalent construction uses the area under the folded surface as a proxy for the volume of deformation (Fig. 3-6 inset diagram). For this method, an estimate of the depth to detachment is required, but it is not necessary to assume conservation of bed lengths. The area under the folded surface, below the regionally interpreted near-top-Middle-Siwalik horizon is 121 100 m^2 (Fig. 3-6). We estimate the depth to detachment to be 1350 m resulting in an estimated slip of 90 m, closely similar to the estimate of 97 m obtained by comparing line lengths on the same seismic line.

Our estimates of slip from the fault bend folds under the Bhadrapur High range from 90 m to 112 m. Our results are relatively consistent with each other, overlapping within error. The Bhadrapur High slip estimates also overlap with the pull-apart basin estimates, suggesting the same amount of slip is deforming both structures. This supports our interpretation that the tear faults and basal décollement are a connected network, moving blocks of the foreland basin.

3.4.4 Strike slip estimated from pull-apart basin subsidence

For any 3D area that undergoes shortening or extension, the volume between the original elevation of a horizon and its deformed elevation (volume of structural relief; V_{sr}) is equivalent to the volume of shortening or extension (Fig. 3-3)(Suppe, 1983), provided neither volume is affected by erosion or compaction. In a plane-strain situation (such as a linear rift or a straight thrust belt), these volumes can be represented by areas in cross-sections drawn parallel to the transport direction (Fig. 3-6). However, in a situation such as a pull-apart basin, plane strain cannot be assumed and the methodology must be applied in 3D.

To calculate the volume of accommodation (equivalent to V_{sr}), we worked with two 2D profiles that imaged a releasing and restraining bend of the same fault; one strike profile and one dip profile. To avoid the effects of erosion at the restraining bend, we worked only with accommodation in the releasing bend. First, we identified a reflection that marked the base of accommodation. This was picked as the deepest continuous reflection that had onlapping reflections above, and no divergence of reflections below. The regional 'original' elevation of the bed was then determined from adjacent lines with flat, layer-cake stratigraphy. We then calculated how much the base of accommodation pick had subsided from its regional level along the two perpendicular seismic profiles.

We then used these two perpendicular profiles to interpolate a total volume of subsidence over the inferred area affected by extension. First, we measured the amount of subsidence (Z_x) at 25 m intervals along the strike-parallel seismic line, and correspondingly (Z_y) along the dip-parallel line. We also recorded the subsidence at the intersection point (Z_i). We then created a 25 m grid spanning the area that underwent subsidence. We interpolated the amount of subsidence in each grid cell as $Z_x * Z_y / Z_i$. Finally, we multiplied the subsidence value for each cell by its area (625 m^2) to get a volume for each grid cell. The volumes were then summed to obtain a final volume of structural relief V_{sr}.

From the volume of structural relief, shortening can be estimated by dividing V_{sr} by the depth to the detachment, and the width of the pull apart basin (Suppe, 1983). Depth to the detachment was identified on the seismic profile, as well as the width of the pull apart basin.

Because the pull apart basin is at relatively shallow depths (< 500 m), early sediments within the basin would be expected to compact significantly as they underwent burial. Because of this, our estimate of deformed volume will be an underestimate, and our estimates of slip from this methodology should be lower than reality. Accommodation volume generated within the pull-apart basin (V_{sr}) is estimated to be between 1.9 and 3.0 x 10^8 m^3. Depth to the detachment surface (from the stratigraphic level where accommodation began being generated) is estimated between 2200 and 3500 m, 2525 m being the best estimate. Finally, the width of the stepover is approximated as 1850 m, using the apparent width of the pull apart basin on the intersecting E-W line. These parameters are used to determine the minimum amount of slip to create the observed pull apart.

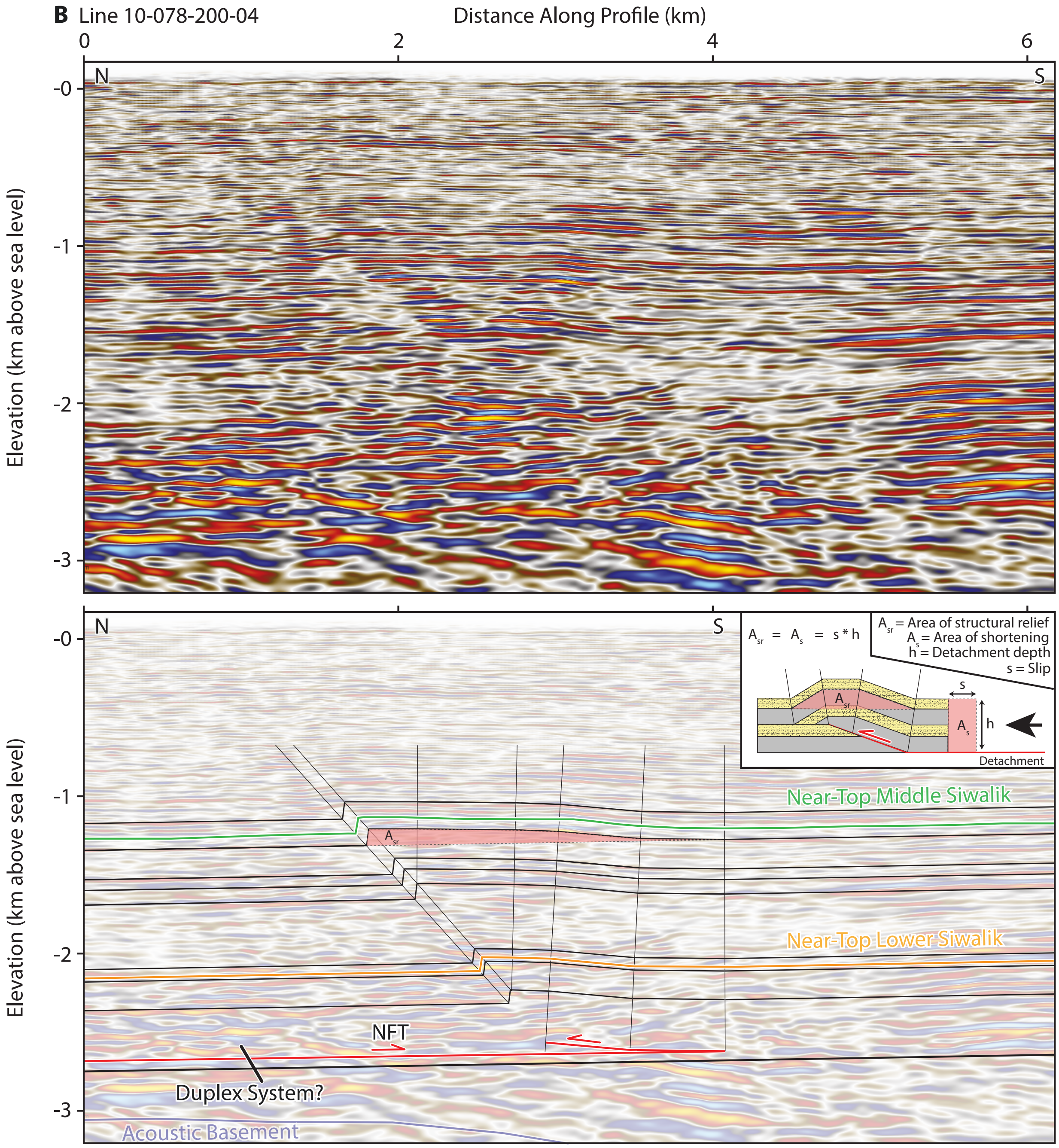

Fig. 3-6: Slip calculation for the Bhadrapur High fault-bend fold

Uninterpreted (top) and interpreted (bottom) natural scale, depth converted seismic profiles along line 10-078-200-04. A series of fault-bend folds are interpreted above blind thrust; the NFT. The lower panel shows the results of a kink construction completed on the structure. The kink construction allows us to calculate the area of structural relief for any horizon, and calculate the total slip. The inset panel shows the slip calculation for an idealized fault bend fold. Inset diagram in bottom half based on Suppe (1983)

We used two methods to infer an amount of slip from the volume of extension (Fig. 3-3). In the first, corresponding to a simple pull-apart basin at an isolated releasing bend above a flat detachment, the volume of extension corresponds to the volume of a vertical prism with parallelogram cross-section (Fig. 3-3b). In this case,

$$V_{sr} = \text{slip x stepover width x depth to detachment}$$

A more realistic estimate, however, recognizes that stepovers typically show flower-structure geometry in 3D. In the seismic profiles, damage zones along the strike-slip faults appear to narrow downwards toward the basal detachment, suggesting a smaller volume of extension. The second model assumes that paired releasing and restraining bends decrease in amplitude linearly to the basal detachment, resulting in pyramidal volumes of deformation (Fig 3-3c). In this case,

$$V_{sr} = 1/3 \text{ x slip x stepover width x depth to detachment}$$

We infer that the true slip lies between these extremes. In the case of the structure illustrated, using a volume of extension estimated from the seismic profiles of 1.9 x 10^8 m^3, a depth to the detachment of 2525 m, and a stepover width of 1850 m, we infer a minimum slip of 41 m. The more realistic second method implies 124 m of slip.

3.4.5 Southward propagation of the Main Himalayan Thrust

The data presented show that Himalayan deformation and faulting does not strictly stop at the Main Frontal Thrust – deformation continues into the subsurface of the foreland basin in the form of a basal décollement, the NFT, and tear faults (Fig. 3-2). The NFT extends 37 km in front of the MFT, and is interpreted as the subsurface extension of the MHT. This propagation distance is several orders of magnitude greater than the inferred slip at the thrust front. The tear and thrust faults deform strata all the way to the top of the seismic survey, or near surface. This constrains their timing to be the Quaternary, and the modern topographical highs above the thrust fault (the Bhadrapur High), and the restraining bend of one of the tear faults (Fig. 3-1c) suggests they are actively developing. The observed system of tear and thrust faults appears to accommodate differential slip along strike, segmenting the upper layers of the foreland basin into blocks. These fault-bounded blocks provide a mechanism to explain salient formation in the Himalayan thrust system, and we view the Bhadrapur High (Fig. 3-2) as a juvenile salient.

3.4.6 Implications for seismicity

Our results may have important implications for seismicity and seismic hazard. Figure 3.7 summarizes the record of seismicity in the region of Block 10 and the section of the Himalaya that lies immediately to the north. Although significant earthquake damage has occurred in the Ganga Alluvial Plain in the past, most seismicity has been attributed either to slip on the MFT or faults to the north (Fig. 3-7). Minor earthquakes to the south of the MFT have been inferred to originate in the Indian crustal units below the Himalayan foreland basin (Ghimire and Kasahara, 2007). Our results suggest that slip over a subhorizontal surface beneath the Ganga plain at least 591 km^2 in area has occurred since ~0.5 Ma.

Seismic moment is defined as the product of the fault area, the average displacement on the fault, and the rigidity of the material (Sleep and Fujita, 1997). We estimate the total slipped area (on both the detachment and the tear faults) to be 1052 km^2 if deformation intersects the MFT in the subsurface (assuming the MFT dips at 30°; Fig. 3-2). A rigidity modulus of 3.3 x 10^4 MPa is commonly assumed for the crust and upper mantle (Sleep and Fujita, 1997). For an estimated 100 m of slip over ~0.5 Ma, this lower rigidity modulus leads to a total moment of ~ 8.9 x 10^{20} Nm. Bilham (2019) has tabulated current slip potential of segments of the Himalaya, and shows a potential slip >10 m for the segment immediately north of Block 10. For an earthquake with a slip distance of 10 m, the resulting moment would be 1.7 x 10^{20} Nm, corresponding to a moment magnitude (M_w) of 7.5. However, experimental results from Middle Siwalk Subgroup sandstone (Mainak et al., 2018) suggest a much lower rigidity modulus of ~3.7 x 10^2 MPa. In addition, slip at the shallow depths of the NFT beneath block 10 may be accommodated by creep and episodic tremor and slip (Rogers and Dragbert, 2003). Although these factors, and the presence of subvertical tear faults that limit the potential slip area may mitigate any seismic hazard associated with the NFT, the high density of population and the poorly consolidated nature of the surficial sediments in the Ganga Basin increase the destructive potential of even a moderate earthquake in this area.

3.5 Conclusions

Fault and related fold geometries in the Ganga Basin show that in eastern Nepal, tear and thrust faults with associated backthrusts have propagated ~40 km south of the Main Frontal Thrust. Observations of releasing and restraining bends allow us to identify a series of tear faults, soling on a detachment surface in the Lower Siwalik Subgroup. These faults are interpreted to

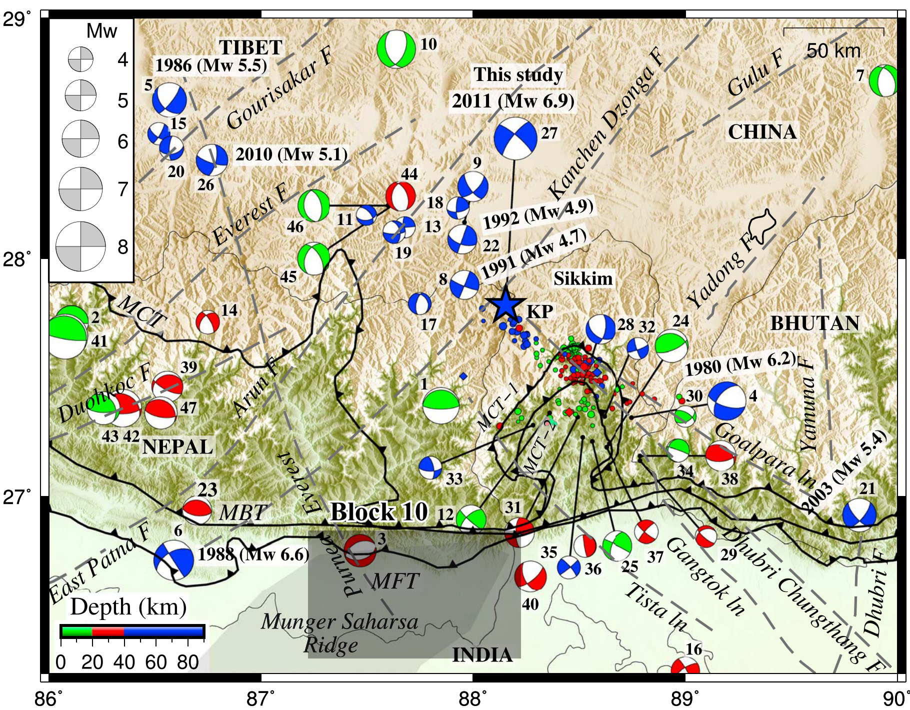

Fig. 3-7: Distribution of seismic events in the Himalaya and adjoining regions north of Block 10. After Sunilkumar *et al.* (2019). Grey rectangle encloses area of Fig. 3-2. Mw: Moment Magnitude. KP: Location of 2011 Mw 6.9 earthquake (blue star) and aftershocks (dots). Numbered focal mechanisms as listed by Sunilkumar *et al.* (2019).

have formed in response to differential slip along strike, thrusting blocks of the foreland basin south at different rates. The Bhadrapur High is recognized as a fault bend fold produced above a subsurface blind thrust here termed the New Frontal Thrust (NFT). This thrust is interpreted as a new splay off the Main Himalayan Thrust and a developing salient in the Himalayan thrust belt. Slip estimates for the fault system have been calculated from the pull-apart basin, as well as the fault bend folds of the Bhadrapur High. We estimate the observed structures represent a minimum of 42-124 m of slip within the foreland basin. The NFT is a potential source of damaging earthquakes, although the potential for a very large event is mitigated by the tear faults, which appear to segment the active thrust surface.

Acknowledgements

We thank John Clayburn and Cairn Energy for their contribution to the project. Schlumberger's Petrel software licenses donated to the University of Alberta assisted data analysis. Participation by JWFW and LG was supported by National Sciences and Engineering Research Council of Canada Discovery Grants.

3.6 References

Baldwin, B., and Butler, C.O., 1985, Compaction Curves: The American Association of Petroleum Geologists Bulletin, v. 69, p. 622–626.

Bilham, R., 2019, Himalayan earthquakes: a review of historical seismicity and early 21st century slip potential, *in* Treloar, P.J. and Searle, M.P. eds., Himalayan Tectonics: A Modern Synthesis, London, United Kingdom, The Geological Society, Geological Society London Special Publications 483, p. SP483.16, http://sp.lyellcollection.org/lookup/doi/10.1144/SP483.16 (accessed August 2019).

Brown, L.D., Zhao, W., Nelson, K.D., Hauck, M., Alsdorf, D., Ross, A., Cogan, M., Clark, M., Liu, X., and Che, J., 1996, Bright Spots, Structure, and Magmatism in Southern Tibet from INDEPTH Seismic Reflection Profiling: Science, v. 274, p. 1688–1690, doi:10.1126/science.274.5293.1688.

Burbank, D.W., Beck, R.A., and Mulder, T., 1996, The Himalayan foreland basin, *in* Yin, A. and Harrison, T.M. eds., The Tectonic Evolution of Asia, Cambridge, Cambridge University Press, p. 149–188.

Cairn Energy, 2006, Seismic Interpretation - Nepal: Cairn UK Internal Report.

Calassou, S., Larroque, C., and Malavieille, J., 1993, Transfer zones of deformation in thrust wedges: an experimental study: Tectonophysics, v. 221, p. 325–344.

Dasgupta, S., Mukhopadhyay, B., Mukhopadhyay, M., and Nandy, D.R., 2013, Role of transverse tectonics in the Himalayan collision: Further evidences from two contemporary earthquakes: Journal of the Geological Society of India, v. 81, p. 241–247, doi:10.1007/s12594-013-0027-5.

DeCelles, P.G., Gehrels, G.E., Najman, Y., Martin, A.J., Carter, A., and Garzanti, E., 2004, Detrital geochronology and geochemistry of Cretaceous–Early Miocene strata of Nepal: implications for timing and diachroneity of initial Himalayan orogenesis: Earth and Planetary Science Letters, v. 227, p. 313–330, doi:10.1016/j.epsl.2004.08.019.

DeCelles, P.G., Gehrels, G.E., Quade, J., and Ojha, T.P., 1998a, Eocene-early Miocene foreland basin development and the history of Himalayan thrusting, western and central Nepal: Tectonics, v. 17, p. 741–765.

DeCelles, P.G., Gehrels, G.E., Quade, J., Ojha, T.P., Kapp, P.A., and Upreti, B.N., 1998b, Neogene foreland basin deposits, erosional unroofing, and the kinematic history of the Himalayan fold-thrust belt, western Nepal: Geological Society of America Bulletin, v. 110, p. 2–21, doi:10.1130/0016-7606(1998)110<0002:NFBDEU>2.3.CO;2.

Gansser, A., 1964, Geology of the Himalayas: London, New York, Interscience Publishers, 289 p.

Ghimire, S., and Kasahara, M., 2007, Source process of the Ms=6.6, Udayapur earthquake of Nepal–India border and its tectonic implication: Journal of Asian Earth Sciences, v. 31, p. 128–138, doi:10.1016/j.jseaes.2007.04.007.

Hauck, M.L., Nelson, K.D., Brown, L.D., Zhao, W., and Ross, A.R., 1998, Crustal structure of the Himalayan orogen at ~ 90 east longitude from Project INDEPTH deep reflection profiles: Tectonics, v. 17, p. 481–500.

Heim, A., and Gansser, A., 1939, Central Himalaya - Geological Observations of the Swiss Expedition 1936: Hindustan Publishing; Delhi, 246 p.

Le Fort, P., 1975, Himalayas: the collided range. Present knowledge of the continental arc: American Journal of Science, v. 275, p. 1–44.

Lyon-Caen, H., and Molnar, P., 1985, Gravity anomalies, flexure of the Indian plate, and the structure, support and evolution of the Himalaya and Ganga Basin: Tectonics, v. 4, p. 513–538.

Mainak, G., Rao, K.S., and Tarun, S., 2018, Strength behaviour of Middle Siwalik sandstone under uniaxial and triaxial conditions, *in* Geomechanics and Geodynamics of Rock Masses, Boca Raton, CRC Press, p. 527–536.

Najman, Y., Johnson, K., White, N., and Oliver, G., 2004, Evolution of the Himalayan foreland basin, NW India: Basin Research, v. 16, p. 1–24, doi:10.1111/j.1365-2117.2004.00223.x.

Nelson, K.D. et al., 1996, Partially Molten Middle Crust Beneath Southern Tibet: Synthesis of Project INDEPTH Results: Science, v. 274, p. 1684–1688, doi:10.1126/science.274.5293.1684.

Ojha, T.P., Butler, R.F., DeCelles, P.G., and Quade, J., 2009, Magnetic polarity stratigraphy of the Neogene foreland basin deposits of Nepal: Basin Research, v. 21, p. 61–90, doi:10.1111/j.1365-2117.2008.00374.x.

Ojha, T.P., Butler, R.F., Quade, J., DeCelles, P.G., Richards, D., and Upreti, B.N., 2000, Magnetic polarity stratigraphy of the Neogene Siwalik Group at Khutia Khola, far western Nepal: Geological Society of America Bulletin, v. 112, p. 424–434.

Pradhan, U.M.S., KC, S.B., Subedi, D.N., Sharma, S.R., Khanal, R.P., and Tripathi, G.N., 2006, Geological Map of Petroleum Exploration Block - 10: Biratnagar, Eastern Nepal: Petroleum Exploration Project, Department of Mines & Geology, Government of Nepal.

Prasad, B., and Pundir, B.S., 2017, Gondwana biostratigraphy of the Purnea Basin (eastern Bihar, India), and its correlation with Rajmahal and Bengal Gondwana basins: Journal of the Geological Society of India, v. 90, p. 405–427, doi:10.1007/s12594-017-0735-3.

Raiverman, V., 1983, Basin geometry, Cenozoic sedimentation and hydrocarbon prospects in north western Himalaya and Indo-Gangetic plains: Petroleum Asia Journal, v. 6, p. 67–92.

Raiverman, V., Chugh, M.L., Srivastava, A.K., Prasad, D.., and Das, S.K., 1994, Cenozoic Tectonics of the Fold Belt of Himalaya and the Indo-Gangetic Fordeep with Pointers towards Hydrocarbon Prospects, *in* Biswas, S.K., Dave, A., Garg, P., Pandey, J., Maithani, A., and Thomas, N.J. eds., Proceedings of the Second Seminar on Petroliferous Basins of India: Himalayan foothills, Vindhyan and Gondwana basins, geoscientific studies and hydrocarbon exploration techniques, Dehra Dun, v. 3, p. 25–54.

Ramsay, J.G., 1967, Folding and Fracturing of Rocks: San Francisco, McGraw Hill, 568 p.

Rao, M.R., 1973, The subsurface geology of the Indo-Gangetic plains: Journal of the Geological Society of India, v. 14, p. 217–242.

Rogers, G., and Dragbert, H., 2003, Episodic Tremor and Slip on the Cascadia Subduction Zone: The Chatter of Silent Slip: Science, v. 300, p. 1942–1943, doi:10.1126/science.1084783.

Sahu, S., Raju, N.J., and Saha, D., 2010, Active tectonics and geomorphology in the Sone-Ganga alluvial tract in mid-Ganga Basin, India: Quaternary International, v. 227, p. 116–126, doi:10.1016/j.quaint.2010.05.023.

Seeber, L., Armbruster, J.G., and Quittmeyer, R.C., 1981, Seismicity and continental subduction in the Himalayan arc, *in* Gupta, H.K. and Delany, F.M. eds., Geodynamics Series, Washington, D. C., American Geophysical Union, v. 3, p. 215–242, doi:10.1029/GD003p0215.

Sleep, N.H., and Fujita, K., 1997, Principles of Geophysics: Malden, Massachusetts, Blackwell Science, 586 p.

Sunilkumar, T.C., Earnest, A., Silpa, K., and Andrews, R., 2019, Rupture of the Indian Slab in the 2011 Mw 6.9 Sikkim Himalaya Earthquake and Its Tectonic Implications: Journal of Geophysical Research: Solid Earth, v. 124, p. 2623–2637, doi:10.1029/2018JB015931.

Suppe, J., 1983, Principles of Structural Geology: Englewood Cliffs, New Jersey, Prentice Hall, 537 p.

Yin, A., 2006, Cenozoic tectonic evolution of the Himalayan orogen as constrained by along-strike variation of structural geometry, exhumation history, and foreland sedimentation: Earth-Science Reviews, v. 76, p. 1–131, doi:10.1016/j.earscirev.2005.05.004.

Zhao, W., Nelson, K.D., Che, J., Quo, J., Lu, D., Wu, C., and Liu, X., 1993, Deep seismic reflection evidence for continental underthrusting beneath southern Tibet: Nature, v. 366, p. 557–559, doi:10.1038/366557a0.

Chapter 4: Conclusions and recommendations

The Ganga Basin of Nepal varies dramatically along its strike, primarily due to inheritance of basement structures.

Seismic interpretation of four regional horizons has allowed us to dissect the geometry of the Ganga Basin of Nepal. A series of fault-bounded basement ridges, oblique to the orogen, dramatically influences the basin geometry. Basement ridges below the Ganga Basin spatially correlate with structural highs in the Cenozoic fill, and the thinnest intervals of Siwalik Group strata. Intervening basement depressions spatially correlate with structural lows, the thickest deposits of foreland basin fill, and the thickest deposits of pre-foreland basin strata. Several locations in the basin changed from areas of minimum deposition during one stage of foreland basin development, to areas of regionally consistent thicknesses during another stage of basin development.

Our observations show that accommodation generation was not constant along-strike. They also show that accommodation generation varied along-strike through time; some regions subsided at slower rates during one phase of basin development, and subsided at the regional rate during a different phase. These along-strike changes in subsidence through time are difficult to explain by differential compaction of underlying strata alone. We infer the longitudinal change in accommodation is due to along-strike changes in basement subsidence. We interpret that basement upwarps have controlled accommodation along-strike, and that changes in the flexural properties of the Indian plate are responsible for these upwarps. The foreland basin oversteps many different mobile belts and cratons that compose the Indian plate, and we interpret that these basement rock domains correspond to changes in the flexural properties of the Indian plate, and produce the observed longitudinal variability of the Ganga Basin.

Faults within the Ganga Basin, particularly within the Cenozoic fill, are not regionally distributed. We interpret a high concentration of subvertical faults striking NNW-SSE and NNE-SSW, interpreted as tear faults, in Eastern Nepal. These faults cut strata all the way from the Lower Siwalik Subgroup to the near surface. Some of the faults are spatially correlated with modern topographic highs, suggesting they are still active. They also are interpreted to sole on a detachment surface within the Lower Siwalik Subgroup. A series of subsurface fault-bend folds have allowed us to delineate a thrust front ~40 km south of the MFT.

We interpret the observed geometry as a series of fault bounded blocks, accommodating along-strike differential slip within the foreland basin. The Bhadrapur High is recognized as the surficial expression of a fault bend fold, formed above a subsurface blind thrust termed the New Frontal Thrust (NFT). We interpret the NFT to be a subsurface splay off the Main Himalayan Thrust. The interpreted geometry suggests a Sub-Himalayan salient is in the early stages of development in Eastern Nepal, providing a mechanism to explain MFT salient formation along the orogen. Finally, the NFT and associated tear faults are a record of slip within the foreland basin, and may be a source of damaging earthquakes.

This work has spawned several directions for future research to address. Future research questions include the following.

- How do basement features affect the rigidity of the Indian plate? This question should be addressed by flexural modelling of the variations in accommodation interpreted in the Ganga Basin.
- Do longitudinal variations in interval thickness and the spatial distribution of foreland basin faults play a role in MFT/MBT salient development?
- Can we use the strata from the pull apart basins in Eastern Nepal to better constrain the frequency and rupture extent of major earthquakes? This would require coring and/or high-resolution seismic studies of the Quaternary and Upper Siwalik Subgroup deposits.
- Three of the nine Himalayan foreland basin ridges/spurs show some evidence of subsurface fault propagation. Are foreland basin faults propagating above the other basement ridges and spurs? This would require availability of additional seismic data in areas outside the current study.
- How do the observed thickness changes in pre-foreland basin strata influence the development of the Lesser Himalaya? Detailed stratigraphic work in the Lesser Himalaya might permit identification of analogous longitudinal variations.
- And most broadly: How do longitudinal variations in the Ganga Basin and the Indian plate relate to transverse structures that segment the entire Himalayan orogen, such as those identified by Soucy La Roche and Godin (2019)?

From this work, it is clear that crustal structures on the Indian plate have had a profound impact on the along-strike development of the Himalayan foreland basin. There is no reason that the influence of these structures would stop at the MFT. The Himalayan foreland basin is deeply intertwined with the Himalaya, and it is reasonable that the same processes that segment the foreland basin, may segment the orogen, either directly or indirectly.

Bibliography

Aditya, S., Raju, A.T.R., and Shukla, S.N., 1979, Assessment of hydrocarbon prospects of the sub-Himalayan, Punjab and Ganga basins-India, *in* Himalayan Geology Seminar New Delhi 1976: Section 3 - Oil and Natural Gas Resources, Geological Survey of India Miscellaneous Publications, v. 41, p. 127–140.

Almeida, R.V., Hubbard, J., Liberty, L., Foster, A., and Sapkota, S.N., 2018, Seismic imaging of the Main Frontal Thrust in Nepal reveals a shallow décollement and blind thrusting: Earth and Planetary Science Letters, v. 494, p. 216–225, doi:10.1016/j.epsl.2018.04.045.

Anders, A.M., Roe, G.H., Hallet, B., Montgomery, D.R., Finnegan, N.J., and Putkonen, J., 2006, Spatial patterns of precipitation and topography in the Himalaya, *in* Willett, S.D., Hovius, N., Brandon, M.T., and Fisher, D.M. eds., Tectonics, Climate, and Landscape Evolution, Geological Society of America Special Paper, v. 398, p. 39–53, doi:10.1130/2006.2398(03).

Appel, E., Rösler, W., and Corvinus, G., 1991, Magnetostratigraphy of the Miocene-Pleistocene Surai Khola Siwaliks in West Nepal: Geophysical Journal International, v. 105, p. 191–198, doi:10.1111/j.1365-246X.1991.tb03455.x.

Avouac, J.-P., 2003, Mountain Building, Erosion, and the Seismic Cycle in the Nepal Himalaya: Amster, Elsevier, Advances in Geophysics, v. 46, 80 p., doi:10.1016/S0065-2687(03)46001-9.

Balakrishnan, T.S., Unnikrishnan, P., and Murty, A.V.S., 2009, The tectonic map of India and contiguous areas: Journal of the Geological Society of India, v. 74, p. 158–168.

Baldwin, B., and Butler, C.O., 1985, Compaction Curves: The American Association of Petroleum Geologists Bulletin, v. 69, p. 622–626.

Banks, C.J., and Warburton, J., 1986, 'Passive-roof' duplex geometry in the frontal structures of the Kirthar and Sulaiman mountain belts, Pakistan: Journal of Structural Geology, v. 8, p. 229–237, doi:10.1016/0191-8141(86)90045-3.

Bashyal, R.P., 1998, Petroleum exploration in Nepal: Journal of Nepal Geological Society, v. 18, p. 19–24.

Basuyau, C., Diament, M., Tiberi, C., Hetényi, G., Vergne, J., and Peyrefitte, A., 2013, Joint inversion of teleseismic and GOCE gravity data: application to the Himalayas: Geophysical Journal International, v. 193, p. 149–160, doi:10.1093/gji/ggs110.

van der Beek, P., Litty, C., Baudin, M., Mercier, J., Robert, X., and Hardwick, E., 2016, Contrasting tectonically driven exhumation and incision patterns, western versus central

Nepal Himalaya: Geology, v. 44, p. 327–330, doi:10.1130/G37579.1.

Bernet, M., van der Beek, P., Pik, R., Huyghe, P., Mugnier, J.-L., Labrin, E., and Szulc, A., 2006, Miocene to Recent exhumation of the central Himalaya determined from combined detrital zircon fission-track and U/Pb analysis of Siwalik sediments, western Nepal: Miocene to Recent exhumation of the central Himalaya: Basin Research, v. 18, p. 393–412, doi:10.1111/j.1365-2117.2006.00303.x.

Bhattacharyya, A., 1996, Recent advances in Vindhyan geology: Geological Society of India Memoir, v. 36, 331 p.

Bilham, R., 2019, Himalayan earthquakes: a review of historical seismicity and early 21st century slip potential, *in* Treloar, P.J. and Searle, M.P. eds., Himalayan Tectonics: A Modern Synthesis, London, United Kingdom, The Geological Society, Geological Society London Special Publications 483, p. SP483.16, http://sp.lyellcollection.org/lookup/doi/10.1144/SP483.16 (accessed August 2019).

Biswas, S.K., 1999, A review on the evolution of rift basins in India during Gondwana with special reference to western Indian basins and their hydrocarbon prospects: Proceedings of the Indian National Science Academy - Part A, v. 65, p. 261–284.

Bollinger, L., Avouac, J.P., Beyssac, O., Catlos, E.J., Harrison, T.M., Grove, M., Goffé, B., and Sapkota, S., 2004, Thermal structure and exhumation history of the Lesser Himalaya in central Nepal: Thermal Structure of the Lesser Himalaya: Tectonics, v. 23, p. n/a-n/a, doi:10.1029/2003TC001564.

Bose, P.K., Sarkar, S., Das, N.G., Banerjee, S., Mandal, A., and Chakraborty, N., 2015, Proterozoic Vindhyan Basin: configuration and evolution, *in* Mazumder, R. and Eriksson, P.G. eds., Precambrian Basins of India: Stratigraphic and Tectonic Context, Geological Society of London Memoir, v. 43, p. 85–102, http://mem.lyellcollection.org/lookup/doi/10.1144/M43.6 (accessed February 2018).

Bouilhol, P., Jagoutz, O., Hanchar, J.M., and Dudas, F.O., 2013, Dating the India–Eurasia collision through arc magmatic records: Earth and Planetary Science Letters, v. 366, p. 163–175, doi:10.1016/j.epsl.2013.01.023.

Brown, L.D., Zhao, W., Nelson, K.D., Hauck, M., Alsdorf, D., Ross, A., Cogan, M., Clark, M., Liu, X., and Che, J., 1996, Bright Spots, Structure, and Magmatism in Southern Tibet from INDEPTH Seismic Reflection Profiling: Science, v. 274, p. 1688–1690, doi:10.1126/science.274.5293.1688.

Burbank, D.W., Beck, R.A., and Mulder, T., 1996, The Himalayan foreland basin, *in* Yin, A. and Harrison, T.M. eds., The Tectonic Evolution of Asia, Cambridge, Cambridge University Press, p. 149–188.

Burchfiel, B.C., Zhiliang, C., Hodges, K.V., Yuping, L., Royden, L.H., and Changrong, D., 1992, *in* The South Tibetan detachment system, Himalayan orogen: Extension contemporaneous with and parallel to shortening in a collisional mountain belt, Geological Society of America - Special Paper, v. 269.

Burgess, W., Yin, A., Dubey, C.S., Shen, Z.-K., and Kelty, T.K., 2012, Holocene shortening across the Main Frontal Thrust zone in the eastern Himalaya: Earth and Planetary Science Letters, v. 357–358, p. 152–167, doi:10.1016/j.epsl.2012.09.040.

Cairn Energy, 2006, Seismic Interpretation - Nepal: Cairn UK Internal Report.

Calassou, S., Larroque, C., and Malavieille, J., 1993, Transfer zones of deformation in thrust wedges: an experimental study: Tectonophysics, v. 221, p. 325–344.

Casshyap, S.M., and Khan, A., 2000, Basin of central India: evidence of pre-Trap doming, rifting and palaeoslope reversal: Journal of African Earth Sciences, v. 31, p. 65–76.

Chatterjee, N., and Ghose, N.C., 2011, Extensive Early Neoproterozoic high-grade metamorphism in North Chotanagpur Gneissic Complex of the Central Indian Tectonic Zone: Gondwana Research, v. 20, p. 362–379, doi:10.1016/j.gr.2010.12.003.

Cohen, K.M., Harper, D.A.T., Gibbard, P.L., and Fan, J.-X., 2013, The ICS International Chronostratigraphic Chart v2018/08: Episodes, v. 36, p. 119–204.

Corvinus, G., and Rimal, L.N., 2001, Biostratigraphy and geology of the Neogene Siwalik Group of the Surai Khola and Rato Khola areas in Nepal: Palaeogeography, Palaeoclimatology, Palaeoecology, v. 165, p. 251–279.

Dasgupta, S., 1993, Tectono-geologic framework of the eastern Gangetic foredeep, *in* Bihar Nepal Earthquake (August 20, 1988), Geological Survey of India Special Publication, v. 31, p. 61–69.

Dasgupta, S., Mukhopadhyay, B., Mukhopadhyay, M., and Nandy, D.R., 2013, Role of transverse tectonics in the Himalayan collision: Further evidences from two contemporary earthquakes: Journal of the Geological Society of India, v. 81, p. 241–247, doi:10.1007/s12594-013-0027-5.

DeCelles, P.G., Gehrels, G.E., Najman, Y., Martin, A.J., Carter, A., and Garzanti, E., 2004, Detrital geochronology and geochemistry of Cretaceous–Early Miocene strata of Nepal: implications for timing and diachroneity of initial Himalayan orogenesis: Earth and Planetary Science Letters, v. 227, p. 313–330, doi:10.1016/j.epsl.2004.08.019.

DeCelles, P.G., Gehrels, G.E., Quade, J., LaReau, B., and Spurlin, M., 2000, Tectonic implications of U-Pb zircon ages of the Himalayan orogenic belt in Nepal: Science, v. 288, p. 497–499.

DeCelles, P.G., Gehrels, G.E., Quade, J., and Ojha, T.P., 1998a, Eocene-early Miocene foreland basin development and the history of Himalayan thrusting, western and central Nepal: Tectonics, v. 17, p. 741–765.

DeCelles, P.G., Gehrels, G.E., Quade, J., Ojha, T.P., Kapp, P.A., and Upreti, B.N., 1998b, Neogene foreland basin deposits, erosional unroofing, and the kinematic history of the Himalayan fold-thrust belt, western Nepal: Geological Society of America Bulletin, v. 110, p. 2–21, doi:10.1130/0016-7606(1998)110<0002:NFBDEU>2.3.CO;2.

DeCelles, P.G., Robinson, D.M., Quade, J., Ojha, T.P., Garzione, C.N., Copeland, P., and Upreti, B.N., 2001, Stratigraphy, structure, and tectonic evolution of the Himalayan fold-thrust belt in western Nepal: Tectonics, v. 20, p. 487–509.

Dhital, M.R., 2015, Geology of the Nepal Himalaya: Cham, Springer, Regional Geology Reviews, 498 p.

Duncan, C., Masek, J., and Fielding, E., 2003, How steep are the Himalaya? Characteristics and implications of along-strike topographic variations: Geology, v. 31, p. 75–78.

Fuloria, R.C., 1996, Geology and hydrocarbon prospects of the Vindhyan sediments in Ganga valley (A. Bhattacharyya, Ed.): Memoirs of the Geological Society of India, v. 36, p. 235–256.

Gahalaut, V.K., and Kundu, B., 2012, Possible influence of subducting ridges on the Himalayan arc and on the ruptures of great and major Himalayan earthquakes: Gondwana Research, v. 21, p. 1080–1088, doi:10.1016/j.gr.2011.07.021.

Gansser, A., 1964, Geology of the Himalayas: London, New York, Interscience Publishers, 289 p.

Garzanti, E., 2019, The Himalayan Foreland Basin from collision onset to the present: a sedimentary–petrology perspective, *in* Treloar, P.J. and Searle, M.P. eds., Himalayan Tectonics: A Modern Synthesis, Geological Society of London Special Publications, v. 483.

Gaur, M., 2009, Havidih-1 & 1z Well Completion Report: Gurgaon, India, Cairn, 64 p.

Gautam, P., and Fujiwara, Y., 2000, Magnetic polarity stratigraphy of Siwalik Group sediments of Karnali River section in western Nepal: Geophysical Journal International, v. 142, p. 812–824, doi:10.1046/j.1365-246x.2000.00185.x.

Ghimire, S., and Kasahara, M., 2007, Source process of the Ms=6.6, Udayapur earthquake of Nepal–India border and its tectonic implication: Journal of Asian Earth Sciences, v. 31, p. 128–138, doi:10.1016/j.jseaes.2007.04.007.

Gill, W.D., 1951, The tectonics of the Sub-Himalayan fault zone in the northern Potwar region and in the Kangra district of the Punjab: Quarterly Journal of the Geological Society, v. 107, p. 395–421.

Godin, L., and Harris, L.B., 2014, Tracking basement cross-strike discontinuities in the Indian crust beneath the Himalayan orogen using gravity data – relationship to upper crustal faults: Geophysical Journal International, v. 198, p. 198–215, doi:10.1093/gji/ggu131.

Godin, L., Soucy La Roche, R., Waffle, L., and Harris, L.B., 2019, Influence of inherited Indian basement faults on the evolution of the Himalayan Orogen, *in* Sharma, R., Villa, I., and Kumar, S. eds., Crustal Architecture and Evolution of the Himalaya–Karakoram–Tibet Orogen, Geological Society of London Special Publication, v. 481.

Gopalan, K., Kumar, A., Kumar, S., and Vijayagopal, B., 2013, Depositional history of the Upper Vindhyan succession, central India: Time constraints from Pb–Pb isochron ages of its carbonate components: Precambrian Research, v. 233, p. 108–117, doi:10.1016/j.precamres.2013.04.014.

Goscombe, B., Gray, D., and Foster, D.A., 2018, Metamorphic response to collision in the Central Himalayan Orogen: Gondwana Research, v. 57, p. 191–265, doi:10.1016/j.gr.2018.02.002.

Harrison, T.M., Copeland, P., Hall, S.A., Quade, J., Burner, S., Ojha, T.P., and Kidd, W.S.F., 1993, Isotopic preservation of Himalayan/Tibetan uplift, denudation, and climatic histories of two molasse deposits: The Journal of Geology, v. 101, p. 157–175.

Hartsink, J., and Pradhan, U.M.S., 1989, Well Completion Report - Biratnagar 1: Kathmandu, Shell Nepal B.V.

Hauck, M.L., Nelson, K.D., Brown, L.D., Zhao, W., and Ross, A.R., 1998, Crustal structure of the Himalayan orogen at ~ 90 east longitude from Project INDEPTH deep reflection profiles: Tectonics, v. 17, p. 481–500.

Heim, A., and Gansser, A., 1939, Central Himalaya - Geological Observations of the Swiss Expedition 1936: Hindustan Publishing; Delhi, 246 p.

Hirschmiller, J., Grujic, D., Bookhagen, B., Coutand, I., Huyghe, P., Mugnier, J.-L., and Ojha, T., 2014, What controls the growth of the Himalayan foreland fold-and-thrust belt? Geology, v. 42, p. 247–250, doi:10.1130/G35057.1.

Hu, X., Wang, J., BouDagher-Fadel, M., Garzanti, E., and An, W., 2016, New insights into the timing of the India – Asia collision from the Paleogene Quxia and Jialazi formations of the Xigaze forearc basin, South Tibet: Gondwana Research, v. 32, p. 76–92, doi:10.1016/j.gr.2015.02.007.

Hughes, N.C., Peng, S., Bhargava, O.N., Ahluwalia, A.D., Walia, S., Myrow, P.M., and Parcha, S.K., 2005, Cambrian biostratigraphy of the Tal Group, Lesser Himalaya, India, and early Tsanglangpuan (late early Cambrian) trilobites from the Nigali Dhar syncline: Geological Magazine, v. 142, p. 57–80, doi:10.1017/S0016756804000366.

Husson, L., and Mugnier, J.-L., 2003, Three-dimensional horizon reconstruction from outcrop structural data, restoration, and strain field of the Baisahi anticline, Western Nepal: Journal of Structural Geology, p. 79–90.

Karunakaran, C., and Rao, A.R., 1979, Status of exploration for hydrocarbons in the Himalayan region-contributions to stratigraphy and structure, *in* Himalayan Geology Seminar New Delhi 1976: Section 3 - Oil and Natural Gas Resources, Geological Survey of India Miscellaneous Publications, v. 41 (5), p. 1–66.

Kellett, D.A., Cottle, J.M., and Larson, K.P., 2019, The South Tibetan Detachment System: history, advances, definition and future directions, *in* Himalayan Tectonics: A Modern Synthesis, Geological Society London Special Publications, v. 483, http://sp.lyellcollection.org/lookup/doi/10.1144/SP483.2 (accessed August 2019).

Kellett, D.A., and Grujic, D., 2012, New insight into the South Tibetan detachment system: Not a single progressive deformation: South Tibetan Detachment System: Tectonics, v. 31, p. n/a-n/a, doi:10.1029/2011TC002957.

Krishnan, M.S., 1949, Geology of India and Burma: Madras Law Journal Office; Madras.

Kumar, P.S., Menon, R., and Reddy, G.K., 2009, Heat production heterogeneity of the Indian crust beneath the Himalaya: Insights from the northern Indian Shield: Earth and Planetary Science Letters, v. 283, p. 190–196, doi:10.1016/j.epsl.2009.04.015.

Kumar, R., and Tandon, S.K., 1985, Sedimentology of Plio-Pleistocene Late orogenic deposits associated with intraplate subduction—the Upper Siwalik Subgroup of a part of Panjab Sub-Himalaya, India: Sedimentary Geology, v. 42, p. 105–158.

Le Fort, P., 1975, Himalayas: the collided range. Present knowledge of the continental arc: American Journal of Science, v. 275, p. 1–44.

Lyon-Caen, H., and Molnar, P., 1985, Gravity anomalies, flexure of the Indian plate, and the structure, support and evolution of the Himalaya and Ganga Basin: Tectonics, v. 4, p. 513–538.

Mainak, G., Rao, K.S., and Tarun, S., 2018, Strength behaviour of Middle Siwalik sandstone under uniaxial and triaxial conditions, *in* Geomechanics and Geodynamics of Rock Masses, Boca Raton, CRC Press, p. 527–536.

Martin, A.J., Burgy, K.D., Kaufman, A.J., and Gehrels, G.E., 2011, Stratigraphic and tectonic implications of field and isotopic constraints on depositional ages of Proterozoic Lesser

Himalayan rocks in central Nepal: Precambrian Research, v. 185, p. 1–17, doi:10.1016/j.precamres.2010.11.003.

Mathur, N.S., 1978, Biostratigraphical aspects of the Subathu Formation, Kumaun Himalaya: Recent Researches in Geology, v. 5, p. 96–112.

McKenzie, N.R., Hughes, N.C., Myrow, P.M., Xiao, S., and Sharma, M., 2011, Correlation of Precambrian–Cambrian sedimentary successions across northern India and the utility of isotopic signatures of Himalayan lithotectonic zones: Earth and Planetary Science Letters, v. 312, p. 471–483, doi:10.1016/j.epsl.2011.10.027.

McQuarrie, N., Tobgay, T., Long, S.P., Reiners, P.W., and Cosca, M.A., 2014, Variable exhumation rates and variable displacement rates: Documenting recent slowing of Himalayan shortening in western Bhutan: Earth and Planetary Science Letters, v. 386, p. 161–174, doi:10.1016/j.epsl.2013.10.045.

Meert, J.G., Pandit, M.K., Pradhan, V.R., Banks, J., Sirianni, R., Stroud, M., Newstead, B., and Gifford, J., 2010, Precambrian crustal evolution of Peninsular India: A 3.0 billion year odyssey: Journal of Asian Earth Sciences, v. 39, p. 483–515, doi:10.1016/j.jseaes.2010.04.026.

Mitra, S., Kainkaryam, S.M., Padhi, A., Rai, S.S., and Bhattacharya, S.N., 2011, The Himalayan foreland basin crust and upper mantle: Physics of the Earth and Planetary Interiors, v. 184, p. 34–40, doi:10.1016/j.pepi.2010.10.009.

Mohanty, S., 2012, Spatio-temporal evolution of the Satpura Mountain Belt of India: A comparison with the Capricorn Orogen of Western Australia and implication for evolution of the supercontinent Columbia: Geoscience Frontiers, v. 3, p. 241–267, doi:10.1016/j.gsf.2011.10.005.

Monsalve, G., Sheehan, A., Schulte-Pelkum, V., Rajaure, S., Pandey, M.R., and Wu, F., 2006, Seismicity and one-dimensional velocity structure of the Himalayan collision zone: Earthquakes in the crust and upper mantle: Journal of Geophysical Research, v. 111, doi:10.1029/2005JB004062.

Mugnier, J.L., Leturmy, P., Mascle, G., Huyghe, P., Chalaron, E., Vidal, G., and Husson, L., 1999, The Siwaliks of western Nepal: I. Geometry and kinematics: Journal of Asian Earth Sciences, v. 17, p. 629–642.

Mukhopadhyay, G., Mukhopadhyay, S.K., Roychowdhury, M., and Parui, P.K., 2010, Stratigraphic correlation between different Gondwana Basins of India: Journal of the Geological Society of India, v. 76, p. 251–266, doi:10.1007/s12594-010-0097-6.

Najman, Y.M.R., 1997, Laser 40Ar/39Ar dating of single detrital muscovite grains from early foreland-basin sedimentary deposits in India: Implications for early Himalayan evolution: Geology, v. 25, p. 535–538.

Najman, Y., Burley, S.D., Copley, A., Kelly, M.J., Pander, K., and Mishra, P., 2018, The Late Eocene-Early Miocene Unconformities of the NW Indian Intraplate Basins and Himalayan Foreland: A Record of Tectonics or Mantle Dynamics? Tectonics, v. 37, p. 3970–3985, doi:10.1029/2018TC005286.

Najman, Y., Carter, A., Oliver, G., and Garzanti, E., 2005, Provenance of Eocene foreland basin sediments, Nepal: Constraints to the timing and diachroneity of early Himalayan orogenesis: Geology, v. 33, p. 309–312.

Najman, Y., Jenks, D., Godin, L., Boudagher-Fadel, M., Millar, I., Garzanti, E., Horstwood, M., and Bracciali, L., 2017, The Tethyan Himalayan detrital record shows that India–Asia terminal collision occurred by 54 Ma in the Western Himalaya: Earth and Planetary Science Letters, v. 459, p. 301–310, doi:10.1016/j.epsl.2016.11.036.

Najman, Y., Johnson, K., White, N., and Oliver, G., 2004, Evolution of the Himalayan foreland basin, NW India: Basin Research, v. 16, p. 1–24, doi:10.1111/j.1365-2117.2004.00223.x.

Nakayama, K., and Ulak, P.D., 1999, Evolution of fluvial style in the Siwalik Group in the foothills of the Nepal Himalaya: Sedimentary Geology, v. 125, p. 205–224.

Negi, B.S., and Eremenko, N.A., 1968, Tectonic Map of India: Oil and Natural Gas Commission.

Nelson, K.D. et al., 1996, Partially Molten Middle Crust Beneath Southern Tibet: Synthesis of Project INDEPTH Results: Science, v. 274, p. 1684–1688, doi:10.1126/science.274.5293.1684.

Ojha, P.S., 2012, Precambrian sedimentary basins of India: an appraisal of their petroleum potential, *in* Geology and Hydrocarbon Potential of Neoproterozoic–Cambrian Basins in Asia, Geological Society of London Special Publications, v. 366, p. 19–58, http://sp.lyellcollection.org/lookup/doi/10.1144/SP366.11 (accessed June 2018).

Ojha, T.P., Butler, R.F., DeCelles, P.G., and Quade, J., 2009, Magnetic polarity stratigraphy of the Neogene foreland basin deposits of Nepal: Basin Research, v. 21, p. 61–90, doi:10.1111/j.1365-2117.2008.00374.x.

Ojha, T.P., Butler, R.F., Quade, J., DeCelles, P.G., Richards, D., and Upreti, B.N., 2000, Magnetic polarity stratigraphy of the Neogene Siwalik Group at Khutia Khola, far western Nepal: Geological Society of America Bulletin, v. 112, p. 424–434.

Parkash, B., Sharma, R.P., and Roy, A.K., 1980, The Siwalik group (Molasse) — Sediments shed by collision of continental plates: Sedimentary Geology, v. 25, p. 127–159, doi:10.1016/0037-0738(80)90058-5.

Pilgrim, G.E., 1913, The correlation of the Siwaliks with mammal horizons of Europe: Records of the Geological Survey of India, v. 42, p. 264–326.

Pradhan, U.M.S., KC, S.B., Subedi, D.N., Sharma, S.R., Khanal, R.P., and Tripathi, G.N., 2006, Geological Map of Petroleum Exploration Block - 10: Biratnagar, Eastern Nepal: Petroleum Exploration Project, Department of Mines & Geology, Government of Nepal.

Prasad, B., and Asher, R., 2001, Acritarch biostratigraphy and lithostratigraphic classification of Proterozoic and Lower Paleozoic sediments (Pre-unconformity sequence) of Ganga Basin, India: Dehra Dun, Geoscience Research Group, Keshava Deva Malaviya Institute of Petroleum Exploration, Oil and Natural Gas Corporation.

Prasad, B.R., Klemperer, S.L., Rao, V.V., Tewari, H.C., and Khare, P., 2011, Crustal structure beneath the Sub-Himalayan fold–thrust belt, Kangra recess, northwest India, from seismic reflection profiling: Implications for Late Paleoproterozoic orogenesis and modern earthquake hazard: Earth and Planetary Science Letters, v. 308, p. 218–228.

Prasad, B., and Pundir, B.S., 2017, Gondwana biostratigraphy of the Purnea Basin (eastern Bihar, India), and its correlation with Rajmahal and Bengal Gondwana basins: Journal of the Geological Society of India, v. 90, p. 405–427, doi:10.1007/s12594-017-0735-3.

Quade, J., Cater, J.M., Ojha, T.P., Adam, J., and Mark Harrison, T., 1995, Late Miocene environmental change in Nepal and the northern Indian subcontinent: Stable isotopic evidence from paleosols: Geological Society of America Bulletin, v. 107, p. 1381–1397.

Raiverman, V., 1983, Basin geometry, Cenozoic sedimentation and hydrocarbon prospects in north western Himalaya and Indo-Gangetic plains: Petroleum Asia Journal, v. 6, p. 67–92.

Raiverman, V., 2002, Foreland sedimentation in Himalayan tectonic regime: a relook at the orogenic process: Dehra Dun, Bishen Singh Mahendra Pal Singh.

Raiverman, V., Chugh, M.L., Srivastava, A.K., Prasad, D.N., and Das, S.K., 1994, Cenozoic Tectonics of the Fold Belt of Himalaya and the Indo-Gangetic Fordeep with Pointers towards Hydrocarbon Prospects, *in* Biswas, S.K., Dave, A., Garg, P., Pandey, J., Maithani, A., and Thomas, N.J. eds., Proceedings of the Second Seminar on Petroliferous Basins of India: Himalayan foothills, Vindhyan and Gondwana basins, geoscientific studies and hydrocarbon exploration techniques, Dehra Dun, v. 3, p. 25–54.

Ramsay, J.G., 1967, Folding and Fracturing of Rocks: San Francisco, McGraw Hill, 568 p.

Rao, M.R., 1973, The subsurface geology of the Indo-Gangetic plains: Journal of the Geological Society of India, v. 14, p. 217–242.

Rao, N.P., Tiwari, V.M., Kumar, M.R., Hazarika, P., Saikia, D., Chadha, R.K., and Rao, Y.J.B., 2015, The M w 6.9 Sikkim–Nepal earthquake of September 2011: a perspective for wrench faulting in the Himalayan thrust zone: Natural Hazards, v. 77, p. 355–366, doi:10.1007/s11069-015-1588-y.

Rasmussen, B., Bose, P.K., Sarkar, S., Banerjee, S., Fletcher, I.R., and McNaughton, N.J., 2002, 1.6 Ga U-Pb zircon age for the Chorhat Sandstone, lower Vindhyan, India: Possible implications for early evolution of animals: Geology, v. 30, p. 103–106.

Ratschbacher, L., Frisch, W., Liu, G., and Chen, C., 1994, Distributed deformation in southern and western Tibet during and after the India-Asia collision: Journal of Geophysical Research: Solid Earth, v. 99, p. 19917–19945.

Ravikant, V., Wu, F.-Y., and Ji, W.-Q., 2011, U–Pb age and Hf isotopic constraints of detrital zircons from the Himalayan foreland Subathu sub-basin on the Tertiary palaeogeography of the Himalaya: Earth and Planetary Science Letters, v. 304, p. 356–368, doi:10.1016/j.epsl.2011.02.009.

Ray, J.S., 2006, Age of the Vindhyan Supergroup: a review of recent findings: Journal of Earth System Science, v. 115, p. 149–160.

Ray, J.S., Martin, M.W., Veizer, J., and Bowring, S.A., 2002, U-Pb zircon dating and Sr isotope systematics of the Vindhyan Supergroup, India: Geology, v. 30, p. 131–134.

Regumi, A., Dhital, M., Gadtaula, R., Tamrakar, N., and Yoshida, K., 2011, Lithostratigraphy and structures of the Siwaliks rocks in the southern part of Dang and its surrounding area, Southwestern Nepal: Journal of the Faculty of Science Shinshu University, v. 43, p. 1–42.

Rogers, G., and Dragbert, H., 2003, Episodic Tremor and Slip on the Cascadia Subduction Zone: The Chatter of Silent Slip: Science, v. 300, p. 1942–1943, doi:10.1126/science.1084783.

Rösler, W., Metzler, W., and Appel, E., 1997, Neogene magnetic polarity stratigraphy of some fluviatile Siwalik sections, Nepal: Geophysical Journal International, v. 130, p. 89–111, doi:10.1111/j.1365-246X.1997.tb00990.x.

Sahni, M.R., and Mathur, L.P., 1964, Stratigraphy of the Siwalik group: New Delhi, BC Roy, International Geological Congress, v. 7.

Sahu, S., Raju, N.J., and Saha, D., 2010, Active tectonics and geomorphology in the Sone-Ganga alluvial tract in mid-Ganga Basin, India: Quaternary International, v. 227, p. 116–126, doi:10.1016/j.quaint.2010.05.023.

Sakai, H., 1983, Geology of the Tansen Group of the Lesser Himalaya in Nepal.: Memoirs of the Faculty of Science, Kyushu University, v. 25, p. 27–74.

Sakai, H., 1989, Rifting of the Gondwanaland and uplifting of the Himalayas recorded in Mesozoic and Tertiary fluvial sediments in the Nepal Himalayas, *in* Taira, A. and Masuda, F. eds., Sedimentary facies in the active plate margin, Tokyo, Terra Scientific Publishing

Company, p. 723–732.

Sakai, H., 1991, The Gondwanas in the Nepal Himalaya, *in* Tandon, S.K., Pant, C.C., and Casshyap, S.M. eds., Sedimentary Basins of India: Tectonic Context: Proceedings of the seminar held at Department of Geology, Kumaun University, Nainital, Nainital : Gyanodaya Prakashan, p. 202–217.

Sakai, H., Hamamoto, R., and Arita, K., 1992, Radiometric ages of alkaline volcanic rocks from the upper Gondwana of the Lesser Himalayas, western Central Nepal and their tectonic significance: Kathmandu: Bulletin of the Department of Geology, Tribhuvan University, v. 2, p. 65–74.

Sastri, V.V., Bhandari, L.L., Raju, A.T.R., and Datta, A.K., 1971, Tectonic framework and subsurface stratigraphy of the Ganga basin: Jornal of the Geological Society of India, v. 12, p. 222–233.

Searle, M.P., Law, R.D., Godin, L., Larson, K.P., Streule, M.J., Cottle, J.M., and Jessup, M.J., 2008, Defining the Himalayan main central thrust in Nepal: Journal of the Geological Society, v. 165, p. 523–534.

Seeber, L., Armbruster, J.G., and Quittmeyer, R.C., 1981, Seismicity and continental subduction in the Himalayan arc, *in* Gupta, H.K. and Delany, F.M. eds., Geodynamics Series, Washington, D. C., American Geophysical Union, v. 3, p. 215–242, doi:10.1029/GD003p0215.

Sengupta, S.N., 1962, Basement configuration of the Indo-Gangetic plains shown by aeromagnetic surveys, *in* Proceedings of the Seminar on Oil Prospects in the Ganga Valley, Oil and Natural Gas Corporation Technical Publications, v. 1, p. 52–54.

Sharma, K.K., and Rahman, A., 2000, The Early Archaean–Paleoproterozoic crustal growth of the Bundelkhand craton, northern Indian shield, *in* Deb, M. ed., Crustal evolution and metallogeny in the northwestern Indian Shield: A festschrift for Asoke Mookherjee, Oxford, Alpha Science International Ltd, p. 51–72.

Shukla, S.N., and Chakraborty, D., 1994, Status of exploration and future programme of hydrocarbon exploration in Vindhyan and Gondwana basins, *in* Biswas, S.K., Dave, A., Garg, P., Pandey, J., Maithani, A., and Thomas, N.J. eds., Proceedings of the Second Seminar on Petroliferous Basins of India: Himalayan foothills, Vindhyan and Gondwana basins, geoscientific studies and hydrocarbon exploration techniques, Dehra Dun, Indian Petroleum Publishers, v. 3, p. 63–100.

Sitaula, R.P., 2009, Petrofacies and Paleotectonic Evolution of Gondwanan and Post-Gondwanan Sequences of Nepal [MSc thesis]: Auburn University, 206 p.

Sleep, N.H., and Fujita, K., 1997, Principles of Geophysics: Malden, Massachusetts, Blackwell Science, 586 p.

Soucy La Roche, R., and Godin, L., 2019, Inherited Cross-Strike Faults and Oligocene-Early Miocene Segmentation of the Main Himalayan Thrust, West Nepal: Journal of Geophysical Research: Solid Earth, v. 124, p. 7429–7444, doi:10.1029/2019JB017467.

Soucy La Roche, R., Godin, L., Cottle, J.M., and Kellett, D.A., 2018, Preservation of the Early Evolution of the Himalayan Middle Crust in Foreland Klippen: Insights from the Karnali Klippe, West Nepal: Tectonics, v. 37, p. 1161–1193, doi:10.1002/2017TC004847.

Srinivasan, S., and Khar, B.M., 1996, Status of Hydrocarbon Exploration in Northwest Himalaya and Foredeep - Contributions to Stratigraphy and Structure, *in* Proceedings of the Symposium on NW Himalaya and Foredeep, Feb 1995, Geological Survey of India Special Publications, v. 21, p. 295–405.

Sunilkumar, T.C., Earnest, A., Silpa, K., and Andrews, R., 2019, Rupture of the Indian Slab in the 2011 Mw 6.9 Sikkim Himalaya Earthquake and Its Tectonic Implications: Journal of Geophysical Research: Solid Earth, v. 124, p. 2623–2637, doi:10.1029/2018JB015931.

Suppe, J., 1983, Principles of Structural Geology: Englewood Cliffs, New Jersey, Prentice Hall, 537 p.

Szulc, A.G. et al., 2006, Tectonic evolution of the Himalaya constrained by detrital 40Ar-39Ar, Sm-Nd and petrographic data from the Siwalik foreland basin succession, SW Nepal: Tectonic evolution of the Himalaya: Basin Research, v. 18, p. 375–391, doi:10.1111/j.1365-2117.2006.00307.x.

de la Torre, T.L., Monsalve, G., Sheehan, A.F., Sapkota, S., and Wu, F., 2007, Earthquake processes of the Himalayan collision zone in eastern Nepal and the southern Tibetan Plateau: Geophysical Journal International, v. 171, p. 718–738, doi:10.1111/j.1365-246X.2007.03537.x.

Tripathy, G.R., and Singh, S.K., 2015, Re–Os depositional age for black shales from the Kaimur Group, Upper Vindhyan, India: Chemical Geology, v. 413, p. 63–72, doi:10.1016/j.chemgeo.2015.08.011.

Upreti, B.N., 1999, An overview of the stratigraphy and tectonics of the Nepal Himalaya: Journal of Asian Earth Sciences, v. 17, p. 577–606, doi:10.1016/S1367-9120(99)00047-4.

Valdiya, K.S., 1980, Geology of Kumaun Lesser Himalaya: Dehra Dun, Wadia Institute of Himalayan Geology.

Valdiya, K.S., 1997, Himalaya, the Northern Frontier of East Gondwanaland: Gondwana Research, v. 1, p. 3–9, doi:10.1016/S1342-937X(05)70002-2.

Valdiya, K.S., 1976, Himalayan transverse faults and folds and their parallelism with subsurface structures of north Indian plains: Tectonophysics, v. 32, p. 353–386.

Veevers, J.J., and Tewari, R.C., 1995, Gondwana master basin of Peninsular India between Tethys and the interior of the Gondwanaland Province of Pangea: Colorado, Geological Society of America, Geological Society of America Memoir, v. 187, 67 p., doi:10.1130/0-8137-1187-8.1.

Verma, A.K., Pati, P., and Sharma, V., 2017, Soft sediment deformation associated with the East Patna Fault south of the Ganga River, northern India: Influence of the Himalayan tectonics on the southern Ganga plain: Journal of Asian Earth Sciences, v. 143, p. 109–121, doi:10.1016/j.jseaes.2017.04.016.

Vögeli, N., Najman, Y., van der Beek, P., Huyghe, P., Wynn, P.M., Govin, G., van der Veen, I., and Sachse, D., 2017, Lateral variations in vegetation in the Himalaya since the Miocene and implications for climate evolution: Earth and Planetary Science Letters, v. 471, p. 1–9, doi:10.1016/j.epsl.2017.04.037.

Wadia, D.N., 1919, Geology of India: London, United Kingdom, Macmillan and Co Ltd, 536 p.

White, N.M., Parrish, R.R., Bickle, M.J., Najman, Y.M.R., Burbank, D., and Maithani, A., 2001, Metamorphism and exhumation of the NW Himalaya constrained by U–Th–Pb analyses of detrital monazite grains from early foreland basin sediments: Journal of the Geological Society, v. 158, p. 625–635, doi:10.1144/jgs.158.4.625.

White, N.M., Pringle, M., Garzanti, E., Bickle, M., Najman, Y., Chapman, H., and Friend, P., 2002, Constraints on the exhumation and erosion of the High Himalayan Slab, NW India, from foreland basin deposits: Earth and Planetary Science Letters, v. 195, p. 29–44, doi:10.1016/S0012-821X(01)00565-9.

Xiao, S., Tang, Q., Hughes, N.C., McKenzie, N.R., and Myrow, P.M., 2016, Biostratigraphic and detrital zircon age constraints on the basement of the Himalayan Foreland Basin: Implications for a Proterozoic link to the Lesser Himalaya and cratonic India: Terra Nova, v. 28, p. 419–426, doi:10.1111/ter.12235.

Yin, A., 2006, Cenozoic tectonic evolution of the Himalayan orogen as constrained by along-strike variation of structural geometry, exhumation history, and foreland sedimentation: Earth-Science Reviews, v. 76, p. 1–131, doi:10.1016/j.earscirev.2005.05.004.

Zhao, W., Nelson, K.D., Che, J., Quo, J., Lu, D., Wu, C., and Liu, X., 1993, Deep seismic reflection evidence for continental underthrusting beneath southern Tibet: Nature, v. 366, p. 557–559, doi:10.1038/366557a0.

Appendix 1. Seismic lines

The following seismic lines were made available for this thesis. Eastings and northings are in Universal Transverse Mercator zone 44N.

Line	Block 10	#Traces	Minimum Easting	Maximum Easting	Minimum Northing	Maximum Northing	Length (m)
109b_part1	West	620	437341	437613	3193803	3201506	7713.74
111 - 1	West	1854	464358	474168	3167842	3188703	23077.24
1	West	640	455720	458167	3174597	3190032	15979.21
1xx	West	1565	456128	462533	3187785	3205071	19487.25
2	West	1315	445995	448707	3163885	3196722	33026.96
1x - 1	West	899	462919	469930	3188612	3197422	11267.63
3	West	3521	431038	509739	3153244	3192353	88078.97
4	West	866	476364	484868	3160265	3180015	21521.06
5	West	832	489094	498662	3153766	3172152	20744.25
4x - 1	West	1912	484123	491595	3177886	3199649	23812.26
5x	West	1982	498129	506113	3171180	3193574	24683.42
6	West	548	503407	509881	3145020	3157001	13618.66
6x	West	1953	505428	519441	3153876	3172987	24258.12
7	West	748	536005	546252	3117461	3133380	18932.13
8	West	2037	531530	579069	3109142	3139662	56794.63
9	West	1004	547050	559597	3107196	3129038	25189.95
10	West	860	560492	571803	3098586	3116876	21544.04
10x	West	699	569175	576071	3111715	3123777	13901.01
11	West	330	555298	561683	3157707	3162933	8251.02
12	West	202	558219	561934	3159229	3162611	5043.05
13	West	326	555725	563735	3160524	3161985	8142.15
14	West	1189	626374	652321	3095901	3110415	29752.64
14x	West	1049	611988	628968	3108148	3120222	20887.16
15	West	473	632176	635998	3098684	3109815	11781.07
16	West	423	640408	645250	3095762	3105131	10546.84
17	West	1134	624178	651128	3097505	3104650	28350.93
17x	West	999	609755	627128	3103714	3113102	19896.35
32	West	2047	501688	545887	3126753	3150842	51011.46
33	West	880	524526	531891	3127060	3147723	21970.99
34	West	489	501900	507821	3146447	3157086	12175.65
45n	West	371	420324	423840	3211231	3214245	4687.69
98	West	489	609393	614288	3111589	3119983	9739.09
99 - 1	West	1368	618695	629427	3094197	3118343	27179.85
100	West	4187	522990	590783	3082070	3129538	83553.49
101	West	1279	587923	599132	3081661	3103455	24676.52
45s - 1	West	1720	409362	420256	3192617	3211139	21502.74
102	West	2376	577626	621180	3093434	3109614	47013.94
103	West	1308	574610	583992	3091023	3114545	25869.52
104a	West	3050		450260		3210192	3275192.65
104b	West	3006	449710	484613	3180682	3194867	37704.56
105 - 1	West	2727	425411	452668	3164813	3185270	34488.9
106 - 1	West	2157	441700	467292	3169899	3177764	27248.29
109a - 1	West	1701	430887	435862	3202349	3222790	21208.71
104c	West	3834	482942	521873	3153975	3181578	47795.1
109b_part2 - 1	West	1926	436938	437425	3171138	3195566	24452.8
97	Central	1315	675930	677946	3043011	3068471	26078.83
95	Central	1499	691421	692155	3040894	3070675	29895.26
31	Central	887	882591	891792	2992168	3012332	22170.13
31ext	Central	1946	888383	897697	3005034	3040046	38197.59
35	Central	972	743208	757657	3041633	3060963	24260.55

Line	Block 10	#Traces	Minimum Easting	Maximum Easting	Minimum Northing	Maximum Northing	Length (m)
36	Central	3799	686887	780171	3041634	3048698	94933.25
36x	Central	899	672156	689813	3047524	3049057	17881
37	Central	998	698623	713288	3038551	3058689	24950.64
38	Central	513	845502	846255	3054991	3067783	12814.53
39	Central	1589	816702	856458	3057091	3058671	39803.56
40	Central	608	822295	829459	3053039	3066486	15265.53
41	Central	1171	790748	804094	3102959	3121354	29260.3
42	Central	893	755747	770169	3175522	3190888	22350.34
43	Central	658	915186	929239	3063483	3071597	16379.08
44	Central	820	923928	940583	3061324	3071537	20502.61
46	Central	2572	869050	912853	3034390	3053861	50756.03
47	Central	1199	865474	869313	2995672	3019319	24079.92
49	Central	1875	894791	904854	2987261	3023404	37641.82
82_part1	Central	2421	746344	788722	3040066	3062119	48372.81
82_part2	Central	3299	688237	752486	3059577	3065284	65564.21
82b	Central	1260	669467	693987	3059161	3061658	25057.48
83	Central	1209	828599	846532	3053120	3068941	24194.54
84	Central	3509	782365	847951	3055833	3069472	69456.28
89	Central	1489	767071	785636	3037034	3058207	29061.03
91	Central	2099	728571	741220	3025598	3065363	41911.55
93	Central	1319	707580	709564	3047315	3073318	26304.08
18	East	1446	1123669	1124583	2936473	2972694	36324.2
19a	East	1189	1099707	1128389	2948536	2956611	29821.85
19b	East	3573	1125100	1210896	2944456	2960807	89896.8
20	East	1602	1198535	1210917	2936061	2974279	40247.67
21	East	1079	1183277	1186735	2942350	2969191	27106.32
22	East	447	1178048	1184836	2945381	2954283	11202.89
23	East	967	1147648	1148699	2940323	2964476	24194.32
24	East	1199	1106889	1116034	2946067	2974647	30009.89
25	East	855		1084283		2961013	3154321.18
26	East	831	1061975	1064884	2939855	2960340	20724.18
27	East	1751	1046719	1090500	2957378	2958197	43899.17
28	East	936	1049552	1050075	2947910	2971337	23460.27
29	East	1095	981610	995117	2952511	2976230	27421.98
30	East	800	970462	989118	2955584	2962646	20003.6
50a_part1	East	3180	925269	987044	2985376	2994615	63618.86
50a_part2	East	3657	983230	1053385	2967225	2987028	73099.9
50b	East	2485	890182	936803	3005795	3016195	49538.56
51	East	1959	912358	915952	2978939	3017867	39312.35
52	East	4670	964920	1051956	2952147	2978758	92885.85
52a	East	5689	866205	970715	2976133	3005575	113726.41
53	East	2369	924466	934422	2966443	3012824	47615.36
55	East	1999	936565	949603	2968962	3006683	40025.78
57	East	1409	955076	962342	2979143	3006045	28112.79
59	East	1420	966270	977100	2977247	3002315	28166.56
61	East	2439	973268	987505	2955498	2998783	47888.08
63	East	1425	1005019	1009418	2958886	2986165	28084.02
65	East	1330	1017924	1028097	2954810	2979382	26616.8
67	East	1169	1032826	1037446	2954966	2977354	23290.81
69	East	1154	1088004	1099418	2954437	2972218	22797.65

Line	Block 10	#Traces	Minimum Easting	Maximum Easting	Minimum Northing	Maximum Northing	Length (m)
71	East	849	1047346	1053583	2959868	2975032	16888
73	East	1179	1068446	1075395	2939565	2960644	23398.99
75	East	1499	989177	996172	2961109	2989511	29662.79
77	East	1280	875041	880630	2993725	3018719	25645.94
10-001-030	Block 10	1577	1129202	1130763	2931932	2971770	39869.88
10-002-042	Block 10	1208	1134541	1136033	2935357	2965676	30422.87
10-003-131	Block 10	1324	1169901	1171082	2939952	2973128	33197.16
10-004-035	Block 10	1370	1131789	1133529	2929982	2964315	34377.35
10-005-141	Block 10	1231	1174020	1175748	2940109	2970917	30886.12
10-006-049	Block 10	1049	1138277	1139606	2938426	2964608	26260.42
10-007-153	Block 10	924	1178818	1179957	2944909	2968092	23211.51
10-008-051-074	Block 10	1444		1148156		2976779	3192571.91
10-009-172	Block 10	877	1187215	1187265	2946986	2968986	22000.11
10-010-060	Block 10	1232	1141757	1143899	2938680	2969385	30905.97
10-011-065	Block 10	975	1144185	1144736	2940484	2964919	24441.24
10-012-178	Block 10	1292	1191388	1192107	2940794	2973245	32459.13
10-013-057-085 - 2	Block 10	1478	1151225	1152197	2939953	2976991	37065.69
10-014-187	Block 10	1353	1193793	1194556	2939383	2973322	33947.73
10-015-094	Block 10	1292	1154075	1155994	2938202	2970466	32321.67
10-016-554	Block 10	694	1190767	1208131	2943953	2944255	17366.63
10-017-216	Block 10	1255	1204532	1204957	2940162	2971555	31402.38
10-018-106	Block 10	1481	1160164	1161277	2935951	2972841	36995.67
10-019-205	Block 10	1611	1200009	1200894	2934953	2975309	40366.89
10-020-118	Block 10	1033	1164797	1167130	2941591	2967338	25924.31
10-021-195	Block 10	1372	1196086	1196863	2938400	2972842	34450.82
10-022-624	Block 10	3542	1122700	1211454	2960900	2963996	88808.18
10-023-576	Block 10	3351	1123386	1207448	2946697	2950424	84150.79
10-024-651	Block 10	957	1189471	1213466	2971090	2971722	24003.34
10-025-024	Block 10	1554	1125838	1128816	2932049	2970876	39009.63
10-026-235	Block 10	879	1209189	1213232	2958698	2980361	22067.49
10-027-602	Block 10	3433	1123068	1209191	2954238	2957644	86203.62
10-028-649 - 2	Block 10	2083	1122346	1174597	2968148	2970562	52308.52
10-029-551	Block 10	2107	1123737	1176467	2939772	2942395	52797.1
10-030-014	Block 10	649	1123560	1124328	2936490	2952769	16297.24
10-031-019	Block 10	714	1125061	1126048	2936393	2954209	17882.69
10-032-781	Block 10	635	1123597	1134803	2930972	2942259	15905.52
10-033-793	Block 10	751	1123232	1136455	2937161	2950558	18823.67
10-035-801	Block 10	653	1128533	1140857	2939553	2950771	16665.13
10-036-810	Block 10	586	1131273	1141613	2943595	2953916	14609.55
10-037-080 - 1	Block 10	952	1149827	1150066	2950202	2974083	23882.8
10-038-564	Block 10	1313	1123678	1156545	2943583	2944195	32892.11
10-039-071	Block 10	699	1145332	1147186	2961504	2978831	17540.64
10-041-797 - 1	Block 10	664	1126764	1138670	2938363	2950015	16659.01
10-042-633	Block 10	602	1139841	1154857	2963552	2964480	15044.67
10-043-806	Block 10	653	1129510	1141457	2941732	2953040	16449.99
10-044-637	Block 10	602	1139811	1154833	2964637	2965334	15038.21
10-045-570 - 2	Block 10	673	1123455	1140341	2945157	2946124	16913.75
10-046-641 - 1	Block 10	783	1139735	1159373	2965731	2966692	19661.5
10-047-581 - 2	Block 10	833	1123355	1144279	2947927	2949123	20958.16
10-050-586	Block 10	704	1126753	1144390	2949653	2950512	17657.91

Line	Block 10	#Traces	Minimum Easting	Maximum Easting	Minimum Northing	Maximum Northing	Length (m)
10-052-591	Block 10	874	1132159	1154116	2951395	2952479	21983.81
10-053-663	Block 10	501	1141544	1154048	2972159	2972809	12520.88
10-054-596	Block 10	960	1132903	1156915	2952923	2954144	24043.26
10-055-645	Block 10	602	1139724	1154810	2966830	2967604	15105.89
10-056-046	Block 10	495	1136559	1136847	2945207	2957610	12406.37
10-058-657	Block 10	533	1141382	1154712	2970310	2971036	13349.82
10-060-055	Block 10	423	1140144	1140435	2947226	2957835	10612.99
10-061-648	Block 10	599	1139602	1154626	2967917	2968700	15044.39
10-063-787	Block 10	361	1128523	1135122	2935191	2941352	9028
10-064-068	Block 10	629	1145608	1146624	2949756	2965474	15767.23
10-065-620	Block 10	648	1139828	1156028	2960398	2961062	16220.09
10-066-114	Block 10	592	1163190	1163445	2953590	2968387	14805.32
10-067-124 - 1	Block 10	656	1167397	1167633	2954383	2970759	16377.77
10-069-613	Block 10	1325		1172342		2959895	3202717.99
10-070-606	Block 10	1379	1138242	1172744	2955631	2958064	34588.13
10-071-063	Block 10	453	1143465	1143674	2948211	2959549	11339.96
10-072-160 - 2	Block 10	1029	1182576	1183775	2942609	2968329	25828.66
10-073-565 - 2	Block 10	779	1189434	1208959	2946003	2947151	19559.01
10-074-222	Block 10	455		1207013		2953472	3191444.5
10-075-218	Block 10	357	1205727	1206108	2954354	2963307	8961.1
10-076-608	Block 10	490	1197737	1210030	2959399	2959746	12297.9
10-077-211	Block 10	827	1202025	1202751	2942351	2963084	20746.54
10-078-200	Block 10	500	1198661	1199006	2942059	2954541	12487.95
10-079-583	Block 10	424	1185476	1196126	2951372	2951905	10663.33
10-080-175	Block 10	378	1189579	1190026	2946503	2955993	9500.52
10-081-631	Block 10	556	1160466	1174397	2964197	2964837	13946.37
10-082-636	Block 10	386	1165385	1175108	2965666	2965928	9727.26
10-083-121	Block 10	316	1166032	1166506	2960221	2968086	7879.33
10-084-618	Block 10	360	1157659	1166298	2960112	2960542	8649.77
10-085-109	Block 10	336	1161398	1161496	2953637	2962055	8418.57

Appendix 2. Well reports

The following well reports were made available for this thesis. Eastings and northings are in Universal Transverse Mercator zone 44N.

Name	Surface Easting	Surface Northing	Latitude	Longitude	Well datum (KB)	Total depth (True vertical depth sub-sea)	Total depth (Measured depth)
Ujhani Deep-1	308893.74	3098816.74	28°00'3.0000"N	79°03'23.5000"E	173.7	1953.49	2127.19
Tilhar Deep #1	377127.63	3101371	28°01'55.0000"N	79°45'0.0000"E	157.9	2067.4	2225.3
Shahjahanpur No. 1	392925.78	3093932.47	27°57'58.2300"N	79°54'40.9200"E	167.1	3184.75	3351.85
Puranpur No.2	410596.09	3157640.96	28°32'33.0000"N	80°05'10.0000"E	186.7	4047.3	4234
Matera-1	560540.91	3066644.61	27°43'22.0000"N	81°36'51.0000"E	138.6	3788.5	3927
Madhuban i- 1	1009074.73	2950737.91	26°35'9.0000"N	86°06'30.0000"E	71.5	5885.6	5957.1
Hadidh-1	1011261.24	2885653.94	25°59'59.0000"N	86°06'16.0000"E	49	1651	1700
Gandak - 1	831584.87	2982013.25	26°55'14.0000"N	84°20'19.0000"E	81	5233	5314
Biratnagar-1	1145330.63	2961688.56	26°37'42.9300"N	87°28'29.5800"E	131	3399	3530

Appendix 3. Field data

Field observations were collected of lithologies and structural orientations on a series of traverses in the Sub-Himalaya. In addition, orientations of strata were interpreted from a digital elevation model (DEM) by fitting planes through topographic features corresponding to interlayered strong and weak strata. These data will be interpreted for a future publication. The projection for the presented data is Universal Transverse Mercator zone 44N.

Location map

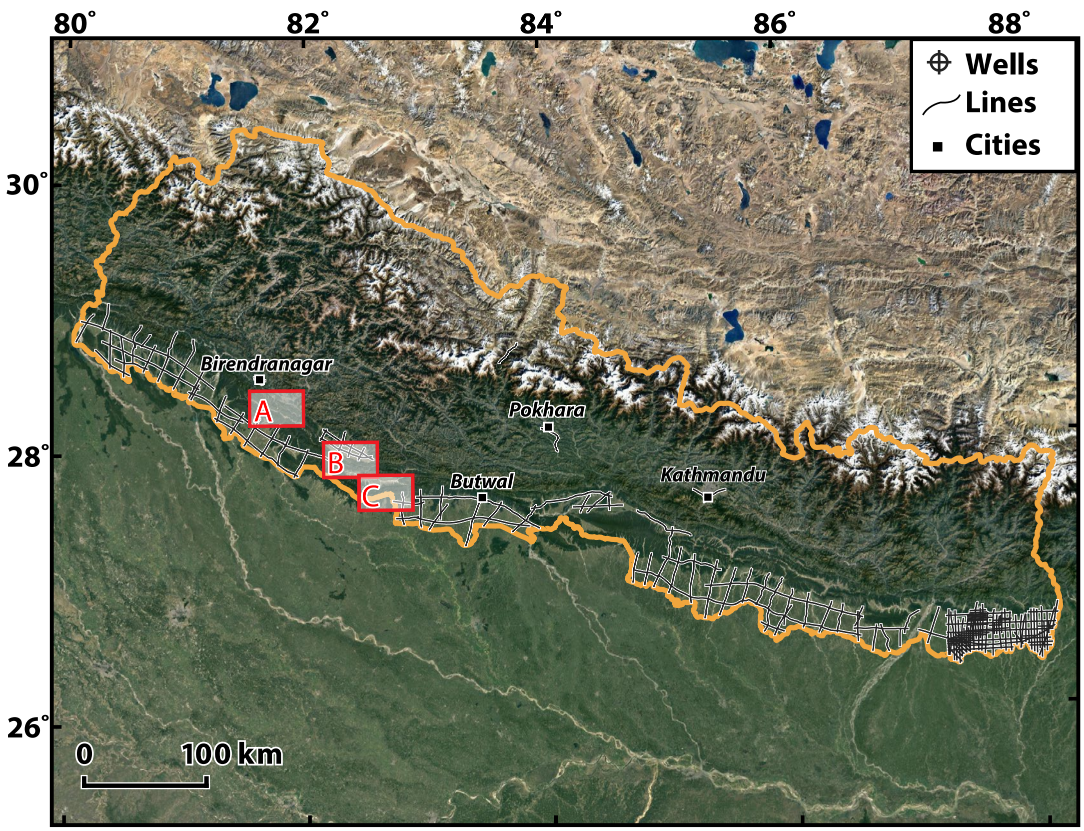

Summary of Abreviations used in the Appendix	
ASL	Above sea level
BU	Upright Bedding
J	Joints
F	Fault
LMS	Lower-Middle Siwalik Subgroup
LS	Lower Siwalik Subgroup
OB	Overturned Bedding
TG	Tension Gash
US	Upper Siwalik Subgroup
UMS	Upper-Middle Siwalik Subgroup
UTM	Universal Transverse Mercator Projection

Table of field measurements

Location ID	UTM Easting	UTM Northing	Elevation (m ASL)	Measurement Type	Strike	Dip	Unit	Comments
QE019	749349	3077251	656.2	OB	100	86	Dumri	
QE019	749349	3077251	656.2	J	335	33	Dumri	
QE020	749329	3077248	639.3	OB	92	71	Dumri	
QE020	749329	3077248	639.3	TG	212	59	Dumri	
QE029	739903	3065948	141.2	BU	306	16	LS	
QE031	681896	3071029	322.1	BU	253	59	LS	
QE033	677753	3074487	435.6	BU	264	56	US	
QE036	678934	3073906	490.5	BU	263	60	UMS	
QE038	681060	3072990	315.1	BU	281	62	UMS	
QE041	681199	3072878	318.3	BU	258	55	UMS	
QE047	650907	3064374	276.3	BU	313	10	LS	
QE049	651578	3065588	583.2	BU	266	32	LMS	
QE051	654187	3067473	729.1	BU	262	46	UMS	
QE053	654691	3068693	563.0	BU	264	54	UMS	
QE054	654655	3070966	314.5	BU	237	65	US	
QE055	654608	3071012	298.3	BU	247	64	US	
QE056	648530	3086573	319.6	BU	255	54	LS	
QE057	648536	3086727	298.3	BU	261	32	LS	
QE058	648585	3086813	289.7	BU	238	17	LS	
QE060	649127	3087384	294.1	BU	250	61	LS	
QE061	649057	3087772	298.7	BU	264	58	LS	
QE062	649137	3087904	306.7	BU	283	59	LMS	
QE064	649272	3089693	291.0	BU	306	31	UMS	
QE066	648648	3089934	299.2	BU	313	41	US	
QE066	648654	3089934	299.2	F	300	54	UMS	
QE067	647202	3093200	658.5	BU	7	54	LS	
QE069	647403	3092820	639.5	BU	113	49	LS	
QE069	647403	3092820	639.5	BU	85	44	LS	
QE071	646944	3090891	502.4	BU	268	38	LMS	
QE073	647008	3090443	326.3	BU	269	79	LMS	
QE073	647008	3090443	326.3	F	149	82	LMS	
QE074	647009	3090270	309.1	OB	261	77	LMS	
QE075	646995	3090298	314.0	BU	286	15	UMS	
QE075	646995	3090298	314.0	OB	261	77	LMS	
QE077	620246	3095365	248.2	OB	325	74	UMS	
QE080	619971	3096096	301.1	OB	274	62	UMS	
QE082	619811	3096271	317.8	OB	303	55	UMS	
QE084	619843	3096514	339.7	OB	289	71	UMS	
QE085	619661	3096694	352.5	OB	311	62	UMS	
QE086	619674	3096764	362.0	OB	299	64	UMS	
QE087	621978	3101045	585.8	OB	309	59	LS	
QE088	622329	3101054	587.5	BU	157	72	LS	
QE089	622220	3101039	596.0	BU	24	17	LS	
QE090	620838	3100132	622.8	BU	128	51	LS	
QE091	622102	3098502	755.0	BU	103	24	LS	

Location ID	UTM Easting	UTM Northing	Elevation (m ASL)	Measurement Type	Strike	Dip	Unit	Comments
QE092	621749	3098084	741.5	OB	297	68	LS	
QE093	621468	3097574	694.7	OB	287	72	LS	
QE094	621032	3097576	714.0	OB	306	75	LS	
QE095	620597	3097985	575.8	OB	291	51	LS	
QE096	620494	3098016	569.1	OB	299	69	LMS	
QE097	619933	3097448	451.0	OB	297	69	LMS	LMS-UMS Contact
QE099	570003	3137072	315.4	BU	273	45	US	
QE100	569952	3137451	340.1	BU	297	67	US	
QE101	569793	3136947	302.1	BU	296	71	UMS	
QE102	568650	3135958	408.0	OB	94	68	UMS	
QE103	568651	3135968	407.9	BU	292	72	UMS	
QE104	567609	3135931	507.3	OB	72	75	LMS	
QE105	567697	3136139	497.5	OB	83	57	LMS	
QE106	566697	3135420	586.8	BU	273	76	LMS	
QE107	566134	3134448	626.8	BU	266	30	LMS	
QE108	566344	3134306	609.0	BU	272	24	LMS	
QE109	567040	3133621	548.5	BU	334	10	LMS	
QE110	566792	3132369	425.4	BU	300	41	LS	
QE111	568229	3138838	485.0	BU	284	23	LS	
QE112	571625	3146004	575.0	BU	313	81	LS	
QE113	571568	3144892	672.2	BU	311	68	LS	
QE115	570669	3143836	814.7	BU	297	40	US	
QE116	570044	3143758	851.4	BU	300	65	UMS	
QE118	567740	3142056	1024.8	BU	283	24	LMS	
QE119	568085	3141223	972.1	BU	252	29	LS	LMS to LS Contact
QE120	567497	3140316	896.4	BU	156	9	LS	
QE122	579270	3105799	183.6	BU	296	17	US	
QE124	582383	3099850	172.0	BU	316	19	UMS	
QE125	582367	3099759	172.4	BU	316	23	UMS	
QE128	586581	3090514	146.5	BU	133	38	US	
QE131	586749	3091138	158.8	BU	131	56	UMS	
QE132	587116	3091445	168.3	BU	136	59	UMS	
QE132	587116	3091445	168.3	F	218	74	UMS	
QE133	587586	3092122	179.2	BU	132	40	UMS	
QE134	587861	3092536	199.9	BU	128	45	LMS	
QE137	565892	3131882	284.6	BU	273	86	LS	
QE138	565896	3131978	282.3	BU	224	44	LS	
QE139	566663	3132777	365.6	BU	274	23	LS	
QE140	566708	3135655	574.9	OB	93	48	LMS	
QE141	570046	3137577	343.3	BU	291	36	US	
QE142	570022	3138111	386.9	BU	301	53	LS	
QE143	569089	3138721	603.5	BU	282	39	LS	
QE144	568726	3140048	687.7	BU	272	20	LS	
QE145	567478	3140970	912.4	BU	268	24	LS	
QE146	567990	3141715	991.0	BU	283	27	LMS	

Location ID	UTM Easting	UTM Northing	Elevation (m ASL)	Measurement Type	Strike	Dip	Unit	Comments
QE147	568510	3142115	980.8	BU	275	36	LMS	
QE149	569448	3142962	907.2	BU	293	58	UMS	
QE152	568437	3137554	295.7	BU	276	72	US	
QE153	568320	3137797	295.5	BU	267	77	US	
QE155	569402	3136132	371.5	BU	116	54	LMS	
QE156	568896	3135977	378.3	BU	286	81	LMS	
QE157	568877	3135959	382.5	BU	288	74	LMS	
QE159	568319	3135556	464.4	BU	292	81	LMS	
QE160	568243	3135454	504.8	BU	320	87	LMS	
QE161	568217	3135342	535.4	OB	111	55	LMS	
QE162	567337	3135902	528.4	OB	77	86	LMS	
QE164	566280	3135145	630.0	BU	130	38	LMS	
QE165	566209	3135025	637.9	BU	302	36	LMS	
QE166	626480	3099447	606.7	OB	317	61	LS	
QE167	626226	3099997	604.0	BU	103	62	LS	
QE168	623081	3100347	592.4	BU	103	79	LS	
QE169	620999	3099446	658.9	BU	114	71	LS	
QE171	619931	3094960	245.6	OB	296	77	US	
QE172	624566	3091985	258.0	BU	104	43	LMS	
QE173	625052	3091902	264.3	BU	136	53	LMS	
QE175	630320	3090130	258.3	BU	70	47	LMS	
QE176	631027	3089098	235.7	BU	94	66	LMS	
QE177	654671	3070733	290.3	BU	251	40	US	
QE178	654630	3070496	299.8	BU	103	63	US	US-UMS Contact
QE179	654589	3070210	336.7	BU	259	69	UMS	
QE180	654678	3069889	379.1	BU	263	55	UMS	
QE181	654689	3069670	372.4	BU	274	48	UMS	
QE183	654784	3069073	472.2	BU	266	64	UMS	
QE184	654550	3069009	502.7	BU	277	61	UMS	
QE186	654350	3066838	793.7	BU	247	23	LMS	
QE187	652715	3066223	718.6	BU	252	38	LMS	
QE188	649690	3066239	300.0	BU	264	76	LMS	
QE189	649676	3065980	299.7	BU	263	73	LMS	
QE190	649482	3065793	298.1	BU	265	73	LMS	
QE192	649633	3065383	275.2	BU	263	64	LMS	
QE193	650062	3065230	241.5	BU	263	76	LMS	
QE194	650354	3065059	233.8	BU	276	64	LMS	
QE195	650446	3064880	217.9	BU	264	60	LMS	LS-LMS Contact
QE199	649166	3089799	161.2	BU	309	19	UMS	
QE200	649580	3089570	234.7	BU	304	31	LMS	
QE202	649936	3089666	268.5	BU	277	16	UMS	
QE204	649850	3089717	269.8	BU	286	24	UMS	
QE205	649749	3089455	269.0	BU	279	22	UMS	
QE207	649765	3089014	271.1	BU	299	37	UMS	
QE208	649737	3088804	280.1	BU	292	63	UMS	

Location ID	UTM Easting	UTM Northing	Elevation (m ASL)	Measurement Type	Strike	Dip	Unit	Comments
QE210	649771	3088930	277.8	BU	289	41	UMS	
QE211	649655	3088715	279.3	BU	282	52	UMS	
QE212	649522	3088666	275.1	BU	294	63	LMS	
QE213	649349	3088456	277.6	BU	273	68	LMS	
QE215	649548	3088147	270.4	BU	288	55	LMS	
QE216	649787	3087806	268.8	BU	249	68	LMS	
QE218	649488	3087719	265.7	BU	318	58	LMS	
QE219	649180	3087613	258.2	BU	276	63	LS	
QE220	649244	3087183	257.8	BU	334	49	LS	
QE222	648979	3086905	256.7	BU	329	58	LS	
QE223	648873	3086916	256.2	BU	347	59	LS	
QE223	648882	3086880	261.7	BU	351	47	LS	
QE224	648886	3086867	259.8	BU	278	35	LS	
QE225	648867	3086880	256.9	BU	249	55	LS	
QE226	648724	3086915	258.8	BU	261	34	LS	
QE227	645689	3090623	316.2	OB	281	74	UMS	
QE228	645513	3090526	326.6	OB	281	88	UMS	
QE229	645274	3090444	333.7	BU	249	13	UMS	
QE230	645277	3090458	335.6	BU	131	25	UMS	
QE231	645289	3090471	339.2	BU	89	61	UMS	
QE232	645314	3090524	344.2	BU	102	90	UMS	
QE233	645389	3090643	347.8	OB	276	87	UMS	
QE234	646054	3090805	335.1	OB	288	51	UMS	
QE236	646984	3090298	316.9	BU	87	79	UMS	
QE240	647090	3090236	306.3	BU	312	23	UMS	
QE241	647389	3092455	578.8	BU	103	42	UMS	
QE242	647397	3092295	578.2	OB	285	84	UMS	
QE243	647324	3092179	561.9	OB	276	72	UMS	
QE244	647196	3091874	503.3	OB	260	68	UMS	
QE245	647189	3091637	478.2	OB	259	89	UMS	
QE246	647198	3091220	408.4	BU	75	87	UMS	
QE247	647318	3090872	375.7	BU	92	86	UMS	
QE248	647440	3090642	353.0	BU	90	89	UMS	
QE249	647625	3090417	331.8	OB	269	79	UMS	
QQ145	676748	3074932	483.7	BU	293	22	US	
QQ147	677451	3074995	449.0	BU	280	31	US	
QQ148	677949	3074163	440.9	BU	289	66	UMS	
QQ149	677782	3074140	418.1	BU	258	67	UMS	
QQ150	679061	3073745	479.4	BU	272	71	UMS	
QQ152	680764	3073481	353.0	BU	264	57	UMS	
QQ155	681708	3071897	259.3	BU	255	64	LS	
QQ156	682025	3071255	293.2	BU	264	62	LS	

Table of measurements interpreted from DEM

Location ID	UTM Easting	UTM Northing	Elevation (m ASL)	Measurement Type	Strike	Dip	Comments
DEM001	640628	3072200	502	B	320	10	
DEM002	639841	3071932	569	B	326	29	
DEM003	637595	3070626	579	B	328	33	
DEM004	642639	3070364	535	B	295	20	
DEM005	642166	3068572	696	B	282	64	
DEM006	644762	3069349	501	B	307	11	
DEM007	643145	3068749	690	B	302	25	
DEM008	647279	3068299	554	B	262	42	
DEM009	645549	3067528	551	B	289	38	
DEM010	665617	3087601	1008	B	268	40	
DEM011	671705	3086673	870	B	311	27	
DEM012	658005	3087803	773	B	279	40	
DEM013	662483	3087660	778	B	264	44	
DEM014	671037	3089391	611	OB	265	56	Inferred as OB
DEM015	651524	3091125	479	OB	243	71	Inferred as OB
DEM016	655386	3088599	712	B	270	57	
DEM017	664513	3087569	962	B	259	43	
DEM018	652677	3088039	612	B	286	47	
DEM019	651249	3087914	567	B	268	53	
DEM020	649845	3090518	477	OB	257	70	Inferred as OB
DEM021	657640	3090735	546	B	118	83	
DEM022	647075	3089734	332	B	294	24	
DEM023	648074	3088764	453	B	320	27	
DEM024	667705	3073901	645	B	265	34	
DEM025	672052	3071685	450	B	265	55	
DEM026	663324	3071795	525	B	256	38	
DEM027	687865	3072994	525	B	265	49	
DEM028	658698	3071585	334	B	259	34	
DEM029	657458	3070502	387	B	255	42	
DEM030	659888	3068638	824	B	254	45	
DEM031	637196	3075162	385	B	306	29	
DEM032	624527	3094234	300	OB	300	64	Inferred as OB
DEM033	629590	3089680	289	B	93	46	
DEM034	608507	3095504	326	B	259	27	
DEM035	638203	3087327	263	B	282	59	
DEM036	653746	3093412	547	OB	271	70	Inferred as OB
DEM037	670565	3090517	880	OB	272	55	Inferred as OB
DEM038	663314	3089738	603	OB	274	75	Inferred as OB
DEM039	666063	3091122	998	OB	268	77	Inferred as OB
DEM040	631215	3097090	667	OB	302	63	Inferred as OB
DEM041	628227	3098449	655	OB	302	55	Inferred as OB
DEM042	589088	3118074	579	B	336	53	
DEM043	577198	3131449	675	B	301	29	
DEM044	571109	3133504	738	B	303	42	

DEM045	574126	3140111	913	B	292	49	
DEM046	584633	3126073	799	B	319	31	
DEM047	586367	3126634	453	B	309	27	
DEM048	597796	3114632	557	B	319	17	
DEM049	599815	3110515	903	B	12	13	
DEM050	597310	3112930	721	B	335	36	
DEM051	595175	3114374	536	B	304	39	
DEM052	595290	3118962	528	B	297	34	
DEM053	563843	3147720	682	B	315	36	
DEM054	555223	3141480	252	B	307	27	
DEM055	559331	3138796	520	B	277	27	
DEM056	565468	3136227	371	B	275	56	
DEM057	559709	3136064	480	B	266	56	
DEM058	550909	3140021	639	B	304	27	
DEM059	553023	3141718	347	B	312	43	
DEM060	548881	3142519	475	B	281	68	
DEM061	555495	3152846	735	B	299	42	
DEM062	609000	3102980	441	OB	300	58	
DEM063	611591	3107378	787	B	305	75	

Map of field locations, Area A

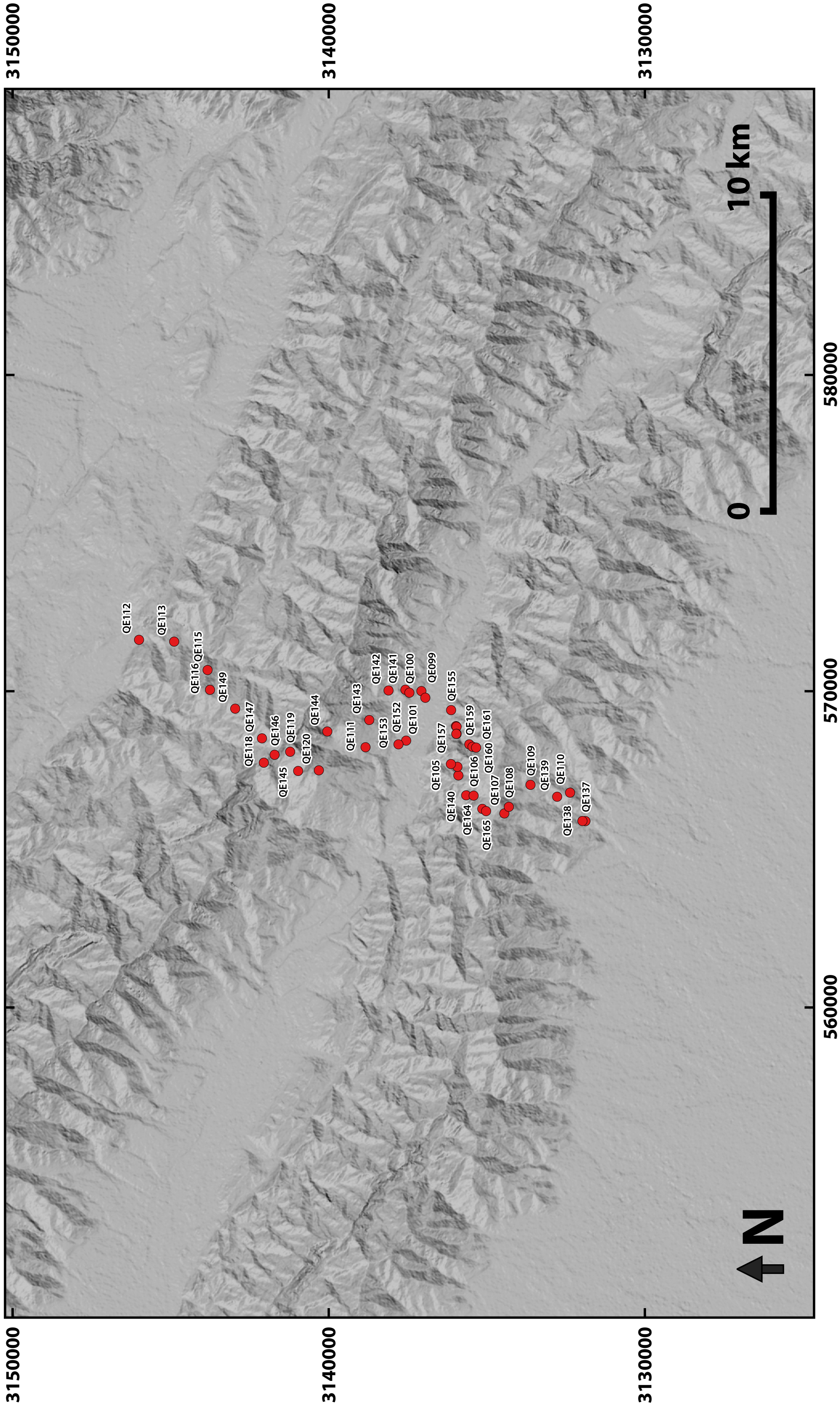

Map of field locations, Area B

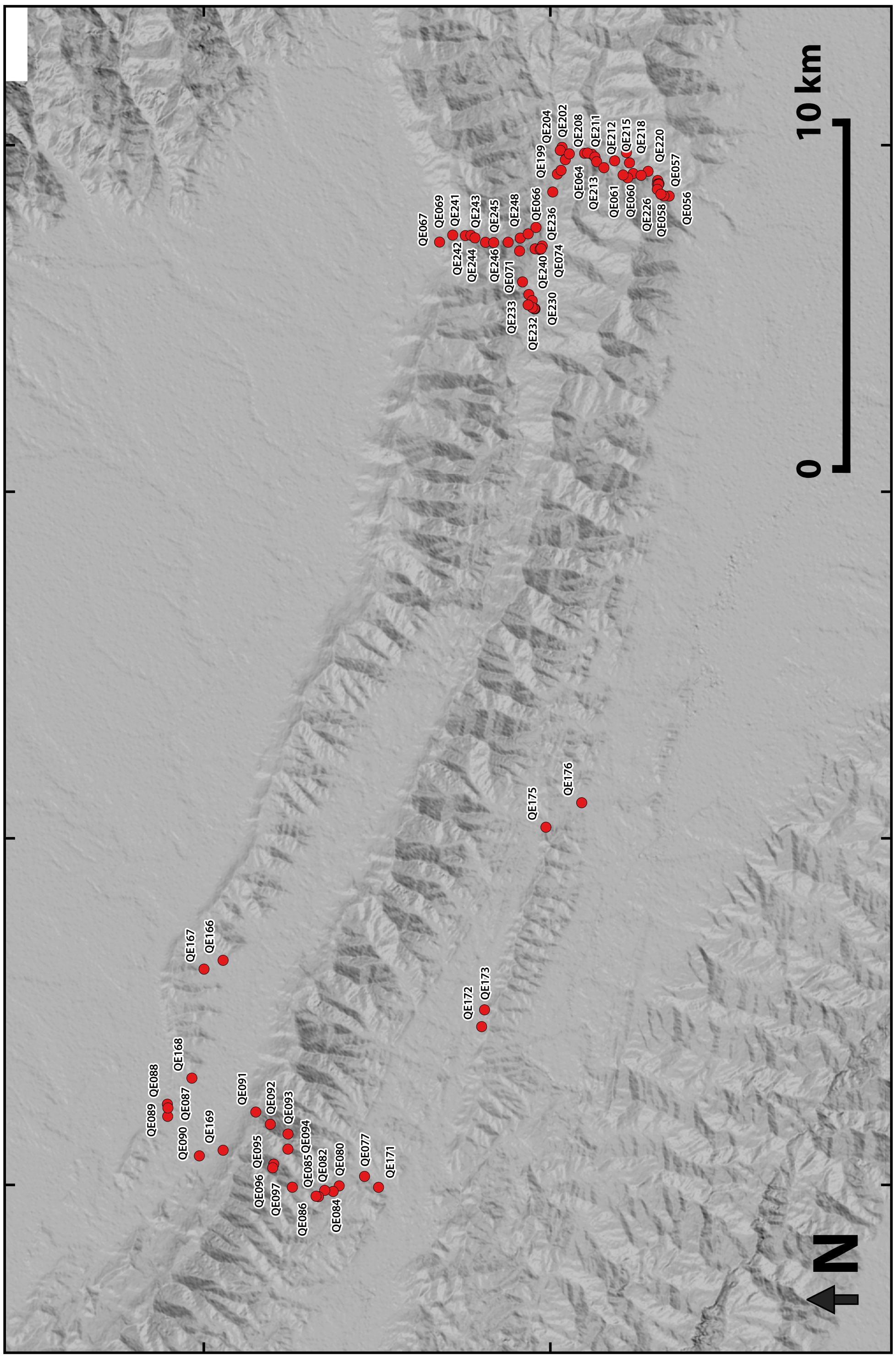

Map of field locations, Area C

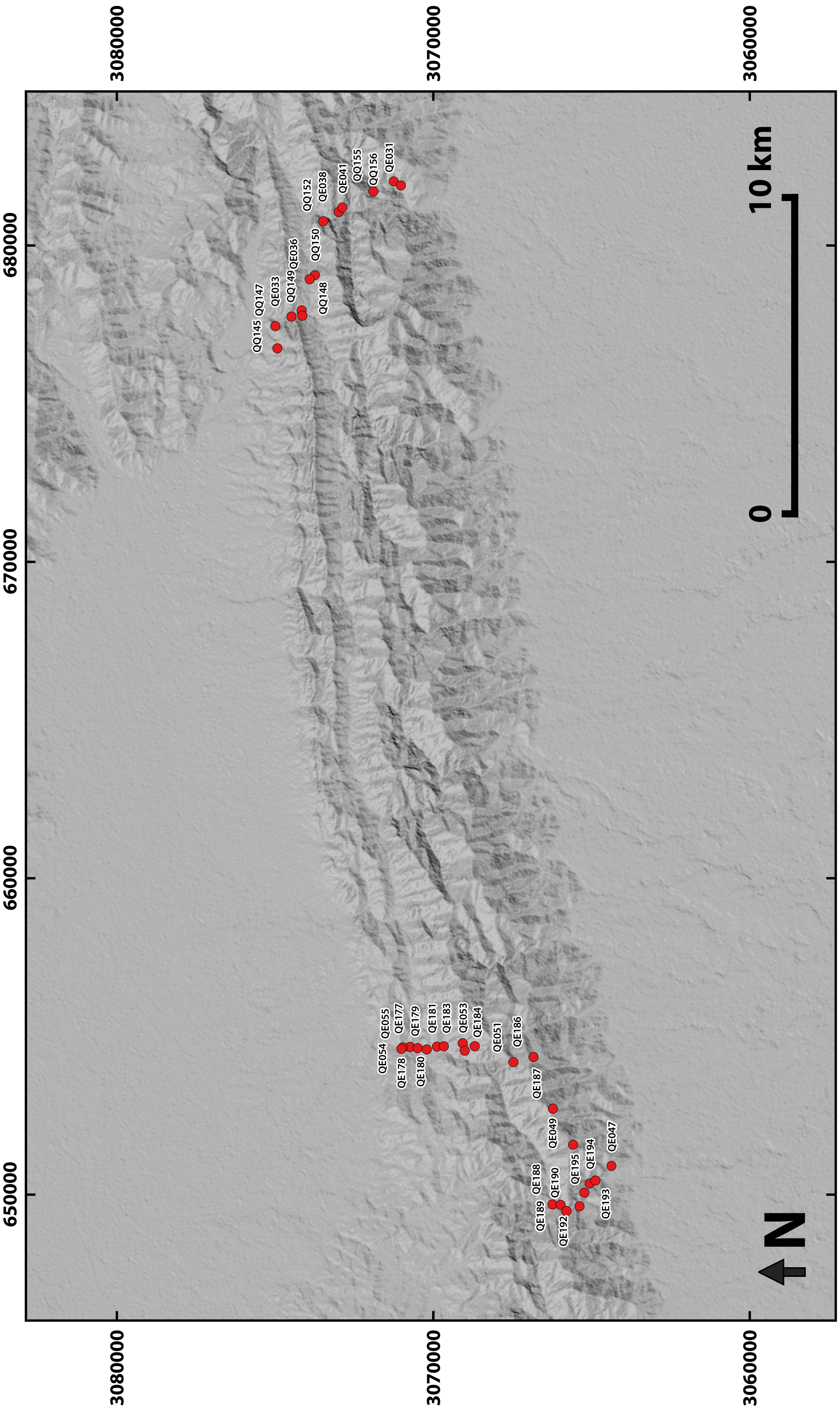

Map of orientations, Area A

Black: field measurements. Green: orientation measurements interpreted from DEM.

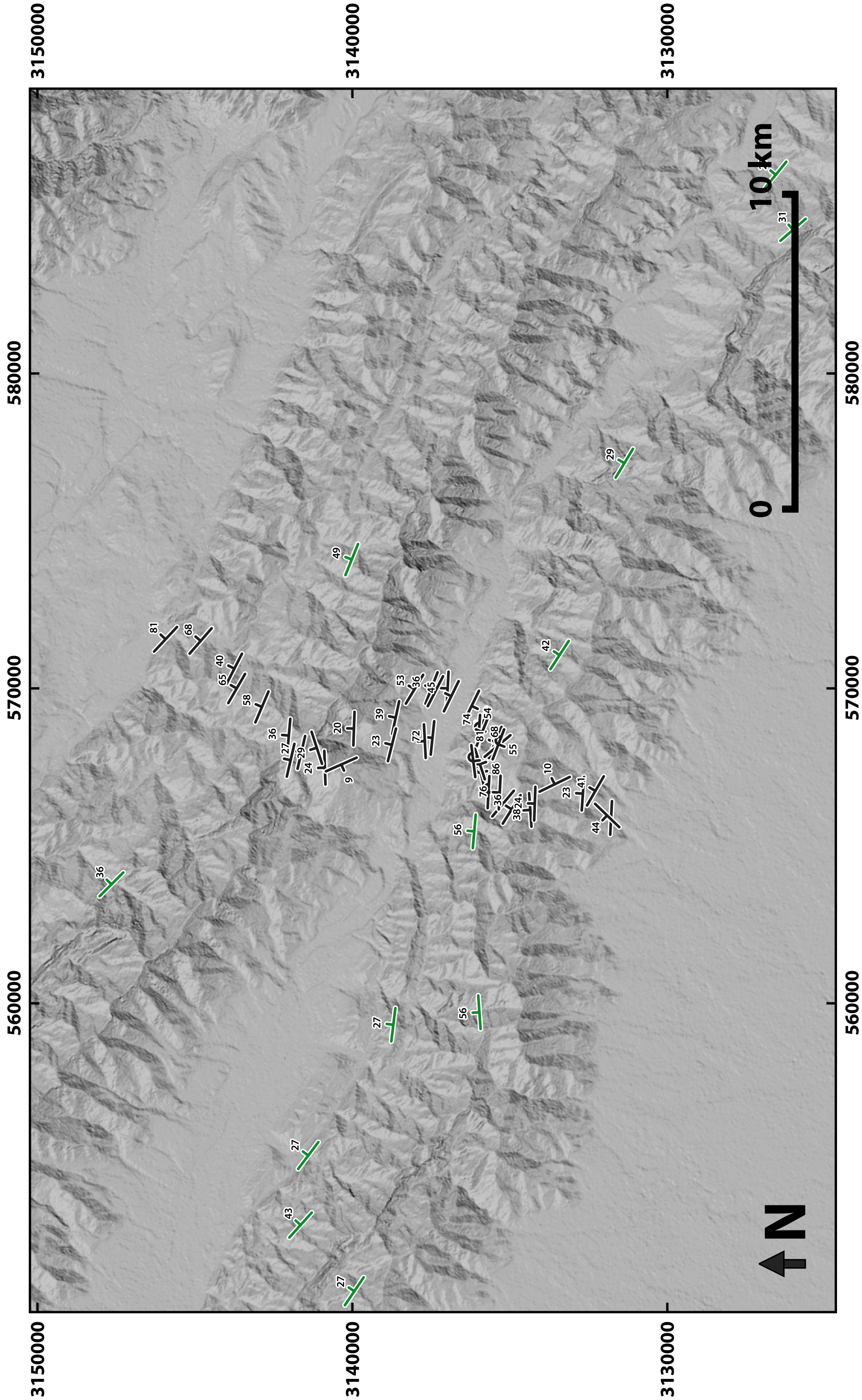

Map of orientations, Area B

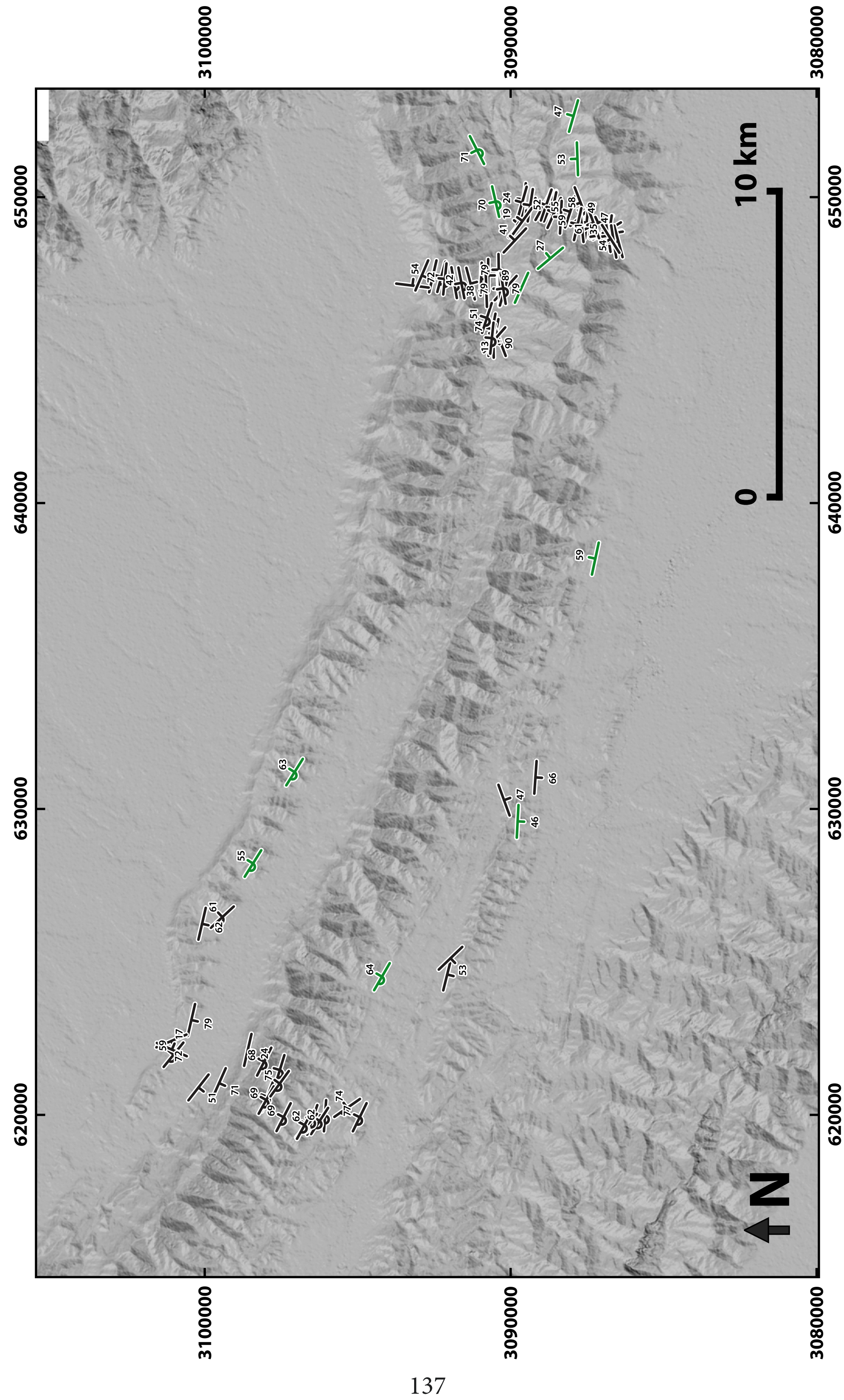

Map of orientations, Area C